ANTITUMORAL PROPERTIES OF EPIDERMAL GROWTH FACTOR DERIVATIVES

Clara Panosa Roqueta

Universitat de Girona

PhD Thesis

ANTITUMORAL PROPERTIES OF EPIDERMAL GROWTH FACTOR DERIVATIVES

Clara Panosa Roqueta

2015

Universitat de Girona

PhD Thesis

ANTITUMORAL PROPERTIES OF EPIDERMAL GROWTH FACTOR DERIVATIVES

Clara Panosa Roqueta

2015

Ciències Experimentals i Sostenibilitat

Vist-i-plau

El co-director de Tesi

Dr. Rafael de Llorens i Duran

Catedràtic de Bioquímica i Biologia Molecular

Vist-i-plau

La co-directora de Tesi

Dra. Anna Massaguer i Vall-llovera

Professora Agregada de Bioquímica i Biologia Molecular

Memòria presentada per optar al títol de doctora per la Universitat de Girona

Agraïments

Gràcies al grup de recerca de Bioquímica del Càncer, que em van donar la oportunitat d'iniciar aquesta tesi. També donar les gràcies als grups de recerca externs que em van acollir, ensenyar i donar tot el que vaig necessitar per completar aquest treball, gràcies Siscu, gràcies Reilly.

Gràcies a tots aquells qui m'heu acompanyat durant aquest temps i que m'heu donat suport en els moments difícils, he tingut la gran sort d'estar envoltada de becaris genials.

Aquesta tesi ha estat realitzada amb el suport de la Universitat de Girona (beques BR08/19 i PUG2007A/10).

Dedicatòria

Júlia, aquest treball te'l dedico a tu, perquè puguis arribar a gaudir també algun dia de les mateixes oportunitats d'aprendre i estudiar que he tingut jo.

Publications arising from this thesis

Panosa C, Tebar F, Ferrer-Batallé M, Fonge H, Seno M, Reilly RM, Massaguer A, De Llorens R. Development of an epidermal growth factor derivative with EGFR blocking activity. PLoS One; 2013; 8 (7): e69325.

Panosa C, Fonge H, Ferrer-Batallé M, Menéndez JA, Massaguer A, De Llorens R, Reilly RM. A comparison of non-biologically active truncated EGF (EGFt) and full-length hEGF for delivery of Auger electron-emitting ^{111}In to EGFR-positive breast cancer cells and tumor xenografts in athymic mice. Nucl Med Biol; 2015; Epub ahead of print.

Abbreviations

^{111}In	Indium-111
^{111}In-DTPA-EGFt	Truncated form of EGF labeled with ^{111}In
^{111}In-DTPA-hEGF	Human EGF labeled with ^{111}In
131I	Iodine-131
186Re	Rhenium-186
211At	Astatine-211
225Ac	Actinium-225
231Bi	Bismuth-231
99mTc	Technetium-99m
Aa	Amino acid
AIDS	Acquired immune deficiency syndrome
Akt	Protein kinase B
AR	Amphiregulin
Arg	Arginine
Asn	Asparagine
Asp	Aspartic acid
ATP	Adenosine Triphosphate
AUC	Area under the curve
BC	Breast cancer
BSA	Bovine serum albumin
BTC	Betacellulin
CBL	Ubiquitin ligase
cDTPAA	Bicyclic anhydride of DTPA
CL	Clearance
CR	Cysteine-rich domain
CTL	Control
Da	Daltons
DMEM	Dulbecco's modified eagle medium
DMSO	Dimethyl sulfoxide
DNA	Deoxyribonucleic acid
DTPA	Diethylenetriamine pentaacetate
DUBs	De-ubiquitylating enzymes
E.coli	Escherichia coli
EC	Electron capture
EDTA	Ethylenediaminetetraacetic acid
EGF	Epidermal growth factor
EGFR	Epidermal growth factor receptor
EGFt	Epidermal growth factor truncated form
ELISA	Enzyme-linked immunosorbent assay
EPG	Epigen
EPR	Epiregulin
ER	Endoplasmatic reticulum
ErbB 1/HER1	Epidermal growth factor receptor
ErbB 2/HER2	Receptor tyrosine-protein kinase erbB-2
ErbB 3/HER3	Receptor tyrosine-protein kinase erbB-3
ErbB 4/HER4	Receptor tyrosine-protein kinase erbB-4
FBS	Fetal bovine serum
FWHM	Full width at half maxiumum
Gln	Glutamine
HB-EGF	Heparin-binding EGF-like growth factor
hEGF	Human epidermal growth factor
HIV	Human immunodeficiency virus
HPLC	High performance liquid chromatography
HRP	Horseradish peroxidase
i.v.	Intravenous
ID	Injected dose
Ig G	Immunoglobulin G
Ile	Isoleucine
IPTG	Isopropyl β-D-1-thiogalactopyranoside
ITLC-SG	Instant thin layer-silica gel chromatography
Kd	Dissociation constant
KDa	Kilodaltons
keV	Kiloelectronvolt
Kvp	Peak kilovoltage

LB	Luria-Bertani medium
LET	Linear energy transfer
Leu	Leucine
mAbs	Monoclonal antibodies
MALDI-TOF MS	Matrix-assisted laser desorption/ionization mass spectometry
MAPK	Mitogen-activated protein kinase
mBq	millibeckerels
MBq	megabeckerels
Met	Metionine
MeV	Megaelectronvolts
Micro SPECT/CT	Micro-single-photon emission computed tomography/computed tomography
ml	milliliters
mM	millimolar
mm	millimeters
MTT	3-(4,5-dimethylthiazol-2-yl)-2,5-diphenyltetrazolium bromide
MVB	Multi vesicular body
NLS	Nuclear localization signal
NPC	Nuclear pore copmplex
NRG	Neuregulin
NSCLC	Non-Small Cell Lung Cancer
OmpA	Outer membrane protein A
OSEM	Ordered subset expectation
p	statistical significance
p.i.	post injection
PBS	phosphate buffered saline
PBS-T	PBS plus Tween-20 buffer
PCI	Potato Carboxypeptidase inhibitor
pCi	picoCurie
PCNA	Proliferating cell nuclear antigen
PDRT	Peptide-directed radiotherapy
PE	Plating efficiency
Phe	Phenilalanine
PI3K	Phosphoinositide 3-kinase
PKC	Protein kinase C
PLCγ	Phospholipase C gamma
PSA	Prostate-specific antigen
PTB	Phospho-tyrosine binding
PVDF	Polyvinylidene difluoride
Ras	Small GTPase proteins
RIT	Radioimmunotherapy
RITC	Rhodamine isothiocyanate
RP-HPLC	Reverse phase HPLC
s.c.	Subcutaneous
SD	Standard deviation
SDS-PAGE	Dodecyl sulfate polyacrylamide gel electrophoresis
SE	Standard error
Ser	Serine
SF	Surviving fraction
SFKs	Src family kinases
SH2	Src homology 2
Src	Proto-oncogene tyrosine kinase
STAT	Signal transducer and activator of transcription
$T_{1/2}\alpha$	Distribution half-life
$T_{1/2}\beta$	Elimination half-life
TGFα	Transforming growth factor alpha
TK	Tirosine Kinase
TKIs	Tyrosine Kinase inhibitors
TMB	3,3',5,5'-Tetramethylbenzidine
Tyr	Tyrosine
UIM	Ubiquitin-interacting motif
V_1	Initial volume of distribution
Val	Valine
Vss	Volume of distribution at steady state
x g	Relative centrifuge force
Y	Tyrosine
mg	milligrams
µm	micrometers

List of figures

List of tables

Summary

The members of the epidermal growth factor (EGF) / ErbB family are prime targets for cancer therapy. However, the therapeutic efficiency of the existing anti-ErbB agents is limited. Thus, identifying new molecules that inactivate the ErbB receptors through novel strategies is an important goal on cancer research. In this thesis work we have developed a shorter form of human EGF (EGFt) with a truncated C-terminal as a novel EGFR inhibitor. EGFt was designed based on the superimposition of the three-dimensional structures of EGF and the Potato Carboxypeptidase Inhibitor (PCI), an EGFR blocker previously described by our group. The peptide was produced in *E. coli* with a high yield of the correctly folded peptide. EGFt induced poor EGFR homodimerization and phosphorylation. Interestingly, EGFt promoted EGFR internalization and translocation to the cell nucleus although it did not stimulate the cell growth. In addition, EGFt competed with EGFR native ligands, inhibiting the proliferation of cancer cells.

The lack of EGFR-mediated growth-stimulatory activity prompted us to evaluate EGFt for targeted delivery of ^{111}In, an Auger electron emitter, into EGFR-positive cancer cells. An ^{111}In-DTPA-EGFt radioconjugate was developed and its properties were analyzed and compared to those of ^{111}In-DTPA-hEGF. First we determined that ^{111}In-DTPA-EGFt displays high specificity and affinity for EGFR. However, the cellular uptake of ^{111}In-DTPA-EGFt resulted to be lower than that of ^{111}In-DTPA-hEGF. Once internalized, ^{111}In-DTPA-EGFt showed a high efficiency to accumulate into the cell nucleus, where the radioactivity emitted by ^{111}In may damage the DNA. In accordance, ^{111}In-DTPA-EGFt showed to be cytotoxic *in vitro* against breast cancer cells, although its cytotoxicity was lower compared to ^{111}In-DTPA-hEGF. *In vivo* studies revealed a longer half-life in blood for ^{111}In-DTPA-EGFt than for ^{111}In-DTPA-hEGF and higher uptake in the kidney, with minor accumulation in other normal

tissues. ^{111}In-DTPA-EGFt accumulated in MDA-MB-468 tumors where, interestingly, ^{111}In-DTPA-EGFt was detected in a great proportion in the cell nucleus.

All the data obtained from this work indicate that EGFt may be a potential EGFR blocker for cancer therapy and also an attractive ligand for delivery of cytotoxic agents into the nucleus of EGFR-positive cancer cells.

Resum

Els receptors i lligands de la família del factor de creixement epidèrmic (EGF) / ErbB són dianes molt importants en el desenvolupament de teràpies contra el càncer. No obstant, l'eficàcia terapèutica dels fàrmacs dirigits a atacar aquesta via i que són utilitzats actualment en clínica és limitada. Per aquest motiu la recerca de noves molècules que inactivin els receptors d'aquesta família mitjançant noves estratègies és avui dia una de les vies més explorades. En aquesta tesi s'ha desenvolupat un pèptid idèntic al factor de creixement epidèrmic EGF que li manca la seva part C-terminal (EGFt) com a nou inhibidor de EGFR. El disseny d'aquest pèptid truncat s'ha basat en la superposició tridimensional de l'estructura de l'EGF i de l'inhibidor de la carboxipeptidasa de patata (PCI), un bloquejador de la via de l'EGFR descrit prèviament pel nostre grup. El pèptid ha estat produït en *E.coli* i s'ha aconseguit obtenir un alt rendiment de la proteïna i amb la seva conformació estructural correcta. Hem observat que l'EGFt in vitro té una capacitat molt menor per induir dímers del receptor i també la seva fosforilació si la comparem amb l'activitat que té l'hEGF natiu. Per altra banda, l'EGFt promou la internalització del receptor i la seva translocació al nucli cel·lular tal i com ho fa l'hEGF, tot i que no estimula el creixement cel·lular. A més, l'EGFt competeix amb els lligands natius de la família i inhibeix la proliferació cel·lular.

La manca d'activitat estimuladora del creixement cel·lular d'aquest pèptid quan s'uneix a l'EGFR ens va portar a provar la utilització de l'EGFt com a vehicle de toxines dirigit a cèl·lules tumorals que sobreexpresessin EGFR. Concretament, es va produir un radioconjugat de EGFt amb l'isòtop radioactiu emissor d'electrons Auger Indi-111. Les propietats d'aquest radioconjugat es van analitzar i es van comparar amb el radioconjugat produït amb hEGF natiu. En primer lloc es va determinar que ^{111}In-DTPA-EGFt té una alta especificitat i afinitat per EGFR. No obstant, la captació cel·lular de ^{111}In-DTPA-EGFt va resultar ser menor que la de ^{111}In-DTPA-hEGF. Un cop internalitzat, ^{111}In-DTPA-EGFt va mostrar una alta eficiència per acumular-se en el

nucli de la cèl·lula, on la radioactivitat emesa per ^{111}In danya l'ADN. ^{111}In-DTPA-EGFt va mostrar ser citotòxic in vitro contra cèl·lules de càncer de mama, encara que la seva citotoxicitat va ser menor en comparació amb ^{111}In-DTPA-hEGF. Els estudis in vivo van revelar una vida mitjana més llarga en sang per ^{111}In-DTPA-EGFt que per ^{111}In-DTPA-hEGF, una major captació en el ronyó i una menor acumulació en altres teixits normals. ^{111}In-DTPA-EGFt es va detectar en els tumors de cèl·lules MDA-MB-468 on el radiocompost es va acumular preferentment en el nucli de la cèl·lula.

Les dades recollides en aquest treball indiquen que l'EGFt pot tenir un gran potencial com a bloquejador en teràpia pel càncer i a més pot ser un bon lligand per utilitzar com a vehicle d'agents citotòxics dirigits al nucli de cèl·lules tumorals positives en EGFR.

Resumen

Los receptores y ligandos de la familia del factor de crecimiento epidérmico (EGF) / ErbB son dianas muy importantes en el desarrollo de terapias contra el cáncer. Sin embargo, la eficacia terapéutica de los fármacos dirigidos a atacar esta vía y que son utilizados actualmente en clínica es limitada. De ahí que la búsqueda de nuevas moléculas que inactiven los receptores de esta familia mediante nuevas estrategias es hoy en día una de las vías más exploradas. En esta tesis se ha desarrollado un péptido idéntico al factor de crecimiento epidérmico EGF que le falta su parte C-terminal (EGFt) como nuevo inhibidor de EGFR. El diseño de este péptido truncado se ha basado en la superposición tridimensional de la estructura del EGF y del inhibidor de la carboxipeptidasa de patata (PCI), un bloqueador de la vía del EGFR descrito previamente por nuestro grupo. El péptido ha sido producido en *E.coli* y se ha logrado obtener un alto rendimiento de la proteína y con su conformación estructural correcta. Hemos observado que el EGFt in vitro tiene una capacidad mucho menor para inducir dímeros del receptor y también su fosforilación si la comparamos con la actividad que tiene el hEGF nativo. Por otra parte, el EGFt promueve la internalización del receptor y su translocación al núcleo celular tal como lo hace el hEGF, aunque no estimula el crecimiento celular. Además, el EGFt compite con los ligandos nativos de la familia e inhibe la proliferación celular.

La falta de actividad estimuladora del crecimiento celular de este péptido cuando se une al EGFR nos llevó a probar la utilización del EGFt como vehículo de toxinas dirigido a células tumorales que sobreexpresaran EGFR. Concretamente, se produjo un radioconjugado de EGFt con el isótopo radiactivo emisor de electrones Auger Indio-111. Las propiedades de este radioconjugado se analizaron y se compararon con el radioconjugado producido con EGF nativo. En primer lugar se determinó que ^{111}In-DTPA-EGFt tiene una alta especificidad y afinidad por EGFR. No obstante, la captación celular de ^{111}In-DTPA-EGFt resultó ser menor que la de ^{111}In-DTPA-hEGF. Una vez internalizado, ^{111}In-DTPA-EGFt mostró una alta eficiencia para acumularse en

el núcleo de la célula, donde la radiactividad emitida por ^{111}In daña el ADN. ^{111}In-DTPA-EGFt mostró ser citotóxico in vitro contra células de cáncer de mama, aunque su citotoxicidad fue menor en comparación con ^{111}In-DTPA-hEGF. Los estudios in vivo revelaron una vida media más larga en sangre para ^{111}In-DTPA-EGFt que para ^{111}In-DTPA-hEGF, una mayor captación en el riñón y una menor acumulación en otros tejidos normales. ^{111}In-DTPA-EGFt se detectó en los tumores de células MDA-MB-468 donde el radiocompuesto se acumuló preferentemente en el núcleo de la célula.

Los datos recogidos en este trabajo indican que el EGFt puede tener un gran potencial como bloqueador en terapia para el cáncer y además puede ser un buen ligando para utilizar como vehículo de agentes citotóxicos dirigidos al núcleo de células tumorales positivas en EGFR .

CONTENTS

INTRODUCTION

1. Cancer overview

1.1. Molecular basis of cancer

Cancer is a genetic disease that occurs when the information in cellular DNA is corrupted leading to abnormal patterns of gene expression. As a result, the effects of normal genes that control cell growth, survival and spread are enhanced and those of genes that suppress these effects are repressed. The main mechanism by which this corruption of the genetic code occurs is through the accumulation of mutations, although there is increasing recognition of the role of non-mutational (epigenetic) changes in the process. Aberrant gene expression leads to a number of key changes in fundamental biological processes within cancer cells, the so-called 'hallmarks' of cancer (Hanahan et al., 2011). The hallmarks of cancer comprise six biological capabilities acquired during the multistep development of human tumours. They include sustaining proliferative signalling, evading growth suppressors, resisting cell death, enabling replicative immortality, inducing angiogenesis, and activating invasion and metastasis. Underlying these hallmarks are two important characteristics that enable the acquisition of these mentioned function capabilities: genome instability, which generates the genetic diversity that expedites their acquisition, and inflammation, which fosters multiple hallmark functions. Conceptual progress in the last decade has added two emerging hallmarks of potential generality to this list—reprogramming of energy metabolism and evading immune destruction (Figure 1). In addition to cancer cells, tumors exhibit another dimension of complexity: they contain a repertoire of recruited, ostensibly normal cells that contribute to the acquisition of hallmark traits by creating the "tumor microenvironment."

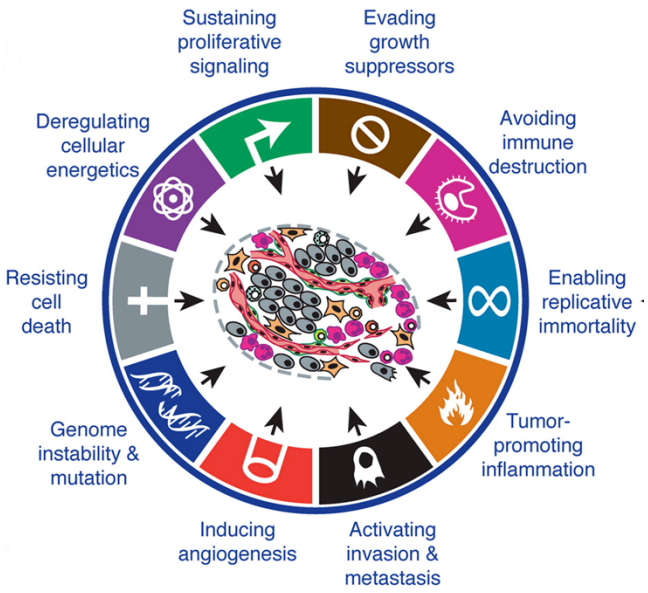

Figure 1. The hallmarks of cancer. The illustration encompasses the six biological capabilities acquired during the multistep development of human tumors, the two new emerging hallmark capabilities and two enabling characteristics crucial to the acquisition of these hallmark capabilities. Extracted from Hanahan and Weinberg, 2011.

1.2. Classification of human cancers

There are many different types of cancer. Cancer can be classified according to the tissue that the malignant cells originate from; the main categories include:

- Adenocarcinoma – tumours derived from secretory epithelial cells (e.g. prostate, breast and colorectal cancers).
- Squamous cell carcinoma – tumours derived from epithelial cells (in skin or in tissues covering some inner organs).
- Sarcoma – tumours derived from connective or supportive tissue (bone, cartilage, fat, muscle and blood vessels).
- Leukaemia – derived from blood-forming tissue (bone-marrow).
- Lymphoma and Myeloma – cancers that originate in the immune system.
- Glioma – tumours derived from brain and spinal cord.

The two first groups represent the most common human cancers – the carcinomas. Carcinomas are responsible for more than 80% of the cancer-related deaths in the Western world (Weinberg, 2007).

1.3. Cancer statistics

Nowadays, cancer accounts for one in every eight deaths worldwide – more than HIV/AIDS, tuberculosis, and malaria combined. In EU a total of 1,359,100 Europeans are projected to die of cancer in 2015 (Malvezzi et al., 2015). And in United States the expected numbers of deaths from cancer in 2015 is estimated in 589,430 Americans, corresponding to about 1600 deaths per day (Siegel et al., 2015).

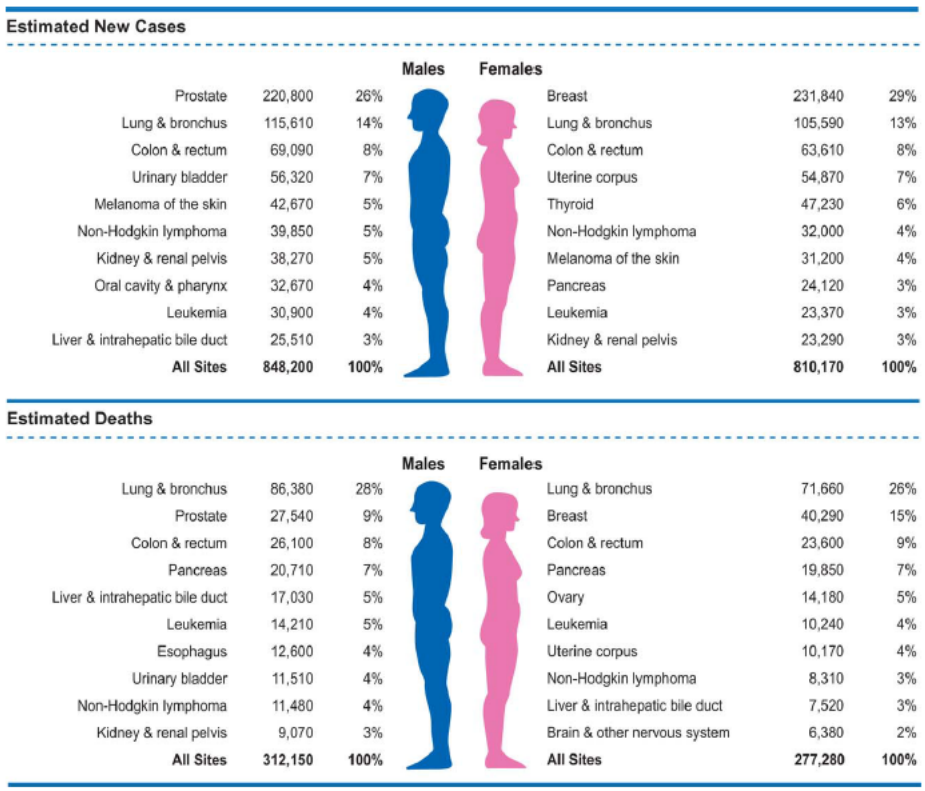

Estimated New Cases

Males				Females		
Prostate	220,800	26%		Breast	231,840	29%
Lung & bronchus	115,610	14%		Lung & bronchus	105,590	13%
Colon & rectum	69,090	8%		Colon & rectum	63,610	8%
Urinary bladder	56,320	7%		Uterine corpus	54,870	7%
Melanoma of the skin	42,670	5%		Thyroid	47,230	6%
Non-Hodgkin lymphoma	39,850	5%		Non-Hodgkin lymphoma	32,000	4%
Kidney & renal pelvis	38,270	5%		Melanoma of the skin	31,200	4%
Oral cavity & pharynx	32,670	4%		Pancreas	24,120	3%
Leukemia	30,900	4%		Leukemia	23,370	3%
Liver & intrahepatic bile duct	25,510	3%		Kidney & renal pelvis	23,290	3%
All Sites	**848,200**	**100%**		**All Sites**	**810,170**	**100%**

Estimated Deaths

Males				Females		
Lung & bronchus	86,380	28%		Lung & bronchus	71,660	26%
Prostate	27,540	9%		Breast	40,290	15%
Colon & rectum	26,100	8%		Colon & rectum	23,600	9%
Pancreas	20,710	7%		Pancreas	19,850	7%
Liver & intrahepatic bile duct	17,030	5%		Ovary	14,180	5%
Leukemia	14,210	5%		Leukemia	10,240	4%
Esophagus	12,600	4%		Uterine corpus	10,170	4%
Urinary bladder	11,510	4%		Non-Hodgkin lymphoma	8,310	3%
Non-Hodgkin lymphoma	11,480	4%		Liver & intrahepatic bile duct	7,520	3%
Kidney & renal pelvis	9,070	3%		Brain & other nervous system	6,380	2%
All Sites	**312,150**	**100%**		**All Sites**	**277,280**	**100%**

Figure 2. Ten leading cancer types for the estimated new cancer cases and deaths by sex, USA, 2015. Estimates are rounded to the nearest 10 and cases exclude basal cell and squamous cell skin cancers and *in situ* carcinoma except urinary bladder. Extracted from Siegel *et al.,* 2015.

Figure 2 indicates the most common cancers expected to occur and deaths in men and women in 2015 in United States (Siegel et al., 2015). Among men, cancers of the prostate, lung and bronchus, and colorectum will account for about half of all newly diagnosed cancers. The 3 most commonly diagnosed types of cancer among women in 2015 will be breast, lung and bronchus, and colorectum, accounting for the half of the estimated cancer cases in women. Breast cancer alone is expected to account for 29% (231,840) of all new cancer cases among women. Cancers of the lung and bronchus, prostate, and colorectum in men and cancers of the lung and bronchus, breast, and colorectum in women account for almost half of the total cancer deaths (Siegel et al., 2015).

1.4. Cancer treatment today

Cancer therapy involves several types of treatment. The principal therapeutic modalities are surgery, radiotherapy and chemotherapy. In the case of solid tumors, the first step is usually surgical removal of the primary cancer together with a margin of normal tissue; as such cancers are commonly irregular in shape. Then, the area around the site may be irradiated to destroy any possible remnants of the tumor. At the same time, cytotoxic drugs can be given to kill residual cancer cells and possible metastases and nowadays, beside standard chemotherapy have emerged the targeted therapy drugs, which inhibit a more specific target in cells. This is the usual pattern of treatment, but there are some situations where alternative approaches are used. In regions of anatomical complexity, such as the head and neck, and in regions of vital biological function, such as the brain and spine, surgery would cause many problems, and so radiotherapy is sometimes the preferred modality. In disseminated cancers such as leukaemia, the only modality that can be used is chemotherapy. The time after the treatment that patient survives without any signs or symptoms of cancer are called the relapse-free survival. The return of the disease or the signs and symptoms after a period of improvement is known as relapse (Figure 3) (King and Robins, 2006).

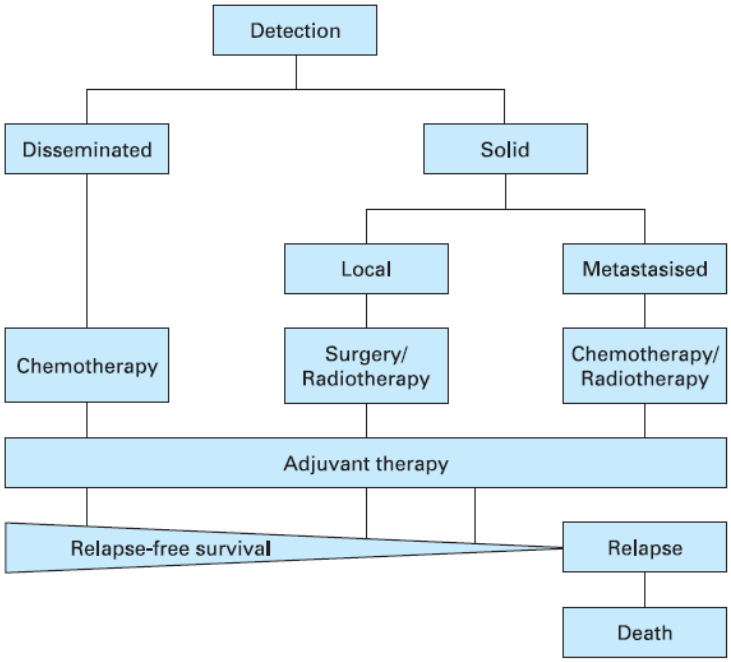

Figure 3. Clinical events in cancer therapy. Extracted from King and Robins, 2006.

1.5. Targeted cancer therapy

Traditional chemotherapy and radiotherapy will destroy not only proliferating cancer cells but also proliferating normal cells; so side effects are almost inevitable. The term *targeted therapy* refers to drugs or other substances that block the growth and spread of cancer by interfering with specific molecules (molecular targets) that are involved in the growth, progression, and spread of cancer. These, targeted therapies are deliberately selected or designed to interact with their target and are often cytostatic (they block tumor cell proliferation), whereas many standard chemotherapies were identified because they kill cells (they are cytotoxic).

As more is understood about the molecular defects that lead to malignancy, more agents targeted towards specific molecules or specific survival functions of cancer cells

are being developed and are demonstrating effective therapeutic benefit while limited toxicity to normal cells (Zahorowska et al., 2009). Targeted cancer therapies approved for use against specific cancers include agents that prevent cell growth signalling, interfere with tumor blood vessel development, promote the death of cancer cells, stimulate the immune system to destroy cancer cells, and deliver toxic drugs to cancer cells. In addition, new fields have emerged lately as promising targets, including cancer metabolism and epigenetic modulation. Cancer immunotherapy is also a promising field for targeted cancer discovery (Huang et al., 2014).

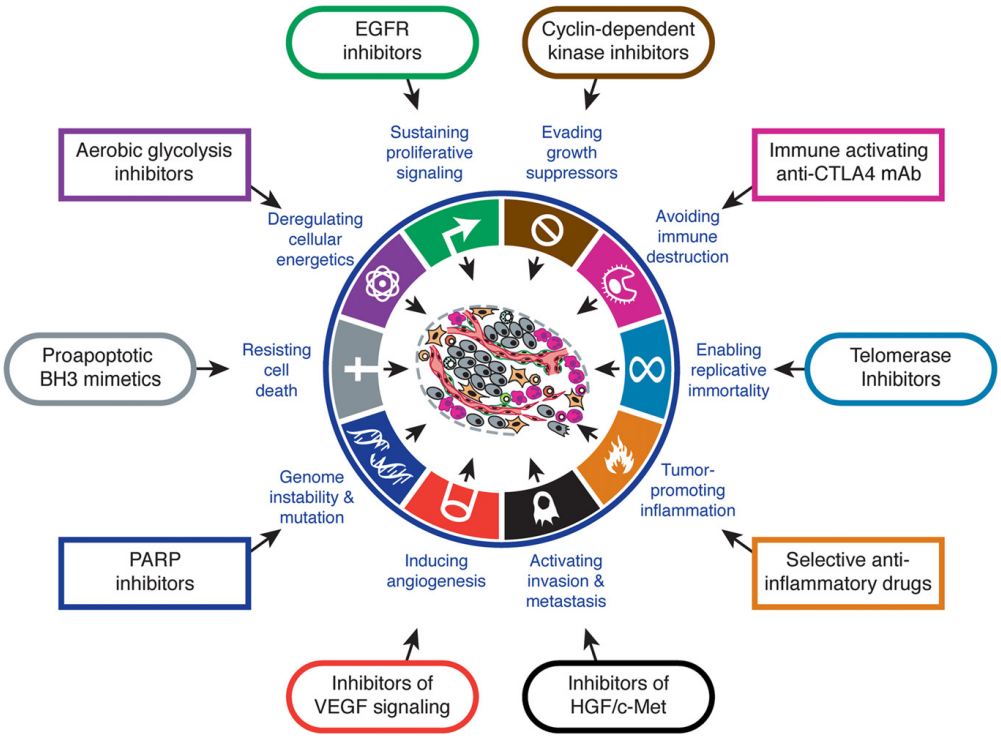

Figure 4. Therapeutic targeting of the Hallmarks of cancer. Drugs that interfere with each of the acquired capabilities necessary for tumor growth and progression have been developed and are in clinical trials or in some cases approved for clinical use in treating certain forms of human cancer. Extracted from Hanahan et al., 2011.

Targeted therapies include monoclonal antibodies (mAbs), small molecules (such as ATP analogues), peptide mimetics, and antisense oligonucleotides (Stoffel, 2010; Imai et al., 2006). Among the targets for therapy, growth factor receptors and downstream signaling molecules continue to be the most actively explored targets for cancer drug discovery. Figure 4 illustrates some examples of targeted therapeutics categorized according to their respective effects on one or more hallmark capabilities.

2. The Epidermal Growth Factor Receptor (EGFR)

2.1. EGFR and its family

The epidermal growth factor receptor (EGFR) belongs to the ErbB family of proteins, which consists of ErbB1/HER1/EGFR, ErbB2/HER2/Neu, ErbB3/HER3 and ErbB4/ HER4 (Stern, 2010). They are transmembrane glycoproteins with molecular weights ranging from 170 to 185 KDa. Structurally, ErbB family members consist of i) a cysteine-rich variable extracellular N-terminal domain, ii) a hydrophobic transmembrane domain and iii) an intracellular, highly conserved, cytoplasmic C-terminal tyrosine kinase domain with several phosphorylation sites. (Seshacharyulu et al., 2012). The extracellular region of EGFR is subdivided into four domains arranged as a tandem repeat of two types of domains (Figure 5). The first and third domains are homologous and have been designated as domains I and III or L1 and L2, respectively. These domains are responsible for binding to different ligands. The second and four domains, are also homologous and have been designated as domains II and IV or CR1 and CR2, respectively. Domains II an IV are involved in the dimerization of ErbB receptors (Leahy, 2004; Normanno et al., 2006; Flynn et al., 2009; Lemmon, 2009).

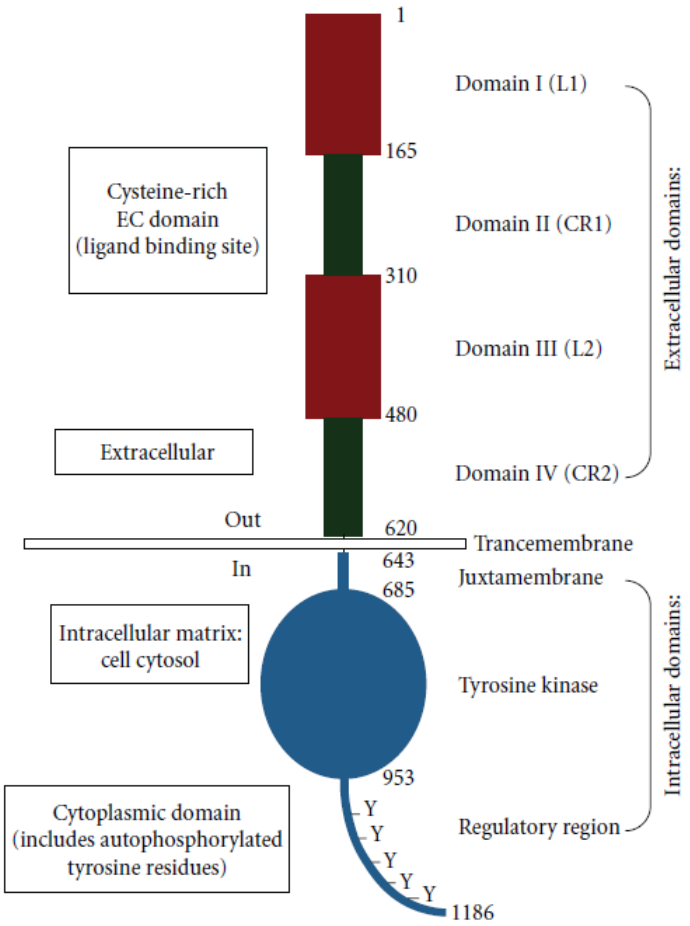

Figure 5.Basic Structure of EGFR demonstrating relevant domains. *(I) The extracellular domains*: (1) domain I: L1; (2) domain II: CR1; domain III: L2; domain IV: CR2. *(II) Transmembrane domains*. *(III) The* intracellular *domains* (1) juxtamembrane domain; (2) tyrosine kinase domain; (3) regulatory region domain. Adapted from Flynn et al., 2009.

ErbB family members can be activated by 13 known ligands, which include EGF, transforming growth factor alpha (TGFα), amphiregulin (AR), betacellulin (BTC), heparin-binding EGF-like growth factor (HB-EGF), epiregulin (EPR), epigen (EPG) and neuregulins 1 -- 6 (NRG) (Citri and Yarden, 2006; Yarden and Sliwkowski, 2001). Among these ligands, EGF, TGFα, AR, BTC and EPR have been demonstrated to bind EGFR.

Among them, EGF and TGFα are considered the main ligands of EGFR (Linggi et al., 2006; Wells, 1999; Köstler et al., 2010). Although, HER2 is closely related to EGFR, no ligands have been described for HER2 to date (Coussens et al., 1980). EGFR and HER2 share 82% homology in the tyrosine kinase domain, (Prigent and Lemoine, 1992) and cross-interactions between EGFR and HER2 receptors are frequent. In fact, HER2 is the preferred binding partner of EGFR (Harari and Yarden, 2000; Yarden and Sliwkowski, 2001). The ligand-binding domain of HER3 demonstrates approximately 40% homology to EGFR and binds neuregulin-1 and neuregulin-2. HER3 has a distinctive feature; its tyrosine kinase domain is functionally defective. Finally, HER4, which is the most recently described family member, is a receptor for HB-EGF, betacellulin, epiregulin, and neuregulins 1-4 (Campbell et al., 2010; Carpenter, 2003).

EGFR is expressed on normal cells at levels ranging from 20,000 to 200,000 receptors per cell (Chow, 1997). Ligand binding induces major conformational changes in the receptor, leading to the exposition of the dimerization arm in domain II. This allows the receptor homodimerization or heterodimerization with other ErbB receptors in the plasma membrane followed by the activation of the receptor tyrosin kinase activity, causing the transphosphorylation of the cytoplasmic tails of each dimer pair. ErbB receptors activation stimulates many complex intracellular signaling pathways that are involved in numerous biological processes such us proliferation (Ullrich and Schlessinger, 1990; Carpenter and Cohen, 1990), apoptosis (Cao et al., 2000; Armstrong et al., 1994), migration, angiogenesis and differentiation (Yarden, 2001; Roskoski, 2004; Wheeler et al., 2010; Bublil et al., 2007). EGFR plays a role during embryogenesis in the morphogenesis of organs like teeth, brain, reproductive tracts, gastrointestinal tracts and cardiovascular system (Goldman et al., 1996; Kato et al., 1995; Thesleff et al., 1995). Physiologically, EGFR has an essential role in wound healing and normal epithelial regeneration of organs such as gastrointestinal, genitourinary, respiratory, skin and corneal epithelia (Schneider and Wolf, 2009; Repertinger, et al., 2011).

2.2. EGFR ligand: Epidermal Growth Factor (EGF)

Human EGF is a small polypeptide composed of 53 amino acid residues that adopts a well-defined three-dimensional structure containing three disulfide bonds that define three loops (namely A, B and C) (Figure 6) (Ogiso et al., 2002). This scaffold is know as a T-Knot and is found in a large number of functional unrelated proteins. Its structure is tightly related to its function (Mas et al., 1998).

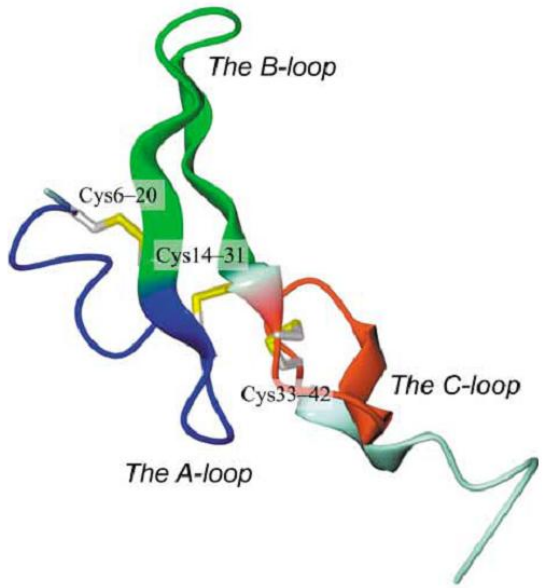

Figure 6. EGF structure. The A, B, and C loops are coloured blue, green, and red, respectively. The other regions are pale green. Adapted from Ogiso et al., 2002.

There are three contact sites described between EGF and the EGFR: the B loop (residues 20-31) of EGF interacts with site 1 in domain I of EGFR, the region containing the A loop (residues 6-19) and Arg41 of EGF interacts with site 2 in domain III of EGFR, and the C-terminal region around Arg45 interacts with site 3 in domain III of EGFR (Figure 7) (Ogiso et al., 2002).

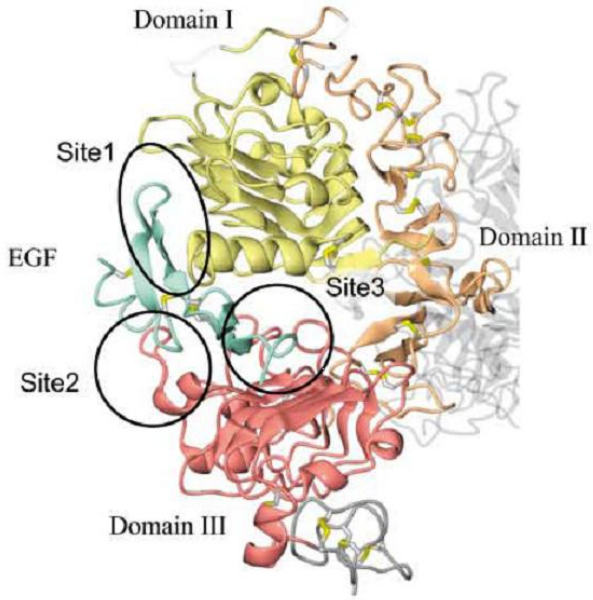

Figure 7. Mapping the interaction sites onto ribbon representations of EGFR and EGF. Three binding sites in the interface are outlined. Domains I, II, III, and IV in the receptor are coloured yellow, orange, red, and gray, respectively. EGF is coloured pale green. Adapted from Ogiso et al., 2002.

In site 1, side chains of Leu14, Tyr45, Leu69 and Leu98 in domain I of EGFR hydrophobically interact with Met21, Ile23, and Leu26 in the B loop of EGF. Furthermore, several hydrogen bonds are involved in the ligand-receptor interactions. Residues 16-18 of EGFR and residues 31-33 of EGF form a short parallel β sheet and the Gln16 side chain of EGFR hydrogen bonds with the Asn32 side chain of EGF.

In site 2, the Val350 and Phe357 side chains in domain III of EGFR hydrophobically interact with Leu15 and Tyr13, respectively, of EGF. The Asp355 side chain of EGFR makes a salt bridge with the Arg41 side chain of EGF. Furthermore, the long aliphatic portion of the Arg41 (EGF) side chain provides Van der Waals contacts with the Tyr13 (EGF) and Phe357 (EGFR) side chains.

In site 3, the side chains of Leu382, Phe412 and Ile438 (EGFR) are involved in hydrophobic interactions with that of Leu47 (EGF). The Gln384 side chain of EGFR hydrogen bonds with the main chain carbonyl and amide groups of Gln43 and Arg45, respectively, of EGF (Jorissen et al., 2002; Ogiso et al., 2002).

2.3. Receptor dimerization

The structure of the ectodomains of EGFR presents two distinct conformations: a closed, inactive conformation (tethered) and an open, active conformation (untethered). In the closed conformation, domains II and IV interact at the intermolecular level, thus preventing domains I and III from interacting with their cognate ligand (Cho and Leahy, 2002; Garrett et al., 2002). Both the open and closed conformations remain in equilibrium (Dawason et al., 2005). The open conformation is facilitated by the moving away of domains II and IV, thereby enabling domains I and III to expose their ligand-binding pocket and interact with their corresponding ligand. As a result, the dimerization arm in domain II then interacts with an identical dimerization arm of another receptor molecule to form a dimer (Figure 8) (Ferguson et al., 2003; Ogiso et al., 2002). The closed conformation is favored in the absence of a ligand. However, the binding of a ligand shifts the equilibrium and stabilizes the open conformation, further enabling the accumulation of active dimers and maintaining active receptor signalling (Dawson et al., 2005).

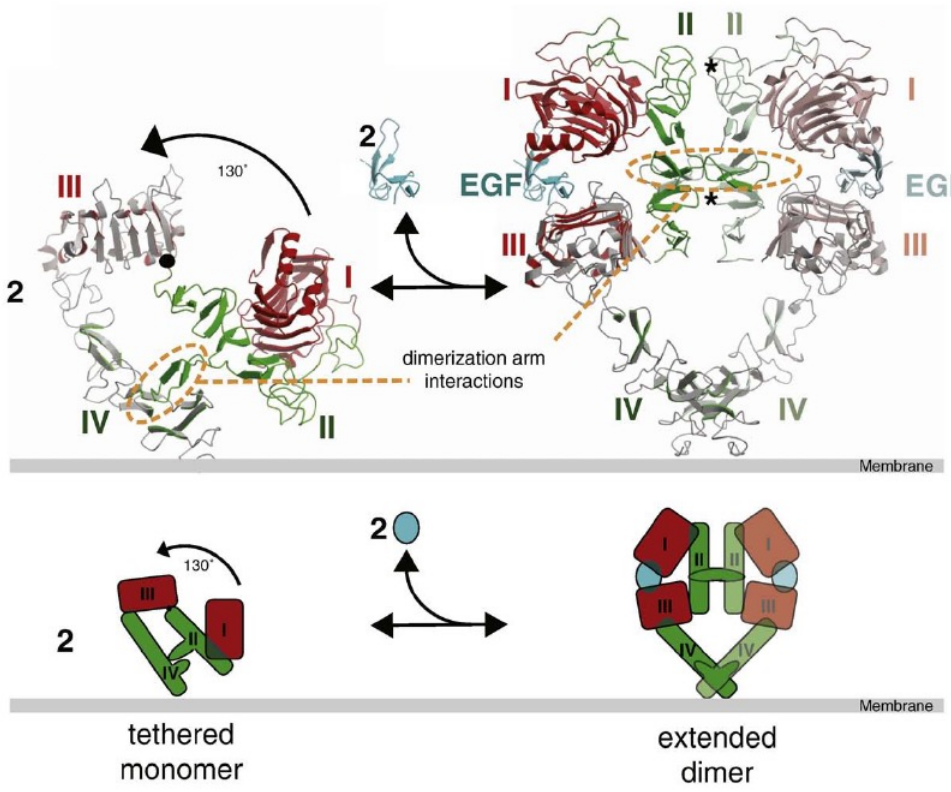

Figure 8. Model for EGF-induced dimerization of the EGFR extracellular region. The top panel shows ribbon representations of extracellular EGFR regions (sEGFR) structures with- and without bound EGF. The left-hand structure shows the domain II/IV tether (ringed with orange oval) that occludes the dimerization arm. EGF binding to this structure induces a conformational change that causes EGFR to adopt the extended conformation, in which the dimerization arm is exposed to drive dimerization as shown in the right-hand panel. Dimerization arm contacts at the dimer interface are ringed with an orange oval. Domains I and III are colored red and red/grey respectively. Domains II and IV are colored green and green/grey respectively. EGF is cyan. The lower panel shows a cartoon representation of this dimerization reaction, with each domain presented as a red or green rectangle. Extracted from Lemmon, 2008.

2.4. Activation of EGFR signaling pathways

The dimerization of HER receptors leads to auto or transphosphorylation of the tyrosine-kinase on specific residues on the cytoplasmic domains. These phosphorylation sites bind adapter proteins and other signaling molecules that possess SH2 (Src-homology domain 2) or PTB (phospho-tyrosine binding) motifs. Several of the phosphorylated tyrosine residues can bind unique effectors and each EGFR ligand is likely to stimulate EGFR phosphorylation at a unique subset of tyrosine residues (Olayioye et al. 2000). Thus, EGFR agonists typically stimulate EGFR coupling to multiple effectors that then activate multiple intracellular pathways including Ras, MAPK, Src, STAT 3/5, phospholipase Cγ (PLCγ), protein kinase C (PKC), and phosphatidyl inositol 3-kinase (PI3K), which lead to different cellular outcomes such as apoptosis, cell survival, migration, growth, adhesion or differentiation (Yarden and Sliwkowski, 2001; Zahnow 2006). The specific docking sites for the mentioned interaction partners could be mapped and are presented together with major pathways of EGFR signalling in Figure 9. Some tyrosine residues are not autophosphorylated by the receptor pair after ligand binding, but are phosphorylated by the c-Src kinases. C-Src-mediated phosphorylation is involved in regulation of receptor function (Biscardi et al., 1999; Jorissen et al., 2003).

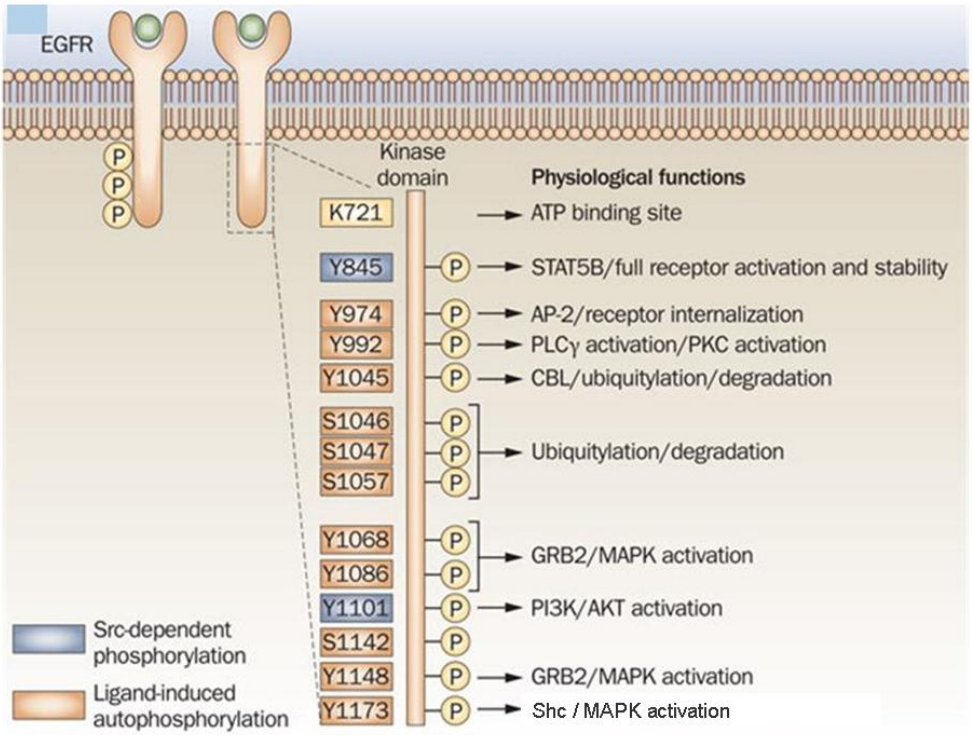

Figure 9. Ligand binding to EGFR causes receptor homodimerization or heterodimerization, which leads to transphosphorylation of the cytoplasmic tail tyrosine residues. Lysine 721 (K721) is the critical site for ATP-binding and kinase activity of EGFR (shown in yellow). Tyrosine phosphorylation in the C-terminus includes Y974, Y992, Y1045, Y1068, Y1086, Y1148 and Y1173 (shown in orange), or Src family kinases (SFKs) can phosphorylate Y845 and Y1101 (shown in blue). Reported biological effects of phosphorylation of each tyrosine are noted (adapted from Wheeler et al., 2010).

2.5. Internalization and endosomal sorting of EGFR

EGFR signaling is primarily attenuated through a highly regulated process of internalization, ubiquitination and lysosomal degradation of the receptor-ligand complex, that results in the transient downregulation of EGFR. In resting cells, a large proportion of EGFR is localized in plasma membrane microdomains termed caveolae, which are lipid rafts enriched in caveolin proteins, glycosphingolipids, and cholesterol.

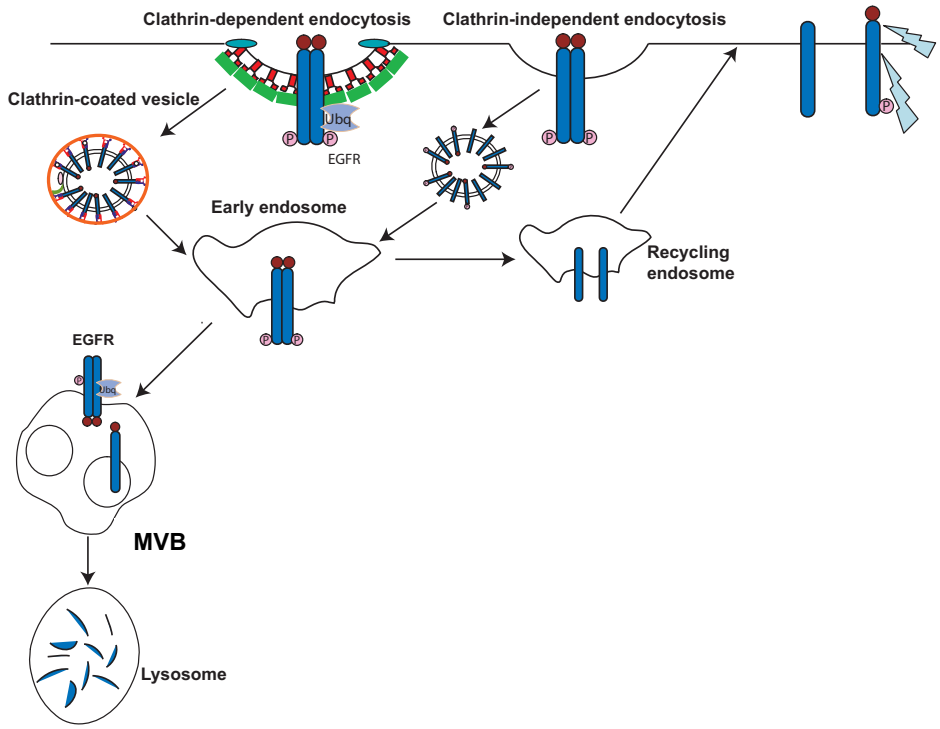

Figure 10. Endocytosis of ligand-activated EGFR molecules. Upon ligand binding, cell surface EGFR may use different routes for entering the cell, clathrin-mediated and clathrin-independent endocytosis. CBL binds to phosphorylated tyrosine residue 1045 and induces receptor ubiquitylation, which is required for receptor sorting by the endocytotic machinery in both early endosomes and the multivesicular body (MVB). Ligand-dissociation in the mildly acidic pH of early endosomes and receptor de-ubiquitylation by de-ubiquitylating enzymes (DUBs) can lead to receptor recycling. Alternately, receptors are sorted from early endosomes to the luminal vesicles in the MVB leading to lysosomal EGFR receptor degradation. Adapted from Mills IG, 2012.

Activated EGFRs migrate from caveole and are sorted into clathrin-coated vesicles; although some EGFR-signaling and non-clathrin-mediated internalization may also occur in caveolae. Then, activated EGFR directly (via phosphorylation of tyrosine residue 1045 or serine residues 1046/47) or indirectly (via GRB2) recruits the ubiquitin ligase CBL (Levkowitz et al., 1999; Theroux et al., 1992), which attaches ubiquitin monomers as well as oligomers to lysine residues of the receptor, thereby tagging the receptor for internalization. Ubiquitylated EGFR is sorted by a set of ubiquitin-interacting motif (UIM) containing adaptors at the early endosome and later into the

luminal vesicles of the MVB (a prelysosomal compartment) leading to lysosomal EGFR receptor degradation (Amit et al., 2004). In some cases, such as low ligand binding affinity to the receptor, EGFR can be recycled back to the plasma membrane after ligand-dissociation in the acidic pH of early endosomes and receptor de-ubiquitylation by de-ubiquitylating enzymes (DUBs) (Sorkin et al., 2008; Köstler et al., 2010; Madshus and Stang, 2009). The receptor endocytosis is represented in Figure 10.

2.6. EGFR nuclear localization

Nuclear localization of EGFR was first reported in regenerating hepatocytes and in primary adrenocortical carcinomas more than two decades ago (Kamio et al., 1990; Marti *et al.*, 1991). Nuclear localization of EGFR was further detected in other cell types and tissues, such as mouse uterus, developing mouse embryos, rat liver, placentas, thyroids, and immortalized epithelial cells of ovary and kidney origins (Lin et al., 2001; Marti et al., 2001). High levels of EGFR were also found in the nuclei of many tumors, including those of skin, breast, bladder, cervix, adrenocortical carcinoma, thyroid, and oral cavity (Kamio *et al.*, 1990; Lin *et al.*, 2001; Lipponen and Eskelinen, 1994; Lo *et al.*, 2005; Marti *et al.*, 2001; Psyrri *et al.*, 2005). Nuclear EGFR is likely to be the phosphorylated form, as shown by a number of studies (Cao et al., 1995; Cordero et al., 2002; Dittmann *et al.*, 2005; Lin et al., 2001; Lo et al., 2005). Furthermore, EGF was reported to also be present in the nucleus (Lin et al., 2001). Although nuclear localization was already well documented, the trafficking mechanism from the cytoplasmic membrane to the nucleus has been elucidated recently. Accumulating evidence suggests a novel pathway where activated EGFR is internalized and redistributed to the Golgi where undergoes COPI-mediated retrograde trafficking to the endoplasmic reticulum (ER) (Wang et al., 2010). Once at the ER, it interacts with the Sec61 translocon mediating receptor retrotranslocation to the cytoplasm (Liao and Carpenter, 2007). In the cytoplasm, the EGFR interacts with importin β via its nuclear

localization signals (NLS) identified in three distinct clusters near the juxtamembrane region (Han et al., 2012).

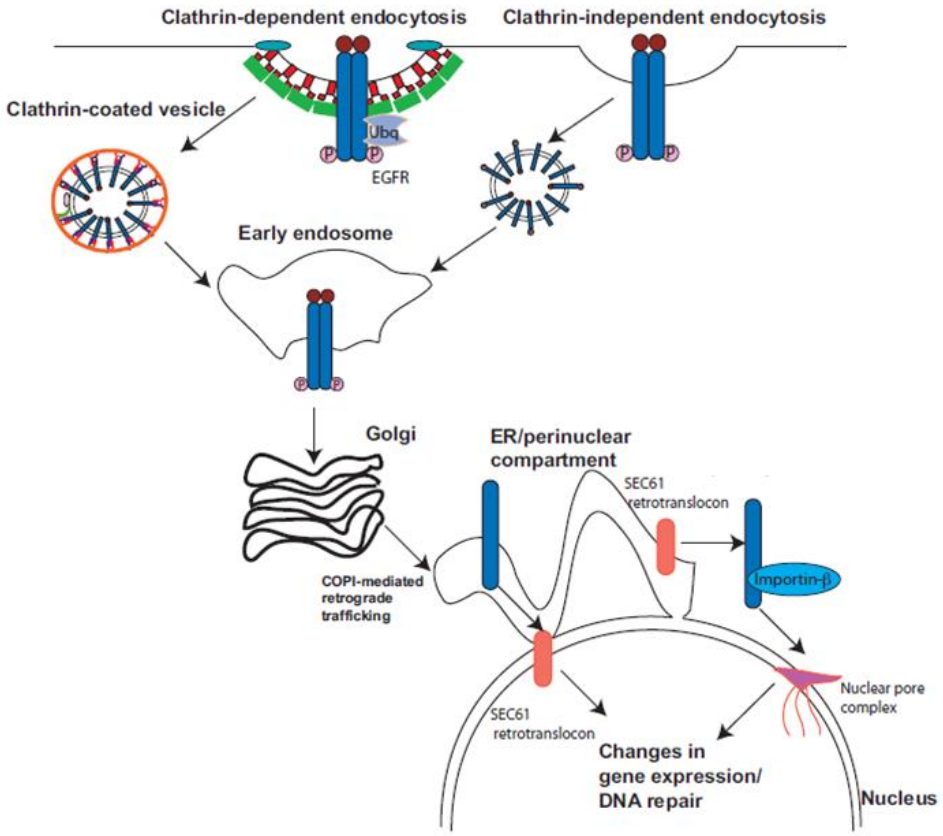

Figure 11. Trafficking of EGFR and routes for nuclear import. The diagram depicts clathrin-dependent and -independent endocytosis of the EGFR highlighting the role of the early endosome as a sub compartment from which retrograde trafficking to the nucleus can occur via the Golgi and endoplasmic reticulum (ER). Once in ER it is believed that the SEC61 retrotranslocon plays a role in expunging EGFR into the cytoplasm, allowing importin-beta to gain access to nuclear localisation signals believed to exist within the receptor. Then occurs the active uptake into the nucleus through the nuclear pore complex. Recently there has also been a suggestion that the SEC61 retrotranslocon is associated within the inner nuclear membrane and can provide a contiguous route for delivering EGFR from the endoplasmic reticulum into the nucleoplasm. Adapted from Mills, 2012.

EGFR transportation to the nucleus is thought to also require chaperones such HSP70 and occurs as a pre-step to active uptake into the nucleus through the nuclear pore complex (NPC) (Hsu and Hung, 2007; Wang et al., 2010) (Figure 11).

Regarding the functions of nuclear EGFR, evidence to date indicates three major roles of EGFR in the cell nucleus: (1) gene regulation, (2) kinase function leading to tyrosine phosphorylation of target proteins, and (3) protein-protein interactions leading to DNA repair (Dittmann et al., 2005; Mills, 2012; Brand et al., 2011). As a transcription co-factor with a functional transactivation domain, nuclear EGFR activates expression of a number of genes, including cyclin D1 (Lin et al., 2001; Brand et al., 2011), inducible nitric oxide synthase (iNOS) (Lo et al., 2005), B-Myb (Hanada et al., 2006), aurora A (Hung et al., 2008), and cyclooxygenase-2 (COX-2) (Lo et al., 2010). Consistent with the fact that EGFR lacks a DNA-binding domain, nuclear EGFR interacts with DNA-binding transcription factors to activate gene transcription. In this context, nuclear EGFR cooperates with signal transducer and activator of transcription-3 (STAT3) to upregulate expression of iNOS and COX-2 genes, with E2F1 to activate B-Myb gene expression, and with STAT5 to enhance aurora A gene expression. In addition to transcriptional regulation, nuclear EGFR retains its tyrosine kinase activity and phosphorylates proliferating cell nuclear antigen (PCNA) to promote cell proliferation and DNA repair (Wang et al., 2006; Brand et al., 2011). Chromatin-bound PCNA protein is phosphorylated on the Tyr211 amino acid residue by nuclear EGFR, leading to increased PCNA stability. This important finding raised the possibility that additional nuclear proteins may be phosphorylated by nuclear EGFR and their functions, stability, and/or subcellular localization altered as a consequence of tyrosine phosphorylation. Furthermore, nuclear EGFR also plays a role in DNA repair following radiation therapy (Dittmann et al., 2005; Mills, 2012).

3. EGFR in cancer

3.1. EGFR signaling network in human cancers

Activation of EGFR initiates intracellular signaling, which results in a range of effects including cell proliferation, differentiation, migration, adhesion, and apoptosis

regulation, all of which are often dysregulated in tumor cells. The discovery that perturbations in the EGFR signaling pathway might contribute to malignant transformation was initially made in the early 1980s in studies that demonstrated that the EGFR is the cellular homolog of the avian erythroblastosis virus v-erbB oncogene, which encodes a truncated protein, that retains the trans-membrane domain and the domain involved in stimulating cell proliferation (De Larco et al., 1980; Downward et al., 1984). Abnormalities in EGFR functions are associated with all key features of cancer development and growth, including autonomous cell proliferation, invasion, angiogenic and metastatic potential (Yarden and Sliwkowski, 2001).

Aberrant EGFR signaling can be initiated by different events. For instance, high levels of EGFR expression are a common feature of the malignant phenotype in many solid human tumors, including those of the head and neck, renal, lung, breast, colon, ovarian, prostate, glioma, pancreas and bladder (Herbst and Shin, 2002; Salomon et al., 1995). In many cases, the number of EGFRs expressed in malignant cells is greater than that expressed in normal cells; for example, up to 2 million EGFRs per cell were reported in breast carcinoma (Filmus et al., 1985; Herbst et al., 2002) compared to 40-100000 receptors per normal cell (Carpenter and Cohen, 1979). In Table 1 the observed percentages of tumors overexpressing EGFR in various types of cancer are listed.

In addition, mutations in the EGFR are observed in some tumors; the most common mutant is EGFRvIII, which lacks an external ligand-binding domain and has a persistent, although attenuated, tyrosine kinase activity. EGFRvIII is commonly overexpress as a result of gene amplification and has been identified in many different tumors such as, brain, lung, breast, prostate, and stomach cancers (Yewale et al., 2013; Baselga, 2002).

Table 1. EGFR overexpression in different tumor types. Table adapted from Herbst et al., 2002.

Tumor type	Percentage of tumors overexpressing EGFR
Colon	**25-77%**
Head and neck	**80-100%**
Pancreatic	**30-50%**
Non-small cell lung carcinoma (NSCLC)	**40-80%**
Breast	**14-91%**
Renal carcinoma	**50-90%**
Ovarian	**35-70%**
Glioma	**40-63%**
Bladder	**31-48%**

Moreover, alterations in the dimerization process, activation of autocrine growth factor loops, limited or enhanced endocytosis of activated receptor, deficiency of specific phosphatases deactivating the phosphorylated EGFR tyrosine residues, and limited turnover are other possible described mechanisms for EGFR pathway deregulation (Sebastian et al., 2006).

3.2. EGFR-targeted therapies

The concept of targeting EGFR as a cancer therapy was initially proposed by Sato et al. (1983) over 30 years ago when they observed that a monoclonal antibody against EGFR led to the inhibition of A431 epidermal carcinoma cell proliferation. Since then, several approaches have been developed that target and interfere with EGFR-mediated effects. The most promising and widely use agents are monoclonal antibodies (mAbs) and small-molecule tyrosine kinase inhibitors (TKIs). There are different mAbs and small-molecule TKIs currently in clinical use for targeting EGFR in various human malignancies. They share the same target but display different mechanisms of action and different specificity for the EGFR. mAbs bind to the extracellular domain of EGFR and compete with endogenous ligands to block the ligand-induced EGFR tyrosine kinase activation by blocking the ligand-binding region.

Small-molecule TKIs compete reversibly with adenosine 5' triphosphate to bind to the intracellular catalytic domain of EGFR tyrosine kinase and inhibit the EGFR autophosphorylation and downstream signaling (Yewale et al., 2013). Although the results are encouraging, there is still a need for the development of novel and more efficient therapies, because many patients are either not sensitive to current drugs/antibodies or develop resistance after a few months of treatment (Carrión-Salip et al., 2012; Yotsumoto et al., 2009; Révillion et al., 2008).

Recently, many other agents like peptides, nanobodies, affibodie (small proteins engineered to bind to an specific target protein), antisense oligonucleotide and others based on binding toxins to molecules to specifically transport toxins to cancer cells have also shown better efficacy in targeting and inhibiting EGFR (Cai et al., 2010; Herbst, 2001; Yewale et al., 2014). Table 2 describes the different strategies and therapies currently in clinical use and also the new strategies.

Table 2. Different types of agent targeting EGFR and their mechanism of action. Adapted from Yewale et al., 2013.

EGFR targeting strategies	Mechanism of action	Examples
Monoclonal Antibodies	Bind to the extracellular domain of EGFR and compete with endogenous ligands to block the ligand-induced EGFR tyrosine activation by blocking the ligand-binding region.	Cetuximab, Panitumumab
Tyrosine Kinase Inhibitors (TKIs)	Compete reversibly with adenosine 5' triphosphate to bind to the intracellular catalytic domain of EGFR tyrosine kinase and inhibit the EGFR autophosphorylation and downstream signaling.	Gefitinib, Erlotinib, Lapatinib, Canertinib
Antibody Based Immunoconjugates	Improves the therapeutic window of chemotherapeutic agents or render the drug inactive (act as prodrug) by altering their in vivo distribution due to conjugation with tumor-targeting monoclonal antibodies.	EQ75-ADR
Antisense oligonucleotides	Decrease the expression of EGFR and regulates the cell proliferation for potential anti-cancer therapy.	GEM 231
Other Novel Agents	Interference with binding mechanism of EGF to its receptor due to structural similarity or having high binding affinity towards EGFR makes them suitable targeting moieties for the delivery of cancer therapeutics.	FR18, Affibodies, Nanobodies, Peptides

4. Potato carboxypeptidase inhibitor: an EGF peptide mimetic with EGFR blocking activity

About two decades ago, our group described the Potato Carboxypeptidase Inhibitor (PCI) as a novel agent against EGFR. Potato carboxypeptidase inhibitor (PCI) is a 39 residue globular protein that competitively inhibits several metallocarboxypeptidases (Hass and Ryan, 1981). It has a 27 residue central core with 3 disulfide bridges that forms a T-Knot scaffold, also found in serine protease inhibitors and in the epidermal growth factor (EGF) superfamily of growth factors (Mas et al., 1998). PCI biological function is the inhibition of insect digestive metallocarboxypeptidases as part of the defense system of the potato plant against insects attack (Hass and Ryan, 1981).

Our studies demonstrated that PCI is structurally similar to EGF (peptide mimetic), and binds to EGFR, interfering with the signaling pathway.

PCI demonstrated anti-tumoral properties (Billings et al., 1989), that were related to their structural similarity to EGF (Figure 12) (Mas et al 1998). Blanco-Aparicio et al. (1998) reported that PCI acts as a competitor of EGF for binding to EGFR, thus inhibiting EGF-induced EGFR activation and cell proliferation. Importantly, PCI was shown to suppress the growth of several human pancreatic adenocarcinoma cell lines, both in vitro and in nude mice (Blanco-Aparicio et al. 1998). Unfortunately, affinity of PCI for EGFR is very low and high concentrations where required to achieve the desired inhibitory activity (Blanco-Aparicio et al. 1998).

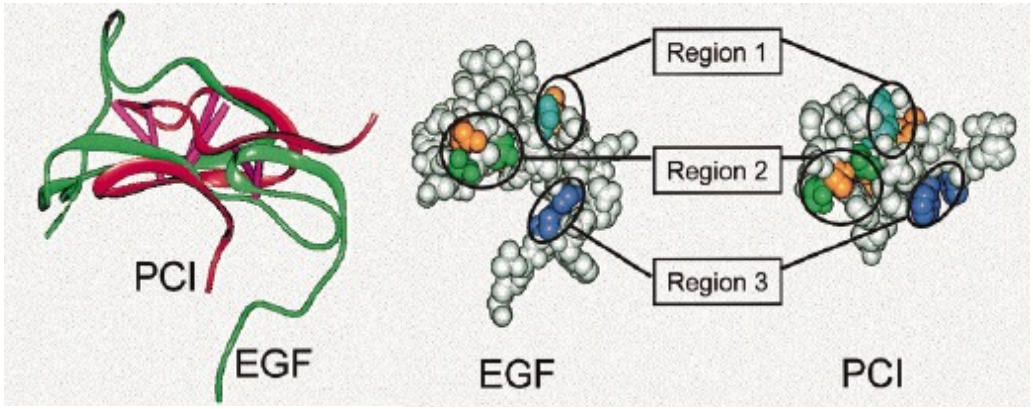

Figure 12. Structural comparison between EGF and PCI structures. EGF and PCI are superimposed by their disulphide-bridge topology and displayed using van der Waals surfaces and ribbon-like representations. In the van der Waals surface representation (right), several residues have been coloured according to their physicochemical properties using the following code: magenta for aromatic, green for polar, blue for basic and orange for non-polar residues. The ribbon-like representations (left) superimpose the α-carbon chains of the PCI (red) and EGF (green). Three regions showing conservative similarities have been encircled. The separation between equivalent residues in both structures is less than 0.7 Å, on average. Adapted from Mas et al., 1998.

The superimposition of the three-dimensional structures of EGF and PCI based on disulfide bridge topology (Figure 12) revealed that PCI lacks the C-terminal part of EGF, one of the important sites described for interaction with domain III of the receptor, which explains the low affinity for EGFR but also the anti-proliferative properties of PCI since EGFR needs a ligand that binds with high affinity to both domains I and III to activate the intracellular signaling pathway that promotes cell division (Ferguson et al., 2003; Dawson et al., 2005).

The structural and clinical interest of PCI opened the possibility of engineering new PCI-like EGF antagonists with improved EGFR affinity. Our group decided to develop this idea following an approach based on the removal of the C-terminal part of human EGF in order to preserve the EGF high affinity for the receptor and the anti-tumour properties of PCI. First, several EGF derivatives were generated from human EGF by

proteolytic procedures after producing EGF in vitro (Ferrer, 2007). The EGF derivatives obtained by this methodology were a mixture of peptides lacking between 5 and 8 amino acids of the C-terminal part of wild type EGF. In vitro experiments demonstrated that these EGF derivatives were less active than wild type EGF to induce EGFR phosphorylation, dimerization, internalization and cell proliferation (Ferrer, 2007). Despite these positive antitumor properties, this strategy provided low concentration of pure EGF derivatives, therefore new methodologies to produce EGF analogues had to be explored.

5. Targeted radiotherapy and molecular imaging

A promising strategy for treating malignancies is targeted delivery of toxins to cancer cells. In this approach, different molecules (mAbs, small molecules, peptide mimetics, and antisense oligonucleotides) that recognize specific or overexpressed tumor components are used as targeting vehicles to deliver into cancer cells therapeutic moieties such as toxins, cytotoxic chemicals, radionuclides, agents blocking gene expression and lytic viruses, chosen for its ability to induce cell death (Brumlik et al., 2008). When the cytotoxic moiety consists of a radionuclide the therapeutic approach is called targeted radiotherapy. In this approach, monoclonal antibodies (mAbs) that recognize tumor-associated antigens or peptide ligands that specifically bind to cell-surface receptors may be used as targeting vehicles to selectively deliver radionuclides to cancer cells for in situ radiation therapy. These two approaches are known as radioimmunotherapy (RIT) or peptide-directed radiotherapy (PDRT), respectively. RIT or PDRT approaches can be also employed for imaging metastatic deposits in order to detect or to non-invasively characterize their phenotype in situ, which is known as molecular imaging. Phenotypic characterization of tumors is nowadays extremely critical to appropriately select patients for treatment with new biologically targeted

anticancer agents, including targeted radiotherapeutics (Abrams et al., 2000; Reilly, 2010).

Radionuclides suitable for targeted *in situ* radiotherapy emit either α–particles (^{213}Bi, ^{225}Ac and ^{211}At), β-particles (^{131}I, ^{186}Re, ^{188}Re, ^{90}Y, ^{64}Cu, and ^{177}Lu), or Auger and conversion electrons (^{125}I, ^{123}I, ^{111}In, and ^{67}Ga) (Reilly, 2010). α-emitters are radionuclides having a proton-to-neutron ratio that exceeds that for stable elements of similar atomic number. Thus in order to reduce the repulsive forces between the positively charged protons, α–particles (consisting of two protons and two neutrons with a 2+ charge) are emitted, which brings the radionuclide to a more stable configuration. In β-particle decay, the radionuclide either carries excess protons or neutrons. In a neutron-excessive radionuclide, neutrons are converted into protons and a β- particle and antineutrino are emitted. However, in a proton excessive radionuclide, protons are converted into neutrons and a β+ particle (positron) and neutrino are emitted. After the emission of beta particles the radionuclide becomes more stable. Generally, in targeted radiotherapy, the most interesting emission is β-decay and not β+ (positron) decay, which is used mainly for PET imaging. For Auger electrons, the radionuclide decays by electron capture (EC). In EC, a proton in the nucleus captures an electron from an inner orbital shell, creating a vacancy in the shell. This vacancy is filled by the decay of an electron from a higher shell. The excess energy released is transferred to an outer orbital electron, which is then ejected from the atom as an Auger electron, creating a 2+ charged nucleus (Khalil MM, 2011; Reilly, 2010).

The important difference between these different forms of radiation is their range in tissue and their linear energy transfer (LET) (Reilly, 2010). The α-particles have the highest LET (100 keV/μm), are densely ionizing, and travel 50-100 μm (5-10 cell diameters) in tissue. α-Emitters are best for eradicating small clusters of cancer cells or micrometastasis (Reilly, 2010). β-Particles have high energy and travel 2-12 mm in

tissues (200-1200 cell diameters). In comparison with α-emitters, the average LET of β-particles is quite low; for instance β-particles emitted by ^{131}I (Eβ=0.6 MeV) have a LET of 0.3 keV/µm over a track length of 2 mm. Moreover, β-particles deposit most of their energy at the end of their track length (Bragg peak). Thus, due to the long range of the β-particle and its small LET, it is possible to kill distant non-targeted tumor or normal cells (cross-fire effect). If these cells are tumor cells, this is advantageous for large lesions i.e. 2-10 mm in diameter in which there is likely to be incomplete targeting of tumor cells by radiolabeled antibodies. However, the cross fire effect contributes to dose-limiting bone marrow toxicity in RIT, due to nonspecific irradiation of the hematopoietic stem cells by circulating radiolabeled antibodies perfusing the marrow (Reilly, 2010). In contrast to high-energy α-emitters (4-9 MeV), Auger electrons have very low energy (<30 keV). As these very low energy Auger electrons travel an extremely short distance in tissue (nm-µm), their LET approaches that of α-emitters (100 keV/µm) (Reilly, 2010). The advantage of the Auger electron emitting radionuclide when it is conjugated to a peptide or mAb is that its cytotoxicity is restricted to those cells in which binding and internalization occurs (due to the short range and the requirement to cause lethal DNA damage) (Martin, 1979; McLean, 1989). Moreover, in contrast to β-emitters, Auger electrons lack the “cross-fire effect”, thus causing the minimum damage to normal tissue Auger electrons are, therefore more useful for treating small tumor deposits or micrometastases for which delivery of radiolabeled antibodies or peptides is more homogeneous (Reilly, 2010).

5.1. EGFR-targeted auger-electron radiotherapy

Auger electron emitting radionuclides such as ^{125}I and ^{111}In, represent an appealing alternative to α and β- emitters for targeted radiotherapy of cancer (Adelstein, 1993). Many different molecular targets overexpressed by cancer cells have been exploited for Auger electron radiotherapy using mAbs and peptides as well as small molecules labeled with ^{111}In, ^{99}mTc, ^{123}I or ^{125}I (Jackson et al., 2013; Kassis, 2003).

Nuclear translocation of EGF/EGFR could be used for the design of novel targeted radiotherapeutics for tumor cells overexpressing EGFR, especially those incorporating subcellular-range Auger electron emitters such as 111In, since these are particularly damaging to DNA when they decay in close proximity to the cell nucleus (Kassis, 2003). The laboratory of Molecular Imaging and Targeted Radiotherapy of the professor Raymond Reilly at the University of Toronto has exploited the nuclear translocation of EGF/ EGFR for the treatment of Breast Cancer (BC) using 111In-labeled diethylenetriaminepentaacetic acid human epidermal growth factor (^{111}In-DTPA-hEGF) (Reilly et al., 2004; Reilly et al., 2000; Chen et al., 2003). ^{111}In-DTPA-hEGF was highly radiotoxic to MDA-MB-468 human BC cells (1×10^6 receptors/cell), reducing their surviving fraction in vitro to <3% at only 111–148 mBq/cell (3–4 pCi/cell) (Reilly et al., 2000). Treatment of athymic mice with five weekly doses of ^{111}In-DTPA-hEGF (a total of 92.5 MBq (17 μg)) slowed the growth of established subcutaneous MDA-MB-468 tumor xenografts threefold and caused the regression of small non-established tumors (Chen et al., 2003). Paradoxically, ^{111}In-DTPA-hEGF did not cause toxicity to the liver and kidneys, which express moderate to high levels of EGFR (approximately 10^5 receptors/cell) (Dunn et al., 1984), even at doses as high as 2220 MBq/kg (Reilly et al., 2006). One possible explanation for the ability of ^{111}In-DTPA-hEGF to kill tumor cells that overexpress EGFR but for its lack of toxicity towards normal tissues may be that it is imported more efficiently into the nucleus of BC cells, resulting in greater deposition of lethal doses of radiation. This could provide a second level of discrimination of ^{111}In-DTPA-hEGF for tumor cells compared to normal cells, in addition to their higher EGFR density.

Although ^{111}In-DTPA-hEGF demonstrated an interesting antiproliferative activity in tumors overexpressing EGFR, since the EGFR pathway is activated following ^{111}In-DTPA-hEGF binding, it may generate different common adverse events in the patients that include flushing, chills, nausea, and vomiting as well as transient hypotension as a

consequence of EGFR pathway activation (Vallis, et al., 2014). Thus it is important to develop new radioconjugates containing a peptide moiety that do not self-activate the EGFR physiological response in order to avoid undesirable side effects.

OBJECTIVES

The aim of this thesis work was to develop a novel strategy to kill cancer cells based on the EGFR pathway, which is one of the most validated target for cancer chemotherapy in different tumors. Our first objective was to produce an EGF peptide mimetic, specifically a shorter form of EGF (EGFt), as a potential EGFR blocker displaying receptor binding affinity without stimulating the EGFR proliferation signaling. The lack of EGFR-mediated growth-stimulatory activity would make EGFt a promising delivery agent to target toxins to tumours over-expressing EGFR. Thus, our second objective was to explore the EGFt analogue to deliver the radiotherapeutic ^{111}In into cancer cells and evaluate their cytotoxic activity.

To achieve these global objectives, seven specific objectives were defined:

1. To produce a recombinant human EGF (hEGF) and the corresponding shorter mimetic (EGFt) by cloning and expressing them in a bacterial extracellular expression system
2. To purify and characterize the recombinant peptides (EGFt and hEGF).
3. To analyse the affinity of EGFt for EGFR and its effect on EGFR ligand binding, dimerization, trans-phosphorylation and internalization in comparison to wild type EGF.
4. To study the effect of EGFt on cancer cell proliferation.
5. To conjugate EGFt with the radioisotope 111-Indium (^{111}In-DTPA-EGFt) and analyse its cellular uptake and distribution.
6. To analyse the *in vitro* cytotoxic activity of ^{111}In-DTPA-EGFt and compare it with that displayed by^{111}In-DTPA-hEGF.
7. To investigate the *in vivo* biodistribution and pharmacokinetics of ^{111}In-DTPA-EGFt *and* ^{111}In-DTPA-hEGF.

METHODS

1. Production of the recombinant human EGF and its truncated derivative EGFt

1.1. Molecular cloning and expression of hEGF and EGFt on small batch culture conditions.

hEGF and EGFt encoding sequences were synthesised by GenScript. The sequences included the *ompA* leader sequence and the enzyme restriction site *XbaI* on the 5' end of the encoding sequences. Next, the sequences were digested with the *XbaI* and *BamhI* restriction enzymes and ligated to the expression vector pIN-III-ompA-2 (Ghrayeb et al., 1984) using T4 DNA ligase (New England Biolabs, Ipswick, MA, USA). The constructed plasmids, ompA_hEGF and ompA_EGFt, were transformed into *E. coli* MC1061 (kindly donated by Dr. Querol, Autonomous University of Barcelona, Spain). The positive clones were identified by diagnostic restriction enzyme digestion and then sequenced to confirm the correct hEGF and EGFt cloning (ABI PRISM 310 Genetic Analyzer, Life Technologies, Carlsbad, CA, USA). *E.coli* MC1061 cells containing ompA_hEGF or ompA_EGFt plasmids were grown at 37ºC in 400 ml culture of M9 minimal medium supplemented with casamino acids (M9 CAS) and with 50 μg/ml ampicillin (Sigma-Aldrich, St.Louis MO, USA). After induction with 0.2 mM isopropyl β-D-thiogalactopyranoside (IPTG) (Sigma-Aldrich) cells were incubated for 24 hours. Next, to determine the presence of the peptides in the extracellular fraction, the culture were harvested by centrifugation at 15,000 × g for 15 min and immediately subjected to cellular fractionation to obtain the different fractions of the culture (Ferrer-Soler et al., 2003).

1.2. Production of hEGF and EGFt in a 10 liter fermentor

OmpA_hEGF or ompA_EGFt MC1061 *E.coli* positive colonies were added into a 100 mL Luria-Bertani medium (LB) supplemented with 50 µg/ ml ampicillin. The culture was grown at 37ºC in a rotary shaker (250 rpm) for a minimum of 5 hours. Then, 5 mL of the culture were inoculated into a flask with 300 mL M9 CAS medium supplemented with 50 µg/ mL ampicillin and grown at 37ºC, over night, in a rotary shaker (250 rpm). The entire 300 mL grown culture was inoculated in 5000 mL of the same medium in a 10-L fermentor. The temperature was maintained at 37ºC, the partial pressure of O_2 at 65% and the pH at 7. The culture was continuously fed from the 2 early hours of the fermentation to the 6 hours with 50% of casamino acids and glycerol. 1-2 hours later M9 salts (33% of the total volume) and 0.4 mM of IPTG were added into the cell culture. After that, the culture was continuously fed with M9 salts, oligoelements, and the other 50% of casaminoacids and glycerol, overnight. 24 hours later the culture medium was collected. The fermentation was carried out by the Fermentation Service of the University of Barcelona using a Biostat B 10L laboratory fermenter (Sartorius Stedim, Goettingen, Germany).

1.3. Protein purification

The culture medium obtained either by flask or by fermentation was centrifuged at 10000 x *g* and 4 ºC for 30 min, twice. The supernatant corresponding to the extracellular medium was then filtered through 0.4 and 0.2 µm membranes, successively, and concentrated by tangential flow filtration using a 3000-Da membrane (Merk-Millipore, Billerica, MA, USA). The concentrated sample was then dialysed against 50 mM Tris-HCl pH 7.5 (solvent A) to subsequently perform HPLC (ÄKTAbasic) (GE Healthcare Bio-Sciences, Little Chalfont, UK) using an anionic-exchange column (HiPrep DEAE FF 16/10 from GE Healthcare Bio-Sciences). The flow rate was 1 ml/min and the elution buffer (solvent B) was: 50 mM Tris-HCl, 1M NaCl at pH 7.5. The samples were eluted with a linear gradient from 0-10% solvent B for 40

min, 10-30% for 80 min and 30-50% for 40 min. Samples containing the recombinant protein were eluted and collected after 60 min of elution and lyophilised. In the last purification step, the sample was dissolved with elution buffer (50mM Tris-HCl, 200mM NaCl at pH 8) and then separated by a gel-filtration HPLC chromatography column (GE Healthcare Bio-Sciences) at a flow rate of 1.2 ml/min. The recombinant proteins were eluted after about 13 min of elution time.

1.4. Protein analysis

The presence of hEGF or EGFt in each production step was determined on a 16% sodium dodecylsulfate–polyacrylamide gel electrophoresis (SDS-PAGE). A commercial recombinant hEGF (Merk-Millipore) was loaded in the gel as a positive control. The gel was stained with Coomassie brilliant blue or analyzed by Western blotting using a primary rabbit polyclonal antibody against human EGF (Z-12) (sc-275) (Santa Cruz Biotechnology, Dallas, TX, USA) and a secondary antibody coupled to horseradish peroxidase (Dako, Glostrup, Denmark). The total protein quantity present in the samples was determined by Lowry-based Bio-Rad assay (Bio-Rad Laboratories, Hercules, CA, USA). The identity and purity grade of the proteins were assessed by MALDI-TOF MS and N-terminal amino acid sequencing (Proteomics and Bioinformatics facility from Autonomous University of Barcelona, ProteoRed network). The state of folding of the EGF peptides was analyzed by reverse phased high performance liquid chromatography (RP-HPLC using Vydac 218TP C18 column from Grace, Columbia, MD, USA) using the methodology described by Chang et al. (Chang et al., 1995; Chang et al., 2005) that allows the identification of minute concentrations of non-native disulfide scrambling isomers.

2. In vitro characterization of hEGF and EGFt

2.1. Cells and cell culture

The human colorectal adenocarcinoma cell line Caco-2 and the breast adenocarcinoma cell lines MDA-MB-468 and MCF-7 were obtained from the American Type Culture Collection (Manassas, VA, USA). The cells were maintained in Dulbecco's modified Eagle's medium supplemented with 10% fetal bovine serum (FBS) and 1% penicillin-streptomycin (Life technologies) at 37˚C in a humidified atmosphere containing 5% CO_2. Cell growth and morphology were assessed daily using an inverted microscope. The cells were routinely maintained for up to 8 passages by successive trypsinization and seeding and the cell viability was assessed by trypan blue staining (only cultures displaying >90% viability were used for further work). Possible contamination with Mycoplasma was routinely checked using the VenorH GeM Mycoplasma Dection Kit (Minerva Biolabs, Berlin, Germany).

2.2. Immunofluorescence analysis by flow citometry

The quantification of EGFR expression was performed by flow cytometry. The cells were analyzed by double immuno-fluorescence using a mouse monoclonal antibody against human EGFR (GR13 Anti-EGFR (Ab-3)), (Calbiochem, San Diego, CA, USA). The cells were incubated for 30 min at 4˚C with the primary antibody or an irrelevant antibody as negative control. After washing with phosphate-buffered saline (PBS) (Gibco), the cells were incubated for an additional 30 min at 4˚C in the presence of the Alexa-Fluor 488-conjugated goat anti-mouse IgG antibody (Invitrogen). Next, the fluorescence was analyzed using a FACSCalibur flow cytometer (Becton Dickinson Immunocytometry Systems, Franklin Lakes, NJ, USA) equipped with CellQuest™ software (Becton Dickinson). Fluorescence intensity was represented on a four orders of magnitude log scale (1-10,000). In each experiment 10,000 cells were analyzed.

2.3. Western blot analysis

Cells were collected and lysed with ice-cold lysis buffer containing 20 mM sodium phosphate pH 7.4; 150 mM NaCl; 1% Triton X-100; 5 mM EDTA; 5 mM PMSF; 10 µg/ml aprotinin and leupeptin; 250 µg/ml sodium vanadate (Sigma-Aldrich). Protein concentrations were determined by Lowry-based Bio-Rad assay (Bio-Rad Laboratories). Equal amounts of protein extracts were electrophoresed on an 8% SDS-PAGE gel, transferred to a polyvinylidene difluoride membrane (Millipore) for 3 hours at 100V and then blocked for 1 h at room temperature in a blocking buffer containing 2.5% powdered skim milk in PBS-T (10 mM Tris-HCl, pH 8.0, 150 mM NaCl and 0.05% Tween-20) to prevent non-specific antibody binding. Blots were incubated overnight at 4˚C with the corresponding primary antibody diluted in blocking buffer. After washes with PBS-T, blots were incubated for 1 h with the corresponding secondary antibody coupled to horseradish peroxidase (Dako), and revealed with a commercial kit (West Pico Chemiluminescent Substrate, Pierce Biotechnology). Blots were reprobed with an antibody for β-actin (Santa Cruz Biotechnology) to control the protein loading and transfer.

2.4. Dimerization analysis

Chemical cross-linking experiments were designed to examine the ability of hEGF and EGFt proteins to induce receptor dimerization. The protocol for cross-linking was previously described by Canals F (Canals, 1992). MDA-MB-468 cells were seeded in 100-mm dishes and allowed to grow to 50% confluence. Cells were harvested in 0.4 ml ice-cold lysis buffer (20 mM sodium phosphate pH 7.4; 150 mM NaCl; 1% Triton X-100; 5 mM EDTA and protease and phosphatase inhibitor cocktails (Sigma-Aldrich)). The protein concentration in cell lysates was determined by a Lowry-based Bio-Rad assay (Bio-Rad Laboratories). Aliquots of 10 µg of protein were stimulated with 150 nM hEGF, or 150 nM and 15 µM EGFt, and additionally 150 nM hEGF together with 150 nM EGFt, at room temperature. After 30 min incubation, EGFR cross-linking was

induced by addition of 40 mM glutaraldehyde. 1 min later the reaction was stopped with 0.2 M glycine (pH 9). Next, loading buffer with 5% β-mercaptoethanol was added to the samples and heated for 5 min at 100ºC. The samples were electrophoresed on 5% polyacrylamide gels (SDS-PAGE), transferred onto PVDF membranes at 30V overnight at 4ºC and analysed by Western blotting as described. Rabbit polyclonal antibodies against human EGFR (EGFR (1005) (sc-03)) and against HER2 (Neu (C-18)), (both from Santa Cruz Biotechnology) were used as primary antibodies.

2.5. Analysis of EGFR activation and degradation

The ability of EGFt to activate the total phosphotyrosines of the receptor was determined in MDA-MB-468 cells after treating the cells with 3nM, 150 nM hEGF or 150 nM EGFt for 15 minutes at 37 ºC. Next, the same amount of cell lysates were analyzed in parallel by Western blotting with a mouse monoclonal antibody against total phosphotyrosines conjugated to horseradish peroxidase (PY20) (sc-508 HRP, Santa Cruz Biotechnology) and a primary antibody against EGFR (EGFR 1005) (Santa Cruz Biotechnology). EGFR specific phosphoresidues were examined in MDA-MB-468, MCF-7 and Caco-2 cells after treating the cells with 150 nM hEGFR or EGFt at 37 ºC for different incubation times. Samples were analysed by Western blotting using primary monoclonal antibodies against phospho-EGFR Tyr 1068 (#2236), Tyr 1173 (#4407), Tyr 1045 (#2237) and Ser 1046/47 (#2238) (Cell Signaling Technology, Danvers, MA, USA). MAPK and AKT activation was analyzed with polyclonal antibodies against phosphorylated MAPK (ERK1/2) and phospho-Akt (Thr308), both from New England Biolabs (Beverly, MA).

For the analysis of EGFR degradation Caco-2 and MCF-7 cells were incubated at 37ºC with starvation medium containing 10 µg/mL of cycloheximide (Sigma Aldrich) and 3 nM, 150 nM hEGF or 150 nM EGFt at different times. After treatments, cells were

collected and lysed and the different samples were analysed by Western blotting using the anti-EGFR antibody (EGFR 1005) (Santa Cruz Biotechnology).

2.6. EGFR internalization analysis

The capacity of hEGF and EGFt to induce the internalization of EGFR was determined by a cell-ELISA assay. MCF-7 and Caco-2 cells were seeded in 96-well culture plates (Costar 3596; Corning Inc., Corning, NY, USA) at a density of 4000 and 5000 cells/well, respectively. The cells were allowed to attach and grow until they reached 70% of confluence and then 3 nM hEGF, 150 nM hEGF, 150 nM EGFt, or PBS (control cells) were added. Next, the cells were incubated for 30 min at 4ºC to allow the binding of EGF to its receptor and then 15 min at 37ºC to allow internalization. The cells were subsequently washed with PBS, fixed with 2% formaldehyde for 20 min at room temperature and blocked with 1% BSA in PBS for 1 h at room temperature. After removal of the blocking solution, the plates were incubated for 1 h at room temperature with the anti-hEGFR mouse monoclonal antibody (GR13 (Ab-3)) (Calbiochem). The samples were subsequently washed and incubated for 1 h with a peroxidase-conjugated secondary antibody (Polyclonal Goat Anti-Mouse Immunogulobulins/HRP from Dako). Briefly, the plates were washed with PBS, and 100 µl of 3,3'-5,5'-tetramethyl benzidine (TMB) (Roche, Penzberg, Germany) solution was added to each well according to the manufacturer's directions. The plate was incubated for 5 min at room temperature and then the enzymatic reaction was stopped by the addition of 100 µl of 1 M H_2SO_4. The absorbance at 450nm was measured with a microplate reader (ELx800; BioTek, Winooski, VT, USA). Each experiment, including untreated control cells, was carried out in triplicate and the mean absorbance for each treatment was calculated. The EGFR present on the cell surface was determined as a percentage of untreated control cells by dividing the mean absorbance of the three replicates by the mean absorbance of the untreated control cells.

2.7. Immunofluorescence staining of EGFR and cellular localization analysis by confocal microscopy

MDA-MB-468 cells grown on coverslips were treated with 150 nM of hEGF or EGFt for different time periods and then fixed with freshly prepared 4% para-formaldehyde (Electron Microscopy Sciences, Hatfield, PA, USA) for 12 min at room temperature and mildly permeabilized with PBS containing 0.1% Triton X-100 and 0.1% BSA (Roche) for 3 min at room temperature. Coverslips were then incubated in the same buffer, in which Triton X-100 was omitted, at room temperature for 1 h with the anti-hEGFR monoclonal antibody (GR13 (Ab-3)) (Calbiochem) and a monoclonal antibody against the nuclear membrane marker Lamin-B1 (A-11) (sc-377000) (Santa Cruz Biotechnology). Coverslips were washed intensively, and then incubated with adequate secondary antibodies labelled with Alexa Fluor 488 and Alexa Fluor 555 (Invitrogen), respectively. Both primary and secondary antibody solutions were precleared by centrifugation at 14,000 x *g* for 10 min. Hoechst (Invitrogen, Carlsbad, CA, USA), was incubated together with the secondary antibodies to stain the cell nucleus. Next, the coverslips were mounted in Mowiol mounting medium (Calbiochem, San Diego, CA, USA). The images were obtained using a Leica TCS SPS laser-scanning confocal spectral microscope (Leica Microsystems, Wetzlar, Germany). Final analysis of deconvolved images was performed using ImageJ software (http://rsb.info.nih.gov/ij/).

2.8. Fluorescent staining of hEGF and EGFt and cellular localization analysis by confocal microscopy

Purified hEGF and EGFt were fluorescently labeled with rhodamine B isothiocyanate (RITC; Sigma Aldrich). Briefly, 2 mg of purified peptide was dissolved in 0.5 M sodium bicarbonate buffer (pH 9.2) to a final concentration of 1 mg/ml. RITC was dissolved to a final concentration of 1 mg/ml in distilled water. Then, the protein and the dye were mixed in a 5:1 ratio, and incubated for 3 h at room temperature on a rocker

platform. After incubation, the sample was centrifuged at 2000 x g for 1 min to remove any insoluble material and passed through a PD-10 desalting column (GE Healthcare Bio-Sciences) eluted with distilled water to remove free RITC. The intracellular localization of hEGF and EGFt in MDA-MB-468 human breast cancer cells were evaluated by confocal fluorescence microscopy using either RITC-hEGF or RITC-EGFt and the fluorescent nuclear stain Hoechst (Invitrogen). Briefly, MDA-MB-468 cells grown on coverslips were treated with 200 nM of RITC-hEGF or RITC-EGFt at 4ºC or at 37ºC for up to 3 h. Then, coverslips were washed with phosphate-buffered saline (PBS), fixed with freshly prepared 4% paraformaldehyde (Electron Microscopy Sciences) for 12 min at room temperature and washed again with phosphate buffered saline (PBS). Next, coverslips were incubated with Hoechst for 10 min at 37ºC, washed with PBS and mounted in Mowiol mounting medium from Calbiochem. The images were obtained using a Leica TCS SPS laser-scanning confocal spectral microscope (Leica Microsystems). Final analysis of deconvolved images was performed using ImageJ software.

2.9. Cell proliferation assay

First of all, to determine the optimal initial seeding density, different cell concentrations (1000, 2000, 3000, 4000, 5000, 6000, 7000 and 8000 cells per well) were plated into 96-well plates (6 replicates per cell concentration). The cells were allowed to attach and grow for 72h, starved for 24 h and then treated with the highest concentration of hEGF used in the proliferation assay (150 nM) for 72 h (MCF-7 cells) or 96 h (Caco-2 cells). Finally, the proliferation of the cells was determined by an MTT assay and the main absorbance was represented versus the number of seeded cells.

To assess the ability of hEGF and EGFt to promote cell-growth, Caco-2 and MCF-7 cells were seeded in 96-well plates at the optimal cell seeding concentration that was

previously established for both cell types in order to maintain the cells in an exponential growth phase along the experiment. The cells were allowed to attach and grow for 72h in culture medium, then the cells were washed and medium without FBS was added to the cells for 24 h. Next, the cells were treated with concentrations ranging from 0 to 150 nM of hEGF or EGFt for 96 h for Caco-2 cells and 72 h for MCF-7 cells. The treatments were removed, and the cells were washed with PBS and incubated for 3 h with 100 µl of fresh culture medium together with 10 µl of MTT (3-(4,5-dimethylthiazol-2-yl)-2,5-diphenyltetrazolium bromide) (Sigma-Aldrich). Medium was discarded and dimethyl sulfoxide (DMSO) (Sigma-Aldrich) was added to each well to dissolve the purple formazan crystals. Plates were agitated at room temperature for 10 min and the absorbance of each well was determined with an absorbance microplate reader (ELx800, BioTek) at a wavelength of 570 nm. Three replicates were used for each treatment. The cell viability was determined as a percentage of the untreated control cells, by dividing the mean absorbance of each treatment by the mean absorbance of the untreated cells.

3. Production and in vitro and in vivo characterization of the radiopeptides ^{111}In-DTPA-hEGF and ^{111}In-DTPA-EGFt

3.1. Radiolabeling of EGFt and hEGF with ^{111}In

EGFt and hEGF (from Upstate Biotechnology) were derivatized with diethylenetriamine pentaacetic acid (DTPA) (from Sigma-Aldrich) by reacting with a 10 to 20-fold molar excess of cDTPAA as previously described for hEGF (Reilly et al., 2000). The conjugation efficiency was measured by trace labelling an aliquot of the reaction mixture with ^{111}In acetate (from Nordion, Ottawa, ON, Canada) and analyzing the proportion of ^{111}In-DTPA-EGFt or ^{111}In-DTPA-hEGF and free ^{111}In-DTPA by instant thin layer-silica gel chromatography (ITLC-SG) (from Gelman, Michigan, USA) developed in 100 mM sodium citrate buffer pH 5.0. DTPA substitution (moles

DTPA/mole EGFt or hEGF) was calculated by multiplying the conjugation efficiency by the molar ratio of cDTPAA:EGFt or cDTPAA:hEGF used in the reaction. DTPA-EGFt and DTPA-hEGF were purified on a Bio-Gel P-2 column (BioRad), eluted with phosphate buffered saline (PBS), pH 7.6, and then re-concentrated on a centrifugal filter device (from Millipore). DTPA-hEGF and DTPA-EGFt were labeled with ^{111}In by incubation with ^{111}In acetate for 30 min at room temperature. ^{111}In acetate was prepared by mixing equal volumes of trace metal free 1 M sodium acetate buffer pH 6.0 and ^{111}In chloride. For the internalization and nuclear translocation studies, ^{111}In-DTPA-hEGF and ^{111}In-DTPA-EGFt were labeled to a specific activity of 3.7 MBq/µg. For the *in vitro* cytotoxicity assays the radioconjugates were labeled to a higher specific activity of 10-20 MBq/µg. The radiochemical purity of the radioconjugates in the *in vitro* assays was >95% assessed by ITLC-SG developed in 100 mM sodium citrate buffer pH 5.0. For the *in vivo* studies ^{111}In-DTPA-hEGF and ^{111}In-DTPA-EGFt were labelled to a specific activity of 4 MBq/µg and the radiochemical purity was >98%.

3.2. Receptor binding assay

EGFt was derivatized with DTPA and radiolabeled with ^{111}Indium-acetate to a specific activity of 3.7-18.5 MBq/µg as described. The receptor-binding properties of ^{111}In-labeled EGFt were evaluated in a direct radioligand binding assay using MDA-MB-468 human breast cancer cells (1x10^6 EGFR/cell (Reilly et al., 2000)). Briefly, various concentrations of ^{111}In-labeled EGFt (0.6 nM-300 nM) in 120 µL of 150 mM NaCl containing 0.2% bovine serum albumin (BSA) (Roche) were incubated with 1x10^6 cells in 1.5 mL microtubes for 3h at 4ºC. Cell bound radioactivity was separated from free radioactivity by centrifugation at 2,700 x g for 5 min, and then counted in a γ-scintillation counter (Wizard Model 1480, Perkin Elmer). Non-specific binding was determined by conducting the assay in the presence of an excess (30 µM) of unlabeled EGFt. Specific binding was obtained by subtraction of non-specific binding from total binding. The equilibrium dissociation constant value (K_d) was estimated by nonlinear

regression of a plot of the specific binding versus the concentration of ^{111}In-DTPA-EGFt incubated with the cells using GraphPad Prism software (Motulsky et al., 1995). The K_d value of ^{111}In-DTPA-hEGF was obtained from previous work (Reilly et al., 2000).

3.3. Cellular uptake and intracellular distribution of ^{111}In-DTPA-EGFt and ^{111}In-DTPA-hEGF

The intracellular distribution of ^{111}In-DTPA-EGFt was determined by performing cell fractionation studies with MDA-MB-468 cells. Briefly, $1x10^6$ MDA-MB-468 cells in 100 µL PBS containing 0.2% of bovine serum albumin (BSA) were incubated with 10 µL of radiolabeled peptide, ^{111}In-DTPA-hEGF (2.8 MBq/mL, 15 nM) or ^{111}In-DTPA-EGFt (2.8 MBq/mL, 15 nM) for 3 hours at 37°C. Then, the cells were rinsed with PBS and centrifuged at 1500 x g for 5 min to separate cell-bound radioactivity from free radioactivity. The proportion of internalized ^{111}In-DTPA-EGFt or ^{111}In-DTPA-EGF was determined by displacing cell-surface radioactivity with 200 mM sodium acetate/500mM NaCl pH 2.5 at 4°C. The cytoplasmic and nuclear fractions were isolated using a nuclei isolation kit (Nuclei EZ Prep, NUC-101, Sigma-Aldrich) according to the manufacturer's directions. The surface-bound, cytoplasmic, and nuclear radioactivities were measured using the gamma counter. This procedure has previously been described to result in intact nuclei without contamination by cytoplasmic organelles or fragments of cell membrane (Reilly et al., 2000; Rakowicz-Szulczynska et al., 1986).

3.4. Determination of cytotoxicity in vitro of ^{111}In-DTPA-hEGF and ^{111}In-DTPA-EGFt

The selective cytotoxicity *in vitro* of ^{111}In-DTPA-hEGF and ^{111}In-DTPA-EGFt for human breast cancer cells overexpressing EGFR was evaluated by measuring the cell survival using a clonogenic assay (Franken et al., 2006). The surviving fraction (SF) of BC cells

exposed *in vitro* to different treatments was determined after treating T150 flasks of MDA-MB- 468 or MCF-7 cells (1×10^6 and 1×10^4 EGFR receptors/cell, respectively (Reilly et al., 2000)) for 72 h at 37°C and 5% CO_2. The treatment groups were: control (untreated cells), ^{111}In-acetate (1.85 MBq/mL), ^{111}In-DTPA-hEGF (1.0 MBq/mL, 10 nM), ^{111}In-DTPA-EGFt (1.0 MBq/mL, 10 nM or 1.85 MBq/mL, 40 nM), 10 nM unlabeled DTPA-hEGF, 10 nM unlabeled DTPA-EGFt or 40 nM DTPA-EGFt. After the treatment period, unbound radioactivity or peptides were removed by rinsing three times with PBS, pH 7.5. Approximately 13,500 cells (MDA-MB-468) or 3,500 cells (MCF-7) were then seeded into T25 flasks, and the cells were cultured at 37 °C under 5% CO_2 in the appropriate growth medium supplemented with 10% FBS for 7 days for MDA-MB-468 cells or 10 days for MCF-7 cells to allow colony formation. Cultures were rinsed with PBS and stained with methylene blue (1% in a 1:1 mixture of ethanol and water). The number of colonies (>50 cells) in each flask was counted by ImageJ software and customized macros (Cai et al., 2011). The plating efficiency was determined for treated and control untreated cells by dividing the number of colonies formed by the number of cells seeded. The SF for each treatment was calculated by dividing the PE for the treated cells by that for untreated control cells.

3.5. Tumor xenograft mouse model

Human BC xenografts were established in groups of 3-4 female CD1 athymic mice (Charles River Labs) by subcutaneous (s.c.) inoculation of 1×10^7 MDA-MB-468 cells in the right flank and 1.5×10^7 MCF7cells in the left flank. Mice inoculated with MCF-7 cells were implanted intra-dermally one week prior to inoculation with 0.72 mg of 60-day-sustained-release 17-β-estradiol pellet (Innovative Research) required for the growth of these tumors. All animal experiments were carried out in compliance with Canadian Council on Animal Care regulations and were approved by the Animal Care Committee of the University Health Network (Protocol 1577.2).

3.6. Pharmacokinetic studies

When the MDA-MB-468 and MCF-7 xenografts were 5-10 mm in diameter (3-4 weeks post-inoculation) tumor bearing mice (three mice per group) were injected intravenously via the tail vein with 8-9 MBq (2 µg) of ^{111}In-DTPA-hEGF or ^{111}In-DTPA-EGFt in 125 µL of saline. Blood samples were collected via the saphenous vein at different time points (5 min to 48 h) using a heparinized capillary tube. The length of the capillary tube (mm) occupied by blood was measured using a digital calliper. The amount of blood in the capillary tube was converted to µL by multiplying by 0.93 (i.e. 1 mm of capillary tube occupies 0.93 µL of blood). Radioactivity in the blood was measured in a γ-counter and expressed as the percentage of the injected dose per gram (%ID/g) assuming blood constitutes 7% of the total body weight. Pharmacokinetic parameters were calculated by fitting the blood radioactivity concentrations vs. time to a two-compartment model using Scientist® Ver. 3.0 (Micromath®). The areas under the curves (AUC) were calculated using the trapezoidal rule. Clearance (CL) and volume of distribution at steady state (Vss) were also calculated.

3.7. Biodistribution

To determine the tissue biodistribution of ^{111}In-DTPA-EGFt, CD1 athymic mice bearing MDA-MB-468 tumors were injected intravenously (i.v.) via the tail vein with 8-9 MBq (2 µg) of ^{111}In-DTPA-hEGF or ^{111}In-DTPA-EGFt in 125 µL of saline (three mice per group). To determine the specificity of uptake a group of mice was pre-injected with 2 mg of the anti-EGFR antibody nimotuzumab (kindly provided by YM Biosciences) 3 h prior to injection of ^{111}In-DTPA-EGFt to block EGFR and inhibit the binding of radiolabeled EGF (Diaz-Miqueli et al., 2013; Ramakrishnan et al., 2009). Nimotuzumab binds to domain III in the extracellular region of the EGFR, a binding domain which overlaps with that of EGF inhibiting the binding of EGF to the EGFR (Talavera et al., 2009). At 48 h post injection (p.i.), mice were sacrificed; tumor and normal tissues

samples were obtained and weighed in tared tubes; and their radioactivity was measured in a γ-counter. Tumor and normal tissue uptake of ^{111}In-DTPA-EGFt were expressed as the percent injected dose per gram (% ID/g). The tumors were further processed by disaggregation and the proportion of radioactivity internalized by the cells was determined by displacing cell-surface radioactivity with 200 mM sodium acetate/500mM NaCl pH 2.5 at 4°C. Cytoplasmic and nuclear radioactivities were isolated using a nuclei isolation kit (Nuclei PURE Prep, NUC-201, Sigma-Aldrich). The surface-bound, cytoplasmic, and nuclear fractions were measured using a gamma counter.

3.8 MicroSPECT imaging

MicroSPECT/CT imaging was performed in tumor bearing mice at 48 h p.i. of 15-18 MBq (5 µg) of ^{111}In-hEGF or ^{111}In-EGFt. Mice were anaesthetized by inhalation of 2% isoflurane in O_2 and imaging was performed on a nanoSPECT/CT tomograph (Bioscan, Washington, DC) fitted with 1.4 mm multi-pinhole collimators (FWHM ≤ 1.2 mm). A total of 24 projections were acquired in a 256 × 256 matrix with a minimum of 100,000 counts/projection. Images were reconstructed using an ordered subset expectation maximization (OSEM) algorithm with 9 iterations. Cone-beam CT images were acquired (180 projections, 1 s/projection, 45 kVp) prior to SPECT imaging. Co-registration of SPECT and CT images was performed using InvivoScope software (Bioscan).

4. Statistical analysis

Statistical analysis was performed with the SPSS statistical software for Windows (version 15.0; SPSS Inc.). Quantitative variables were expressed as mean and standard error (SE). The normality of the data was tested using the Kolmogorov-Smirnov test. The differences between data with normal distribution and homogeneous variances were analyzed using the parametric Student's t-test,

otherwise the non-parametric Mann-Whitney U test was applied. A value of $P<0.05$ was considered significant.

RESULTS

1. Production of the recombinant human EGF and its truncated derivative EGFt

1.1. Design of an EGF analogue

The ribbon diagram of the crystal structure of an EGFR homodimer in complex with two EGF ligands are represented in Figure 13A.

In the figure, the three main interaction sites between EGF and EGFR as well as the specific residues in site 3 involved in the interaction between the receptor and EGF are indicated. Based on this structure we designed a truncated EGF analogue, EGFt, lacking the 8 C-terminal amino acids, including the Leu47 residue important for the hydrophobic interactions in site 3, in order to generate a peptide with blocking activity and higher affinity than PCI for the receptor. In Figure 13B the ribbon diagram and the amino acid sequence of EGF are represented, with the removed C-terminal aminoacids depicted in black and the Leu47 residue depicted in orange.

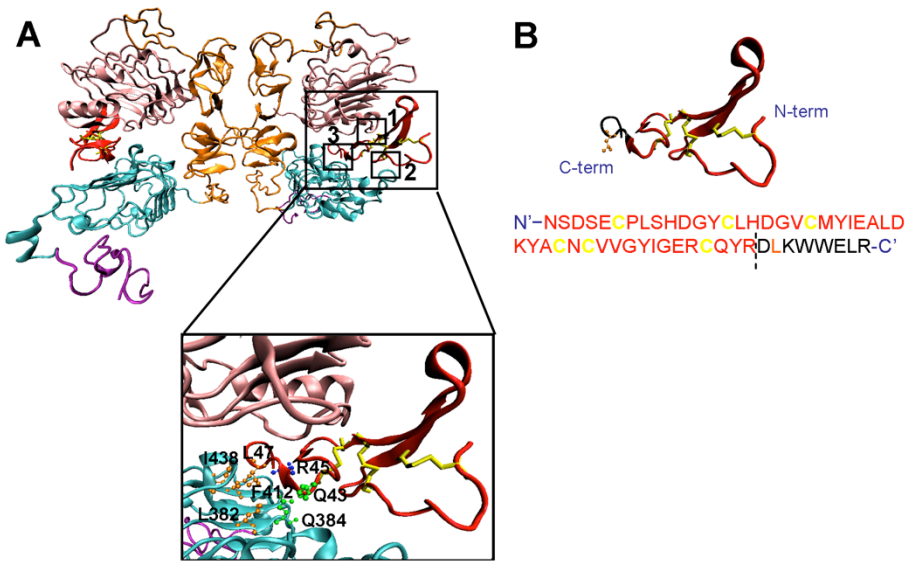

Figure 13. Ribbon diagram of the crystal structure of an EGFR homodimer in complex with two EGF ligands (from Protein Data Bank code 1IVO). (A) The subdomains I, II, III and IV of both receptors are colored pink, orange, cyan and purple, respectively. Held between domains I and III of each receptor are the EGF ligands colored red and their disulfide bridges yellow. The three main interactions sites between EGF and EGFR are outlined (1, 2 and 3). The interaction site 3 between C-terminal part of EGF and domain III of EGFR is magnified. This binding site is composed by two different kinds of interactions: hydrophobic interactions between Leu47 (EGF) and Leu382, Phe412, and Ile438 (EGFR), and the formation of hydrogen bonds with Gln384 side chain of EGFR and carbonyl and amide groups of Gln43 and Arg45, respectively, of EGF. All side chains of residues responsible for these interactions are shown in different colors depending on the type of interaction. (B) Ribbon diagram and amino acid sequence of EGF. The C-terminal part of the molecule is highlighted in black and the side chain of Leu47 is shown in orange in the ribbon diagram. The nucleotides that encode these 8 amino acids were removed from the encoding sequence to construct the EGF truncated form (EGFt).

1.2. Production, purification and analysis of recombinant hEGF and EGFt

Wild type hEGF was produced in parallel to EGFt in order to obtain a positive control for the experiments and for future applications. The encoding sequences of hEGF and EGFt were cloned into a periplasmic secretion system that contains the OmpA (Outer membrane protein A) signal sequence (Sorensen et al., 2005) in order to obtain the

peptides in the supernatant of the cell culture. After 24 h of culture we confirmed by cell fractionation that hEGF and EGFt were mainly in the extracellular fraction of the cell culture (Figure 14 A). The yield of production of these proteins on a shake flask level was about 1 mg/L of culture. To improve this yield, the production of the recombinant proteins was next conducted in a Biostat B 10 L laboratory fermenter under fed-batch fermentation conditions and the production increased by 25-fold.

Next, the proteins were concentrated from the supernatant and purified by two chromatographic steps by HPLC: anion exchange and size exclusion chromatography. Figure 14A shows the SDS-PAGE analysis of the samples obtained in the different purification steps confirming the protein purity in the last step for both peptides. The identities of both proteins were assessed by MALDI-TOF analysis confirming their high purity and expected molecular mass: 6222 Da for hEGF and 5094.7 Da for EGFt (Figure 14B). Additional, N-terminal amino acid sequence analysis confirmed the correct amino acid sequence and the proper cleavage of the ompA signal peptide in the periplasm (data not shown). Figure 14C shows the protein folding analysis by reverse-phase HPLC. Both chromatograms contain a single peak at the retention time described for hEGF indicating its correct folding and the absence of folding scrambles (Chang et al., 1995).

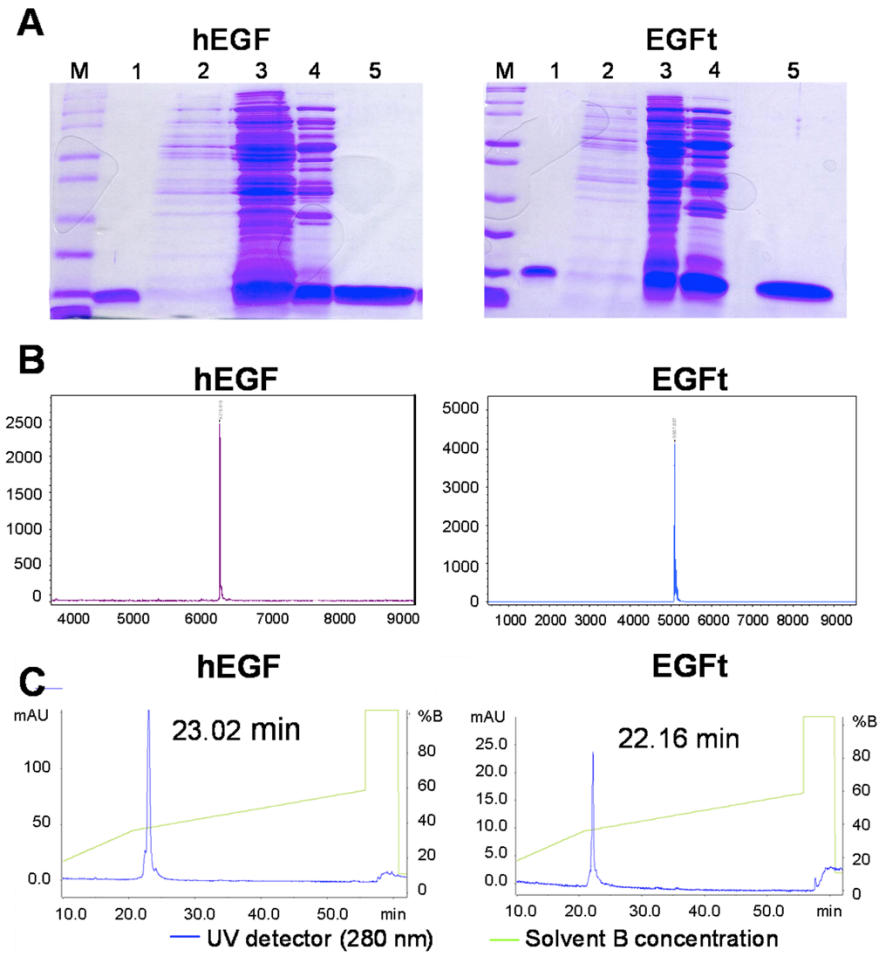

Figure 14. Purification and characterization of hEGF and EGFt. (A) Protein analysis of the different purification steps by Coomassie blue-stained SDS-PAGE. Molecular weights (M); Lane 1: commercial recombinant hEGF. Lane 2: supernatant of the *E.coli* fermentor culture before concentration. Lane 3: 30x concentrated supernatant by tangential flow filtration. Lane 4: product of the first purification step (anionic exchange chromatography). Lane 5: purified product after the final purification step (gel filtration chromatography). (B) Determination of the molecular weight of hEGF and EGFt by mass spectrometry (MALDI-TOF). The analysis confirmed the corresponding molecular weight of the hEGF (6216.6 Da) and EGFt (5087.9 Da). (C) Analysis of the state of folding of purified hEGF and EGFt by RP-HPLC. The peaks on the chromatogram correspond to the elution time of well-folded hEGF (Chang et al., 1995).

2. In vitro charachterization of EGFt

2.1. EGFR expression profile in three EGFR-positive human tumor cell lines

Before conducting the biological assays, we examined EGFR expression levels in MDA-MB468, MCF-7 and Caco-2 human tumor cell lines, by flow cytometry. As represented in Figure 15, MDA-MB-468 cells expressed the highest level of EGFR, while MCF-7 and Caco-2 cells showed similar moderate expression of the receptor.

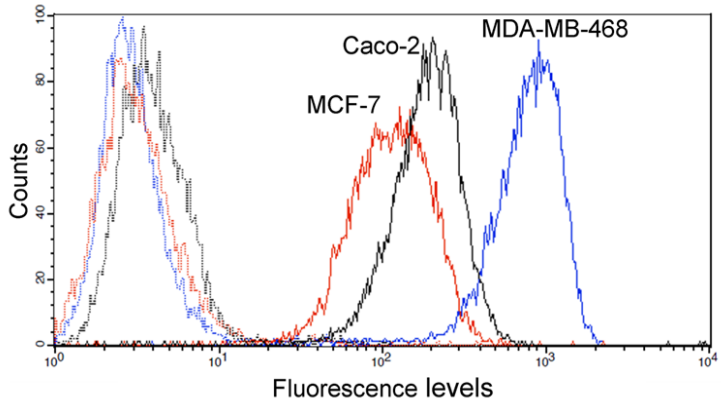

Figure 15. EGFR expression profile in MDA-MB-468, MCF-7 and Caco-2 cells. The expression of EGFR on the cell surface was determined by flow cytometry after indirect immunofluorescence staining with a monoclonal antibody against human EGFR (solid lines) followed by incubation with fluorescent-labelled secondary antibody. An irrelevant primary antibody was used as a negative control (dotted lines). Histograms were obtained after analyzing 10,000 MCF-7 (red), Caco-2 (black) and MDA-MB-469 (blue) cells. The fluorescence intensity is shown on a four-decade log scale.

2.2. EGFR activation

The ability of the recombinant proteins to activate the EGFR was evaluated by analyzing tyrosine residues phosphorylation after hEGF and EGFt cell stimulation. MDA-MB-468 cells were treated with 3 nM, 150 nM hEGF or 150 nM EGFt for 10 min at 37ºC. The cell lysates were analyzed in parallel by Western blotting with an

antibody against total phosphotyrosines and an antibody against EGFR to identify the bands corresponding to EGFR. Figure 16A shows that both recombinant proteins were able to activate the receptor. However, the phosphorylation induced by EGFt was markedly lower, even when hEGF concentration was reduced to 3 nM. These results reveal that EGFR stimulation by EGFt binding leads to an impaired activation of the receptor.

Next, we compared the effect of EGFt and hEGF on the phosphorylation of four EGFR specific residues involved in internalization and proliferation signaling. Figure 16B shows that specific residues involved in the internalization of the receptor, Y1045 and S1046/47, were highly phosphorylated when MDA-MB-468 cells were stimulated with hEGF. The phosphorylation of Y1046/47 was similar when the cells were stimulated with EGFt, while Y1045 was only slightly activated (Figure 16B, left panel). Similar results were obtained in MCF-7 and Caco-2 cells (Figure 16B, central and right panel). On the other hand, while hEGF induced a strong phosphorylation of the tyrosines involved in proliferative signaling pathways, Y1068 and Y1173, EGFt minimally activated them in any assayed cell line (Figure 16C).

In fact, a decrease in a proliferation signal output of EGFR, like MAPK (p-ERK1/2) and PI3K (p-Akt) activation, was observed in EGFt (150 nM) compared to hEGF (3 nM or 150 nM) treatment, being these differences more evident in MCF-7 and Caco-2 than in MDA-MB-468 cell lines (Figure 17). Altogether, the results suggest the induction of EGFR internalization but a less activation of the proliferation signals when treating cells with EGFt.

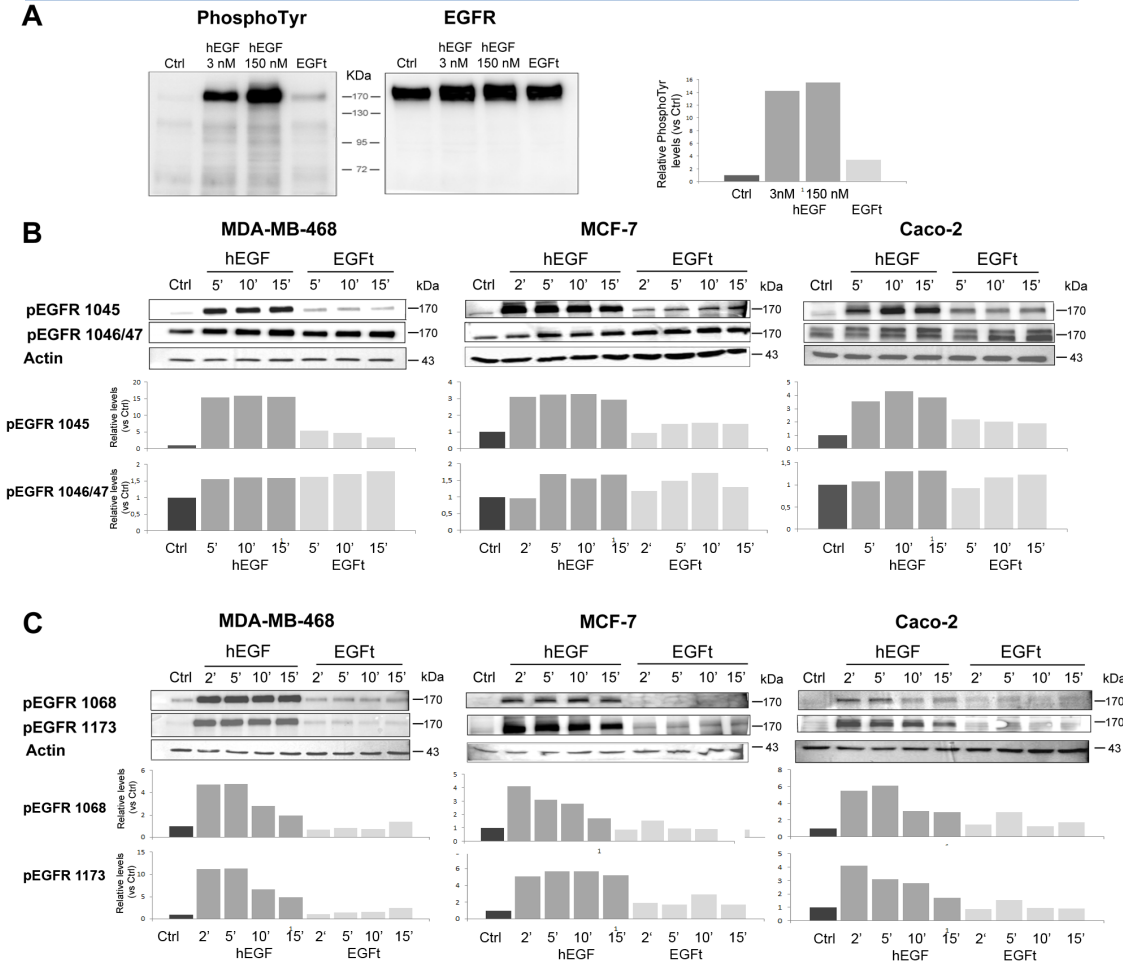

Figure 16. Effect of EGFt on the phosphorylation of EGFR. (A) Analysis of the total phosphorylation of EGFR. MDA-MB-468 cells were treated with 3 nM, 150 nM hEGF or 150 nM of EGFt for 10 min. The whole cell lysates were analyzed in parallel by Western blotting with an antibody against total-phosphotyrosine residues (PY20) and with an antibody against EGFR (EGFR 1005). (B) Analysis of the phosphorylation of the C-terminal residues of EGFR involved in the internalization of the receptor. MDA-MB-468, MCF-7 and Caco-2 cells were treated with 150 nM hEGF or 150 nM of EGFt for the indicated periods of time. The whole cell lysates were analyzed by Western blotting with site-specific antibodies for phospho-EGFR tyrosines 1045 and 1046/47. (C) Analysis of the phosphorylation of the C-terminal residues of EGFR involved in the proliferation signaling pathway. MDA-MB-468, MCF-7 and Caco-2 cells were treated with 150 nM hEGF or 150 nM of EGFt for the indicated periods of time. The whole cell lysates were analysed by Western blotting with site-specific antibodies for phospho-EGFR tyrosines 1068 and 1173. Untreated cells were used as a negative control (Ctl) and β-actin levels were used as the loading control in Western blotting. The signal level of each phosphoresidue was determined by densitometry and normalized versus total EGFR protein (A) or actin levels (B and C). Densitometry values are presented relative to control.

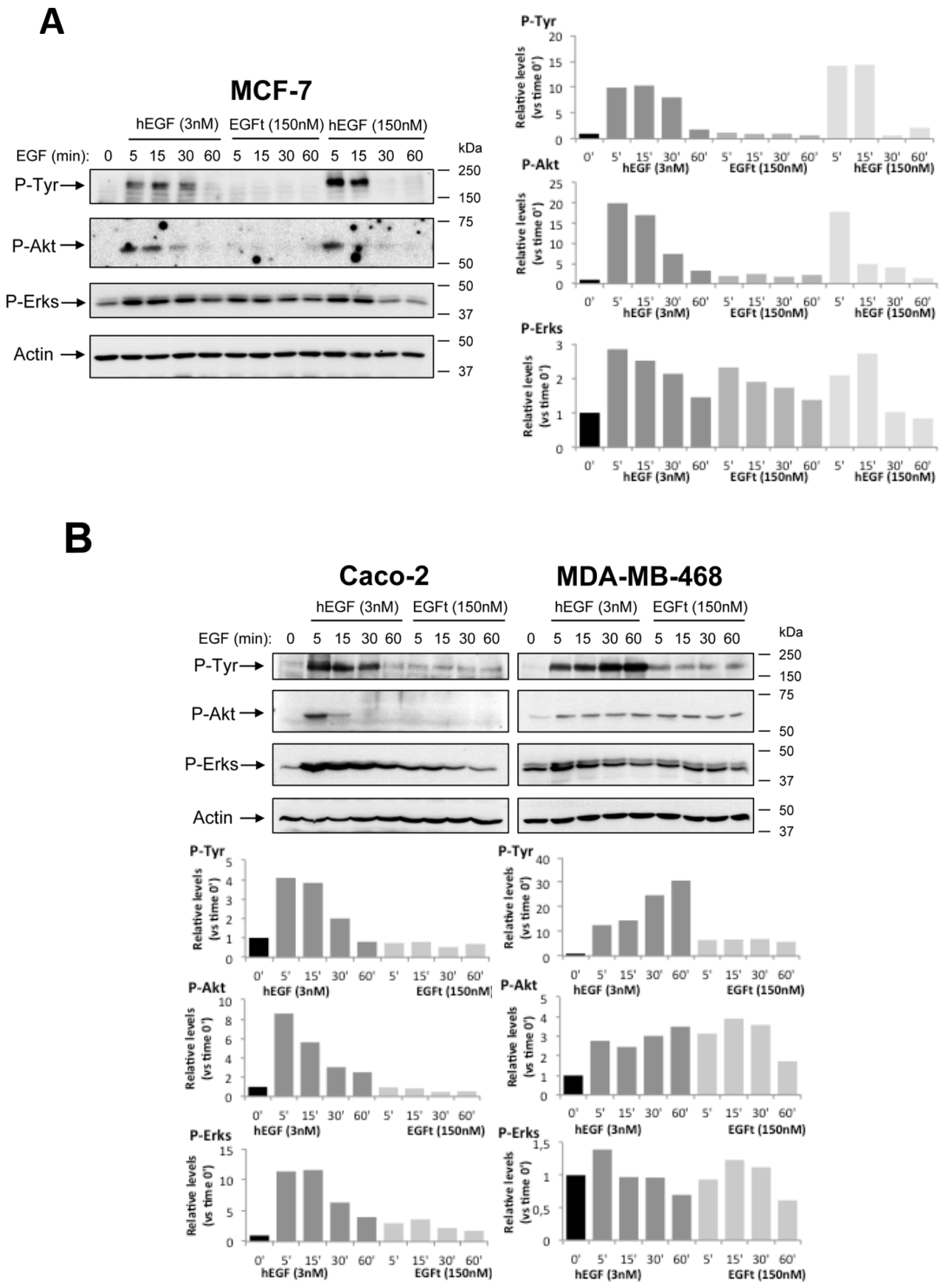

Figure 17. Comparative effect between hEGF and EGFt on MAPK and Akt activation in MCF-7, Caco-2 and MDA-MB-468 cells. Serum starved MCF-7 (A) Caco-2 and MDA-MB-468 (B) cells

growth in 6 well plates were stimulated with 3 nM, 150 nM hEGF or 150 nM EGFt as specified for the period of time indicated at 37ºC. Lysates with equal amount of protein were electrophoresed and phosphorylated EGFR (p-Tyr), MAPK (p-ERK1/2) and Akt/PKB (p-Thr308) were analyzed by Western blotting. Actin detection was used as a loading control. Figure shows one representative experiment from duplicate samples. The signal level of each phosphoresidue was determined by densitometry and normalized versus actin levels. Densitometry values are presented relative to control (time 0 min).

2.3. EGFR dimerization

To determine the effect of EGFt on EGFR dimerization MDA-MB-468 cell lysates were treated with either hEGF or EGFt and in combination for 30 min and then the proteins were cross-linked with glutaraldehyde. The dimer formation was analyzed by Western blotting. As expected, hEGF induced EGFR dimers, while no dimerization of EGFR could be detected after the EGFt treatment, even when the concentration was increased to 15 µM (Figure 18A). These results suggest that the homodimers were not effectively induced or stabilized by EGFt stimulation. EGFt could neither induce EGFR-HER2 heterodimerization (Figure 18B).

Moreover, when hEGF and EGFt were mixed at the same concentration, the EGFR dimer formation decreased compared to hEGF treatment (Figure 18A), indicating that EGFt was competing with hEGF for EGFR binding and competitively decreasing dimer formation.

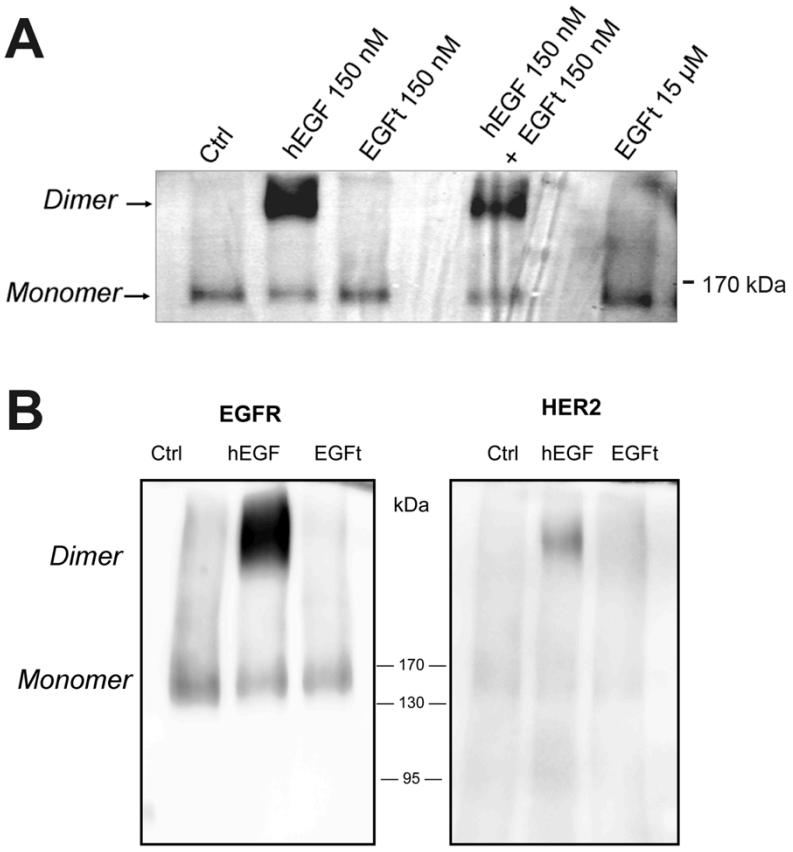

Figure 18. Effect of EGFt on the dimerization of EGFR. (A) Cell lysates from MDA-MB-468 cells were treated with the indicated concentrations of hEGF, EGFt or a mixture of both for 30 min. Untreated cells were used as control. Then the samples were cross-linked by addition of 40 mM of glutaraldehyde and analyzed by Western blotting using and anti-EGFR antibody. The position of the EGFR monomers and dimers are indicated. (B) The effect of EGFt on EGFR heterodimerization with HER2 was examined in either 150nM hEGF or 150nM EGFt treated MDA-MB-468 cells as well as in control cells. After performing the dimerization assay, the samples were analyzed with an antibody against HER2. The position of the EGFR monomers and dimers are indicated.

2.4. Effect of hEGF and EGFt on EGFR internalization

To further explore the ability of EGFt to trigger the internalization of EGFR, we developed a cell-ELISA assay using MCF-7 and Caco-2 cells. In this assay we detected

the EGFR that was not completely internalized and remained on the cell membrane after incubation with either hEGF or EGFt for 15 min at 37ºC. Figure 19A shows the percentage of EGFR on the cell membrane relative to untreated control cells. In MCF-7 cells, EGFR expression on the cell membrane was significantly reduced by 21% by EGFt, while both hEGF treatments induced 50% EGFR internalization. Similar findings were observed in Caco-2 cells regarding to hEGF, which induced 34.5% and 45.6% EGFR internalization at 3nM and 150 nM, respectively, while the effect of EGFt was more moderate, leading to 6.3% EGFR internalization.

2.5. Effect of hEGF and EGFt on EGFR localization

The cellular localization of EGFR after different times of hEGF or EGFt stimulation was analyzed by immunofluorescent confocal microscopy in MDA-MB-468 cells. Triple labelling of the nucleus with Hoescht (blue), the nuclear membrane with a Cy3 anti-lamin B1 antibody (red) and EGFR with a FITC anti-EGFR antibody (green) revealed a similar cellular localization of EGFR after hEGF and EGFt treatments. (Figure 19B). First, in starved condition and before treatments (time 0), EGFR was almost completely located in the plasma membrane. After 10 min with either hEGF or EGFt treatment EGFR were found within the cell near the cell surface. After 90 min, EGFR was observed throughout the whole cytoplasm and plasma membrane in both treatments. Interestingly, after 3 h of treatment a portion of the receptor was observed in several punctuate staining localized in a perinuclear region and some punctuate inside the nucleus (Figure 19B and 19C).

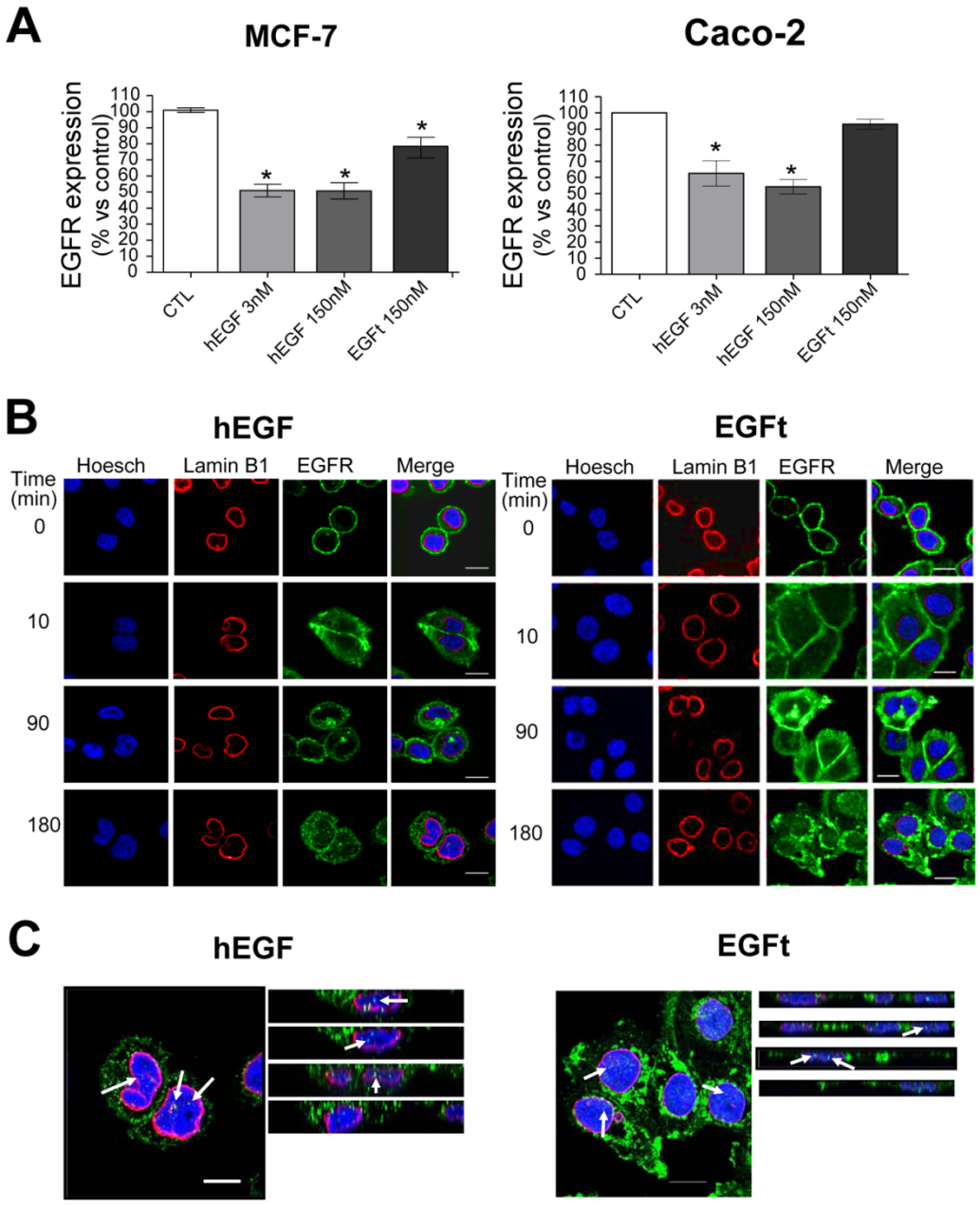

Figure 19. Effect of EGFt on the internalization and localization of EGFR compared to hEGF. (A) MCF-7 and Caco-2 cells were treated with 3 nM, 150 nM hEGF or EGFt for 30 min at 4ºC and then incubated at 37ºC for 15 min. The detection of EGFR in the cell membrane was determined by performing a cell-ELISA assay with specific antibodies. Each column in the graph

represents the relative EGFR expression in the cell membrane versus untreated control cells (CTL) and was the mean ± SEM of three independent experiments (*P<0.05 vs. control cells). (B) MDA-MB-468 cells were exposed for various times to 150 nM hEGF or EGFt and stained for EGFR using FITC anti-EGFR antibody (green). The nucleus and its membrane were stained using Hoescht (blue) and Cy3 anti-lamin B1 antibody (red), respectively. Confocal images were acquired. (C) The merge images corresponding to 180 min of treatment were magnified and some slices of a merged *xz* reconstruction of the stack (slices at 0.3 microns on z axis) are shown. Arrows indicate green signals within the cell nucleus. Scale bar, 10 µm.

2.6. EGFt cellular localization analysis by confocal microscopy

The internalization and intracellular distribution of RITC-labelled EGFt and hEGF in MDA-MB-468 cells was first analyzed by confocal fluorescence microscopy. After 30 minutes incubation at 4ºC, both RITC-hEGF and RITC-EGFt were mainly located in the plasma membrane of the cells, as indicated by the red fluorescent staining (Figure 20). However, when the cells were treated at 37 ºC for 30 minutes, a prominent staining was detected inside the cells, demonstrating an intense internalization of both peptides during this period of time. The peptides were localized both in the cytoplasm and the nuclei of the cells, as indicated by the superimposition of red (hEGF or EGFt) on blue (Hoechst) staining (Figure 20). No significant differences between the intracellular distribution of RITC-hEGF and RITC-EGFt could be observed.

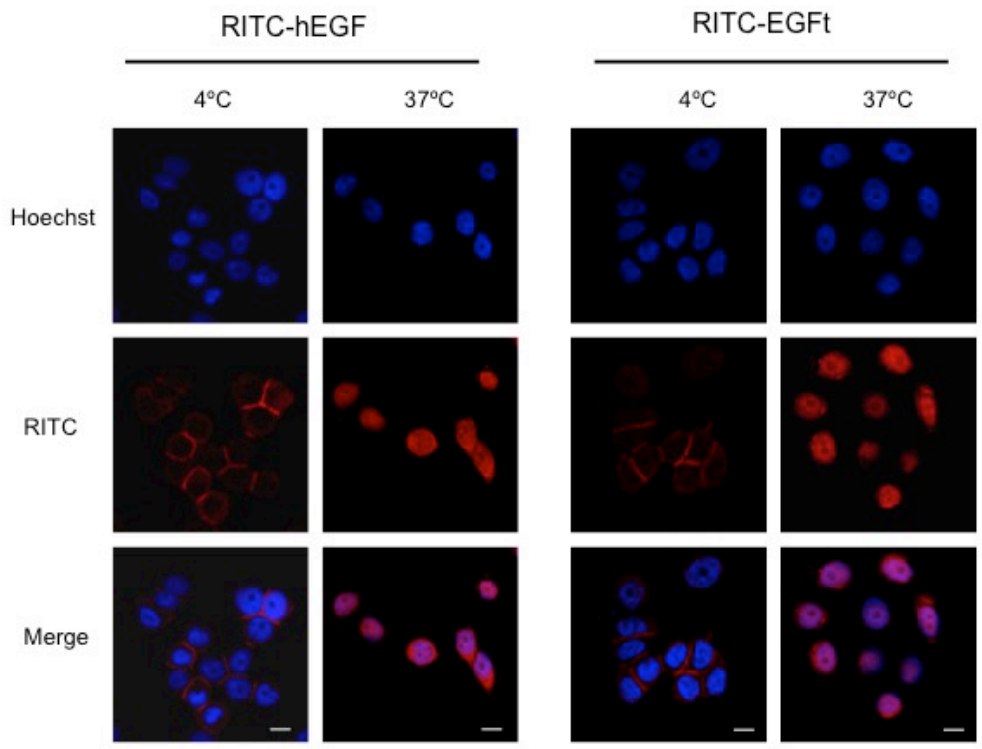

Figure 20. Confocal fluorescence microscopy analysis of the cellular localization of RITC-hEGF and RITC-EGFt after 3 h of exposure. MDA-MB-468 cells were exposed to 200 nM RITC-hEGF or RITC-EGFt (red) at 4ºC or for 3 h at 37ºC. and the nucleus was counter-stained with Hoechst (blue). Confocal images were acquired. Scale bar, 10 µm.

2.7. Effect of hEGF and EGFt on EGFR degradation

The ability of EGFt to trigger the lysosomal degradation of EGFR was also determined. In order to analyze the degradation of the EGFR, MCF-7 and Caco-2 cells were treated with the protein synthesis inhibitor cycloheximide and then the total amount of EGFR was determined by Western blotting after treatment with hEGF or EGFt for 30, 60, 180 and 300 min. As shown in Figure 21 a great proportion of EGFR was degraded after 180 and 300 min following 3 nM or 150 nM hEGF stimulation. In contrast, close to

100% of the initial receptor level was still intact in all the times analyzed after EGFt stimulation.

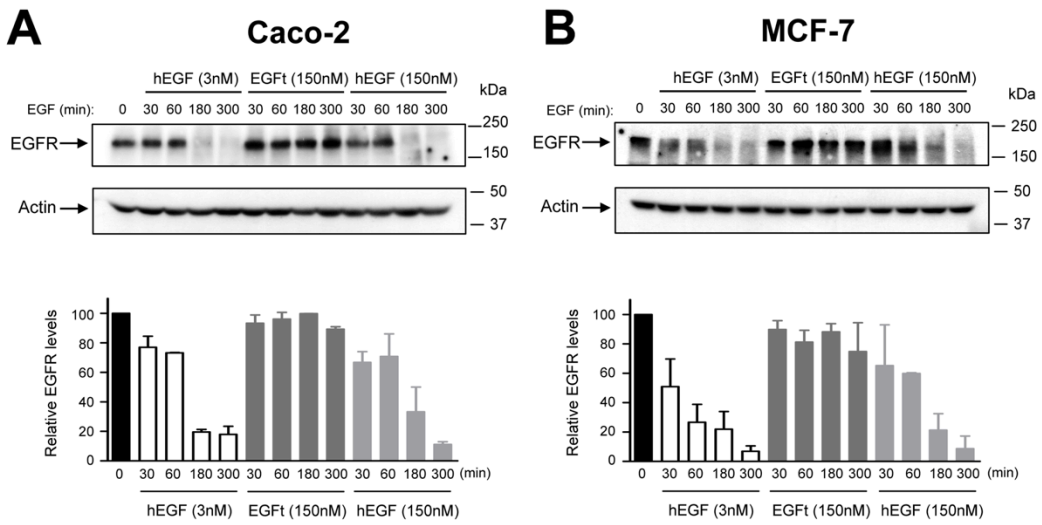

Figure 21. Effect of EGFt treatment on EGFR degradation. MCF-7 (A) and Caco-2 (B) cycloheximide treated cells were incubated with 3 nM hEGF, 150 nM hEGF or EGFt at 37ºC for different time periods as indicated. Cells were lysed, and the amount of EGFR was determined by Western blotting. Actin levels were used as loading control. Levels of EGFR were determined by densitometry and normalized versus actin levels. Each column represents the mean of two replicates + SEM.

2.8. Effect of hEGF and EGFt on cell proliferation

Before analysing the effect of hEGF and EGFt on cell proliferation, we assessed the optimal cell number to be seeded in each well for the proliferation assays, as the cells must be in an exponential growth phase along the experiment. 5000 Caco-2 and 4000 MCF-7 cells/well were selected as optimal initial cell concentrations as these concentrations lied within the linear portion of the plot, indicating that cells were still in an exponential growth rate at the end of the experiment (Figure 22).

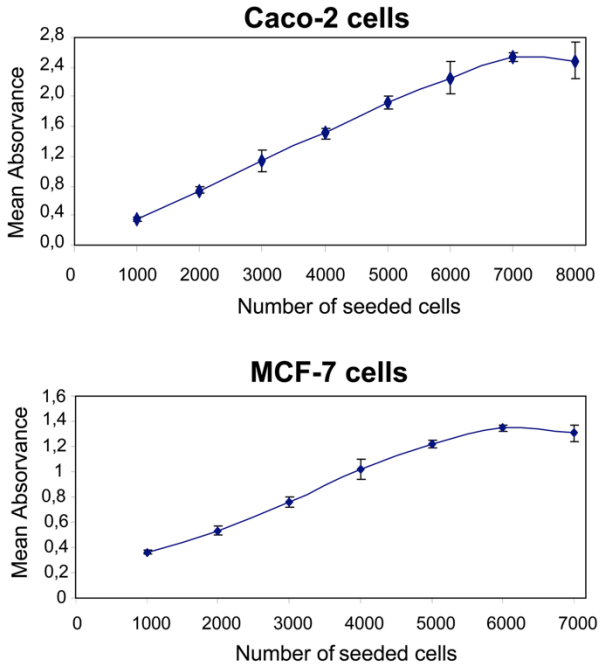

Figure 22. Assessment of the optimal cell concentration for cell proliferation assays. To determine the optimal initial seeding density, different cell concentrations (1000, 2000, 3000, 4000, 5000, 6000, 7000 and 8000 cells per well) were plated into 96-well plates (6 replicates per cell concentration) and incubated as described in the proliferation assay. The proliferation of the cells was determined by an MTT assay and the main absorbance was represented versus the number of seeded cells.

We next compared the ability of EGFt and hEGF, to stimulate MCF-7 and Caco-2 cell proliferation. While hEGF showed a proliferative effect in MCF-7 cells after 3 days of treatment at a concentrations of 20 and 150 nM, EGFt did not significantly modify the proliferation rate at any concentration tested (Figure 23, left panel). On the other hand, after 4 days of treatment, hEGF exhibited a moderated but significant proliferative effect at any concentration tested in Caco-2 cells. In contrast, EGFt induced a dose-dependent inhibition of Caco-2 cells proliferation (Figure 23, right panel). These differences between cell lines were probably due to the presence of a potent stimulatory autocrine loop of TGF-α in Caco-2 cells. As Caco-2 cells characteristically produce enough TGF-α to sustain their own proliferation (Bishop et

al., 1995; Beaulieu et al., 1991; Anzano et al., 1989), the addition of hEGF might not cause a large increase in proliferation. However, when EGFt was added, probably it competed with TGF-α for binding EGFR, causing a decrease in cell proliferation.

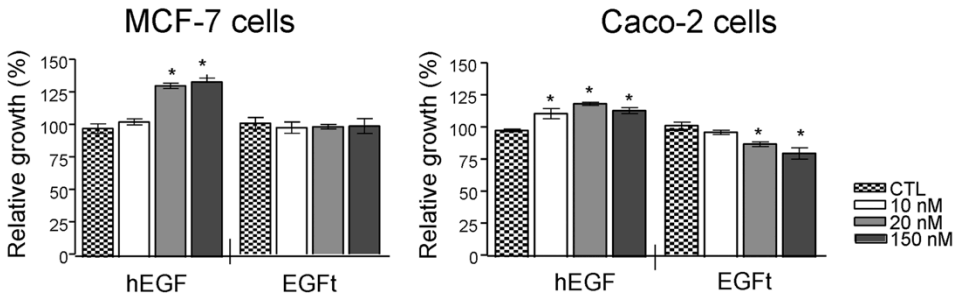

Figure 23. Effect of EGFt on the growth of two human cancer cells. MCF-7 and Caco-2 cells were incubated for 72 h or 96 h in a culture medium without FBS supplemented with 10, 20 and 150 nM hEGF or EGFt. The cell proliferation was assessed by MTT assays. Each column in the graph represents the relative cell proliferation versus untreated cells (control) and was the mean ± SEM of three independent experiments (*P<0.05 vs. control cells).

3. In vitro and in vivo characterization of the radiopeptides ^{111}In-DTPA-hEGF AND ^{111}In-DTPA-EGFt

3.1. Characterization of ^{111}In-DTPA-EGFt

The conjugation efficiency of DTPA-EGFt was measured to know the number of DTPA molecules present in each EGFt molecule. We obtained a ratio of 0.36 ± 0.16 DTPA/EGFt, which indicated that not all the EGFt peptides were derivatized with DTPA molecules. The conjugation efficiency for DTPA-hEGF was 0.58 ± 0.12 (Reilly et al., 2004). The radiochemical purity for both radioconjugates was routinely >98% as determined by ITLC-GC. The level of the radioactivity of the radioconjudates was adjusted according to the experiment to be carried out.

3.2. EGFR binding affinity of EGFt

MDA-MB-468 cells were used to analyze the binding affinity of the truncated EGF analogue for EGFR. In Figure 24, the total, specific and non-specific binding of ^{111}In-DTPA-EGFt has been plotted against increasing concentrations of radiolabelled ligand. The K_d for specific binding of ^{111}In-DTPA-EGFt was calculated using a one-site binding hyperbola nonlinear regression analysis by GraphPad Prism software and indicated that the receptor-binding affinity of ^{111}In-DTPA-EGFt for EGFR (K_d = 6 ± 2.03 M x 10^{-8}) was approximately 46-fold lower than that of ^{111}In-DTPA-hEGF (K_d = 1.3 ± 0.26 M x 10^{-9}).

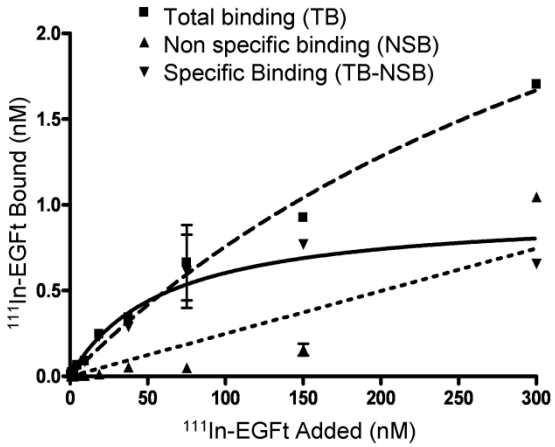

Figure 24. Representative binding curve for ^{111}In-DTPA-EGFt to MDA-MB-468 cells. The total binding curve was obtained by incubating cells with increasing concentration of ^{111}In-labeled EGFt (0-300 nM). The non-specific binding curve is obtained by adding increasing concentrations of the ^{111}In-DTPA-EGFt in the presence of 100-fold excess of unlabeled EGFt (30 μM). The specific binding curve was obtained by subtracting non-specific binding from total binding. The dissociation constant (K_d) for ^{111}In-labeled EGFt measured in this assay was 60.05 ± 2.03 nM. Each point represents the mean ± SEM of 3 assays performed in triplicate.

3.3. Cellular uptake and intracellular distribution of ^{111}In-DTPA-EGFt and ^{111}In-DTPA-hEGF

Cell fractionation studies revealed that the proportion of ^{111}In-DTPA-EGFt bound and internalized into MDA-MB-468 cells (approx. 1.7% of total ^{111}In-DTPA-EGFt incubated with the cells) was considerably lower compared to ^{111}In-DTPA-hEGF (approx. 14.3% of total ^{111}In-DTPA-hEGF added) (Figure 25A). Interestingly, despite substantially lower cell binding of ^{111}In-DTPA-hEGFt, after 3h exposure, 25.4 ± 1.7% of radioactivity remained on the cell surface, 35.6 ± 1.4% was internalized into the cytoplasm and 39.0 ± 0.3% was imported into the cell nucleus. In contrast, ^{111}In-DTPA-hEGF exposure showed a distribution of 47.9 ± 0.1% on the cell surface, 41.1 ± 0.7% in the cytoplasm and 10.9 ± 0.8% in the cell nucleus (Figure 25B). These results revealed greater efficiency of nuclear import of cell-bound and internalized ^{111}In-DTPA-EGFt compared to ^{111}In-DTPA-hEGF despite the lower overall cell-binding of ^{111}In-DTPA-EGFt. As a result, the nuclear accumulation of ^{111}In-DTPA-EGFt was only 2 times lower compared to ^{111}In-DTPA-hEGF, despite 8-fold lower cell-binding and internalization.

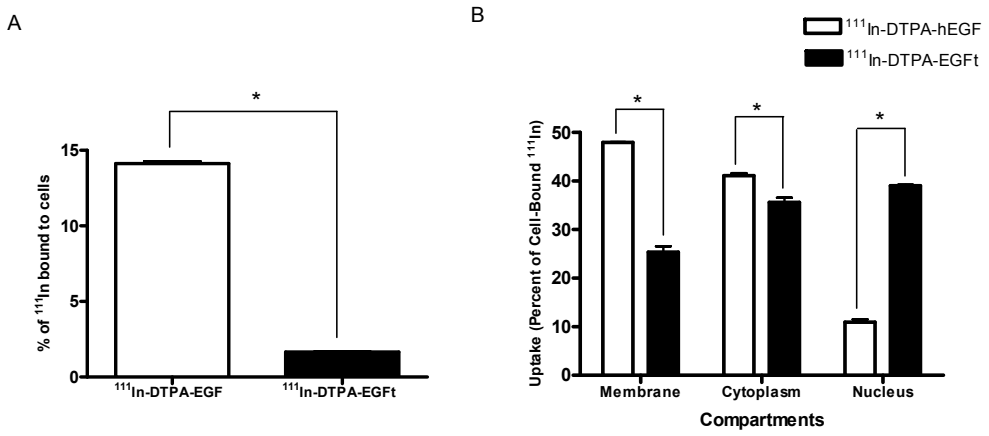

Figure 25. Cellular uptake and intracellular distribution of ^{111}In-DTPA-EGFt and ^{111}In-DTPA-hEGF. MDA-MB-468 cells were incubated with ^{111}In-DTPA-hEGF (2.8 MBq/mL, 15 nM) or with ^{111}In-DTPA-EGFt (2.8 MBq/mL, 15 nM) for 3 h at 37ºC. (A) Percent of ^{111}In bound to cells after unbound fraction removal. (B) Amount of ^{111}In on the cell membrane, in the cytoplasm, or in

the nucleus was measured in cell fractionation experiments and the uptake is presented as the percentage of the cell-bound radioactivity. Significant differences (P<0.05) are indicated by the asterisks.

3.4. In vitro cytotoxicity of ^{111}In-DTPA-EGFt and ^{111}In-DTPA-hEGF

Clonogenic survival assays showed that exposure of MDA-MB-468 cells to 1.85 MBq/mL of ^{111}In-acetate for 3 days followed by culturing for 7 days did not result in any significant cytotoxicity, as the SF was similar to that of the untreated control cells (Figure 26A). However, after exposure to 10 nM (1.0 MBq/mL) of ^{111}In-DTPA-EGFt or ^{111}In-DTPA-hEGF the SF was significantly reduced by 2 and by 19-fold ($p<0.05$), respectively. These results revealed a 9-fold lower cytotoxic potency of ^{111}In-DTPA-EGFt compared to ^{111}In-DTPA-hEGF in MDA-MB-468 cells when incubated at the same concentration. The cytotoxic effectiveness of ^{111}In-DTPA-EGFt was further determined at 40 nM (1.85 MBq/mL), in order to address whether higher concentrations of the radioconjugate may compensate the lower binding affinity and cellular uptake and internalization of EGFt. At this concentration, ^{111}In-DTPA-EGFt markedly decreased the clonogenic survival of MDA-MB-468 cells to only 8%, which supports that EGFt is able to deliver ^{111}In within the cell nucleus, where the nanometer-micrometer range Auger electrons are most damaging to DNA and lethal. Notably, treatment of MDA-MB-468 cells (Figure 26A) with the unlabeled peptides (10 nM DTPA-hEGF, 10 nM and 40 nM DTPA-EGFt) also resulted in a significant decrease in the SF compared to untreated cells, although the cytotoxic potency was lower than those of the corresponding ^{111}In-labeled peptides. It has been previously shown that high concentrations of EGF are growth-inhibitory to MDA-MB-468 cells (Filmus et al., 1985), thus the cytotoxicity of ^{111}In-DTPA-hEGF and ^{111}In-DTPA-hEGFt in these cells are due to these effects combined with the DNA damaging effects of the Auger electrons.

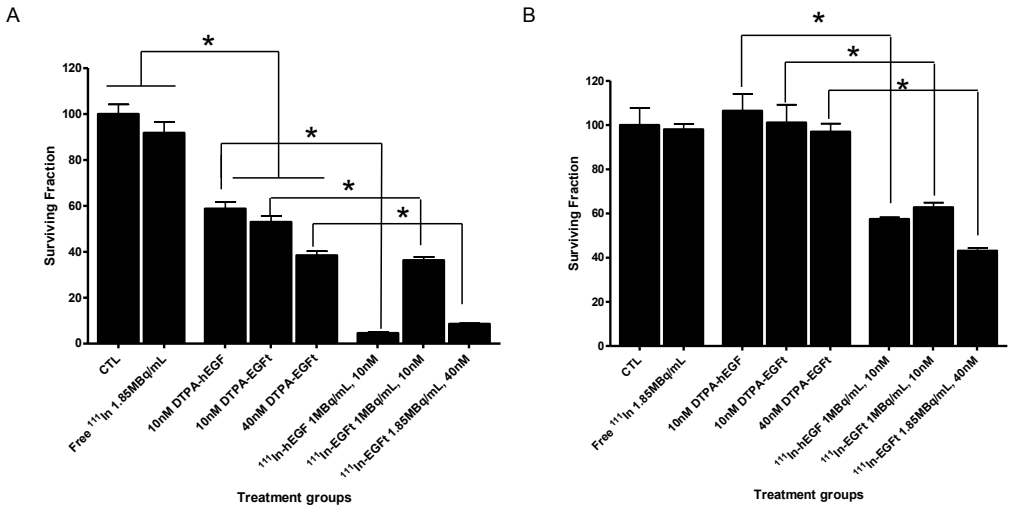

Figure 26. Surviving fraction measured in a clonogenic assay for (A) MDA-MB-468 or (B) MCF-7 cells. Cells were incubated with ^{111}In-acetate (1.85 MBq/mL), unlabeled DTPA-hEGF (10 nM), unlabeled DTPA-EGFt (10 nM or 40 nM), ^{111}In-DTPA-hEGF (1.0 MBq/mL, 10 nM), ^{111}In-DTPA-EGFt (1.0 MBq/mL, 10 nM or 1.85 MBq/mL, 40 nM) for 3 days then cultured for 7 days (MDA-MB-468 cells) or 10 days (MCF-7 cells). Untreated cells were used as control (CTL). Error bars represent SD of mean SF, calculated from 3 experiments. Significant differences (P<0.05) are indicated by the asterisks.

Figure 26B shows the SF of MCF-7 cells, with low EGFR expression, exposed to the same treatments. In this cell line, no cytotoxic effect was observed for the unconjugated peptides DTPA-hEGF and DTPA-EGFt. Interestingly when MCF-7 cells were exposed to 10 nM (1 MBq/mL) of both ^{111}In-DTPA-EGFt or ^{111}In-DTPA-hEGF, the SF was significantly reduced compared to untreated cells or to cells exposed to the equivalent concentrations of unlabeled DTPA-EGFt or DTPA-hEGF, demonstrating that the cytotoxic effect is due to the Auger electron emissions of ^{111}In delivered within the cell. ^{111}In-DTPA-hEGF and ^{111}In-DTPA-EGFt, exhibited a similar cytotoxic potency in MCF-7 cells, with a SF of 57.4% ± 1.3 and SF of 62.8 ± 3.7%, respectively (p = 0.08). At 40 nM, ^{111}In-DTPA-EGFt (1.85 MBq/mL) markedly decreased the clonogenic survival of MCF-7 cells to 43.1 ± 2.1%.

3.5. Pharmacokinetic studies

Pharmacokinetic parameters were obtained for ^{111}In-DTPA-EGFt and for ^{111}In-DTPA-hEGF in CD1 athymic mice bearing both MDA-MB-468 and MCF-7 tumor xenografts following i.v. (tail vein) injection (Table 3). The elimination of radioactivity from the blood for ^{111}In-DTPA-hEGF was significantly faster than ^{111}In-DTPA-EGFt (Figure 27). There was no significant difference in $t_{1/2}\alpha$ for ^{111}In-DTPA-hEGF (0.3 ± 0.2 h) and ^{111}In-DTPA-EGFt (0.3 ± 0.06 h) but the $t_{1/2}\beta$ of ^{111}In-DTPA-EGFt (55.5 ± 18.7 h) was significantly longer than that for ^{111}In-DTPA-hEGF (22.4 ± 8.5 h; $p<0.04$). The AUC for ^{111}In-DTPA-EGFt (0.5 ± 0.2 %ID/mL×h) was 2.5-fold ($p<0.02$) significantly greater than the AUC for ^{111}In-DTPA-hEGF (0.2 ± 0.04 %ID/mL×h). This resulted in a corresponding decrease in CL ($P<0.02$) for ^{111}In-DTPA-EGFt (3.5 ± 1.3 mL/h) compared to ^{111}In-DTPA-hEGF (8.1 ± 1.9 mL/h). Similarly, V_1 for ^{111}In-DTPA-EGFt (12.7 ± 1.6 mL) was significantly lower ($p<0.04$) than for ^{111}In-DTPA-hEGF (32.2 ± 14.1 mL).

Table 3. Pharmacokinetic parameters for elimination of ^{111}In-DTPA-hEGF or ^{111}In-DTPA-EGFt from the blood after intravenous injection in athymic nude mice (n≥3) bearing s.c. MDA-MB-468 and MCF-7 breast cancer xenografts.

Parameters	^{111}In-DTPA-hEGF	^{111}In-DTPA-EGFt
$t_{1/2}\alpha$ (h)	0.26 ± 0.16	0.31 ± 0.06
$t_{1/2}\beta$ (h)	22.40 ±8.50*	55.46 ± 18.69*
CL (mL/h)	8.15 ± 1.89*	3.48 ± 1.28*
AUC (% ID/mL x h)	0.21 ± 0.04*	0.53 ± 0.24*
V_1 (mL)	32.24 ± 14.08*	12.70 ± 1.57*

$t_{1/2}\alpha$ distribution half-life; $t_{1/2}\beta$ elimination half-life; *CL* clearance; *AUC* area under the curve; V_1 initial volume of distribution.

*Significantly different ($p<0.05$)

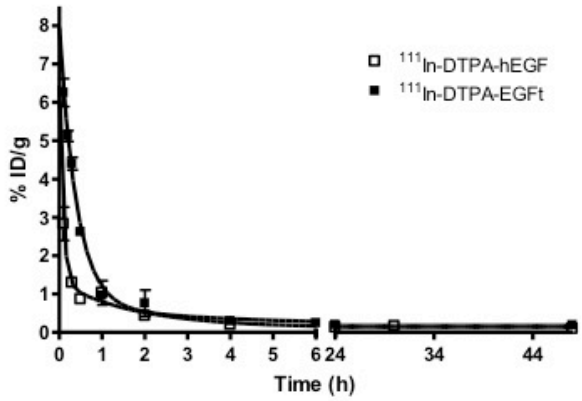

Figure 27. Elimination of ^{111}In-DTPA-hEGF or ^{111}In-DTPA-EGFt from the blood of athymic mice (n≥3) bearing both s.c. MDA-MB-468 and MCF-7 human breast cancer xenografts. Blood radioactivity concentrations vs. time were fitted to a two-compartment pharmacokinetic model. Data are expressed as % injected dose per gram (%ID/g) ± SD.

3.6. Tissue biodistribution and intratumoral distribution of ^{111}In-DTPA-EGFt

The biodistribution of ^{111}In-DTPA-EGFt and ^{111}In-DTPA-hEGF was evaluated in CD1 athymic mice bearing both MCF-7 and MDA-MB-468 tumors (Figure 28). At 48 h.p.i., a significant difference (p<0.05) in the uptake of the radiolabeled peptides was seen in the kidneys, liver, spleen and pancreas, lungs, heart, brain and skin and muscle. ^{111}In-DTPA-EGFt was largely sequestered in the kidneys (23.4 ± 4.8 %ID/g) with only a minor sequestration in the liver, spleen and pancreas (0.9 ± 0.4 and 0.1 ± 0.1 %ID/g, respectively). In contrast, ^{111}In-DTPA-hEGF was mainly accumulated in the kidneys and liver (8.2 ± 2.8 and 7.4 ± 2.0 %ID/g, respectively). Lungs, heart, brain, skin and muscle uptake of ^{111}In-DTPA-EGFt was significantly lower than ^{111}In-DTPA-hEGF (p<0.02) at 48 h p.i. Uptake in MDA-MB-468 tumors of ^{111}In-DTPA-EGFt was also significantly lower (0.6 ± 0.1 %ID/g) compared to ^{111}In-DTPA-hEGF (1.3 ± 0.1 %ID/g; p<0.002). However, the uptake of the radiolabeled peptides in MCF-7 tumors was lower than in MDA-MB-468 tumors as expected since these tumors have low EGFR expression, but was not significantly different for ^{111}In-DTPA-hEGF and ^{111}In-DTPA-EGFt: 0.3 ± 0.1 and 0.2 ± 0.1

%ID/g respectively; *P*>0.49). Pre-administration of nimotuzumab (2 mg) significantly reduced the uptake of ^{111}In-DTPA-EGFt in the skin and in MDA-MB-468 and MCF-7 tumors, indicating specific binding of ^{111}In-DTPA-EGFt to EGFR. However, nimotuzumab did not decrease the uptake of ^{111}In-DTPA-EGFt in the liver or kidneys, which are also known to be tissues that express EGFR (Hu et al., 2007), but also have a large mass, which may require more antibodies to block the uptake of ^{111}In-DTPA-EGFt.

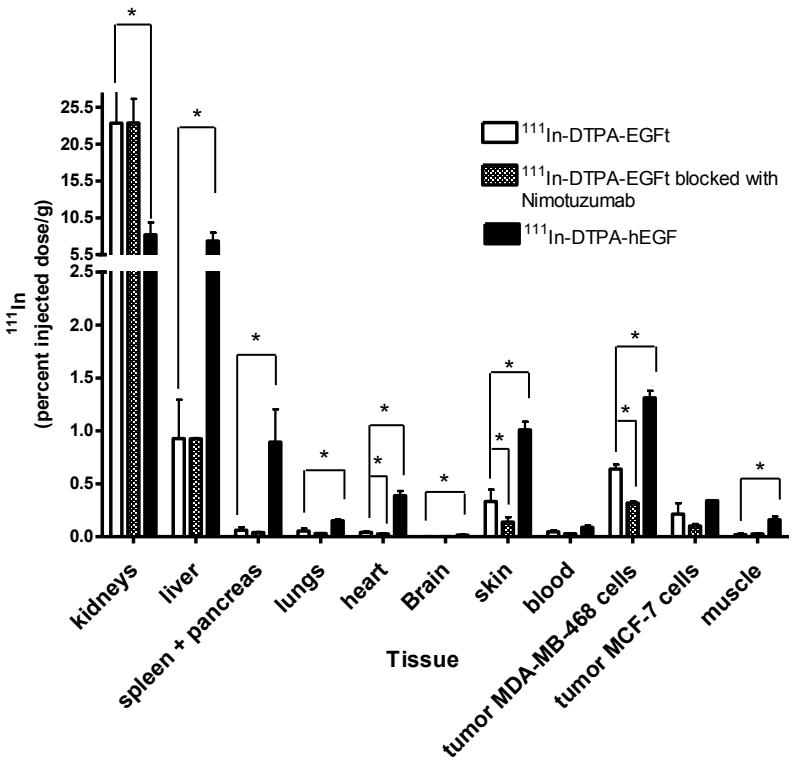

Figure 28. Tumor and normal tissue localization [percent injected dose/g (% ID/g)] of ^{111}In-DTPA-EGFt with/without pre-administration of 2 mg of nimotuzumab or ^{111}In-DTPA-hEGF at 48 h p.i. in athymic mice bearing s.c. MDA-MB-468 or MCF-7 human breast cancer xenografts. Statistically significant differences are indicated by the asterisks (P<0.05). Nimotuzumab binds to a domain on the EGFR that inhibits the binding of EGF to the receptor.

Figure 29 shows the intratumoral distribution of the radioactivity associated with the cells for both treatments. In agreement with *in vitro* intracellular distribution, although

^{111}In-DTPA-hEGF tumor uptake was higher than ^{111}In-DTPA-EGFt, the subcellular localization of each radiolabeled peptide showed that a greater proportion of cell-associated radioactivity in ^{111}In-DTPA-EGFt treatment was translocated to the nucleus of MDA-MB-468 tumor cells compared to ^{111}In-DTPA-hEGF treatment. In the case of ^{111}In-DTPA-hEGF only 8.3 ± 1.2% of tumor cell-associated radioactivity reached the cell nucleus, whereas, 17.3 ± 2.1% of radioactivity reached the cell nucleus for ^{111}In-DTPA-EGFt ($P<0.01$).

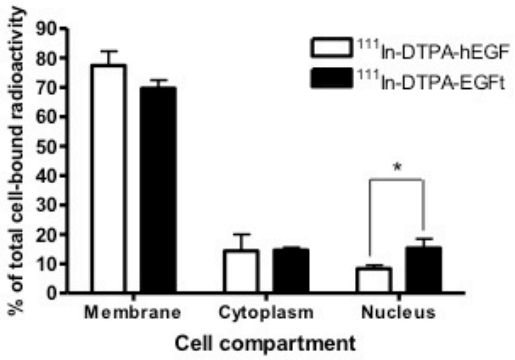

Figure 29. Subcellular distribution of ^{111}In in tumor cells isolated from subcutaneous MDA-MB-468 human breast cancer xenografts in athymic mice at 48 h p.i. with ^{111}In-DTPA-hEGF or ^{111}In-DTPA-EGFt. Subcellular radioactivity was determined by cell fractionation and is expressed as the percentage of total ^{111}In bound to the cells. Values shown represent the mean ± SD. of triplicate determinations. Significant differences in nuclear uptake ($p<0.05$) are indicated by the asterisks.

3.7. MicroSPECT imaging

MicroSPECT/CT imaging was performed at 48 h.p.i. to provide a qualitative assessment of the tissue deposition of ^{111}In-DTPA-hEGF and ^{111}In-DTPA-EGFt in the MDA-MB-468 and MCF-7 tumor-bearing mice (Figure 30). In agreement with the biodistribution data (Figure 28), we observed a significant difference in the main tissue deposition. While

^{111}In-DTPA-hEGF was found to be accumulated in the liver, spleen and kidneys, ^{111}In-DTPA-EGFt was mainly sequestered by the kidneys. Tumors were poorly detected. According to biodistribution data, the highest tumor uptake, 1.31 % ID/g, corresponding to ^{111}In-DTPA-hEGF, was a dose that cannot be fully detected by MicroSPECT/CT.

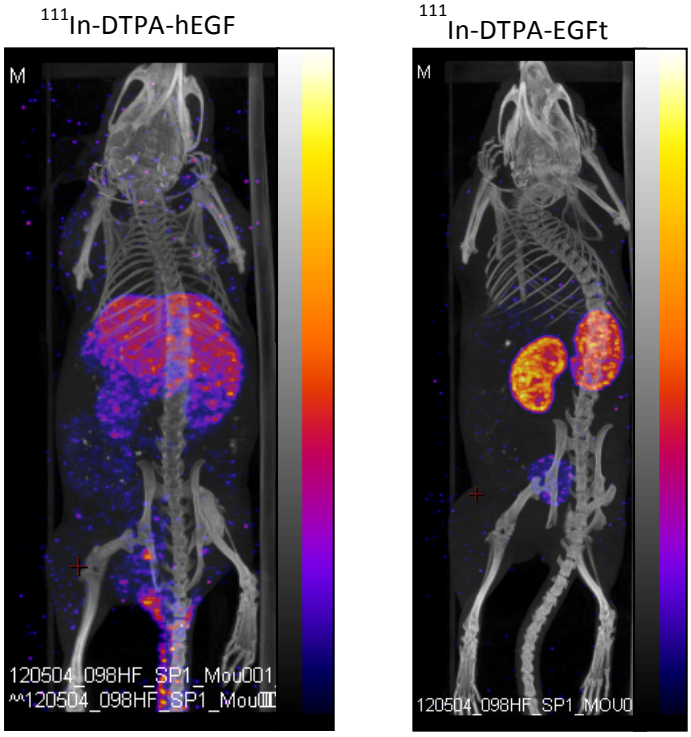

Figure 30. Micro SPECT/CT images illustrating the whole-body transport of ^{111}In-DTPA-hEGF and ^{111}In-DTPA-EGFt, in a representative athymic mouse bearing a s.c. MDA-MB-468 human BC xenograft on the left flank and MCF-7 human BC xenograft on the right flank at 48 h.p.i.

DISCUSSION

1. Production and characterization of an Epidermal Growth factor derivative with EGFR blocking activity

Signaling through ErbB receptors is of crucial importance in the control of cell proliferation, survival and differentiation. Hence, deregulated signaling by these receptors has been implicated in human malignancies. Recently, EGFR has been found to be a validated target for cancer chemotherapy to treat different tumours. However, the marked differences in the clinical efficiency of different EGFR inhibitors in different carcinomas, as well as the development of resistance, have limited the efficacy of these drugs (Ferrer-Soler et al., 2007; Marshall, 2006; Benavente et al., 2009). Thus, identifying additional agents that can target EGFR through novel strategies is an important goal in the treatment of cancer.

The main objective of the present work was to produce a peptide with EGFR-blocking activity as anti-tumour agent, based on the PCI, a peptide previously described by our group as an EGFR blocker, but with a lower affinity for EGFR than EGF. In order to design a peptide with higher receptor affinity but preserving the anti-tumour properties of PCI, EGF and PCI structures were superimposed (Mas et al., 1998; Blanco-Aparicio et al., 1998; Sitjà-Arnau et al., 2005). Interestingly, PCI lacks the C-terminal part of EGF, which is very important for interaction with the receptor. Thus, we hypothesized that the absence of this domain could be responsible for the anti-proliferative activity of PCI. Therefore, we decided to synthesize an EGF analogue without the C-terminal 8 amino acids, preserving the last disulphide bridge. One of the amino acids that we aimed to remove is Leucine 47, a highly conserved residue, important for EGF binding to the EGFR and its mitogenic activity (Matsunami et al., 1991; Ray et al., 1988; Jorissen et al., 2003).

In the present work we have produced both the wild type human EGF and the new truncated EGF peptide (EGFt) by cloning and expressing them in an extracellular

expression system that simplifies the purification protocol to only two chromatographic steps and produces the recombinant proteins with their correct folding, a really important feature because the function of these peptides is tightly related to their 3D structure. Furthermore, we have described a novel production methodology by fermentation that increases several times the yield obtained in small batch shake flask production. This methodology notably improves the production of EGF truncated peptides compared to previous protocols established by our group (Ferrer-Soler et al., 2003). The first strategy was based on production of hEGF by refolding it from *E.coli* inclusion bodies, which involved complicated and costly de-naturation and refolding processes (Choi et al., 2004). Next, our group explored the production of truncated forms of the peptide by enzymatic digestion of hEGF (Ferrer-Soler, 2007) but the recovery yield and purity were very low. In contrast, the methodology established in this work provides a high yield of correctly folded protein, which allows the performance of the *in vitro* assays to characterize the EGFt activity and compare it with that of hEGF in key steps of EGFR activation: ligand binding, dimerization, trans-phosphorylation and internalization.

We first analysed the capability of EGFt to stimulate EGFR and initiate downstream signaling pathways by determining the effects of EGFt in the trans-phosphorylation of the receptor. Our results showed that EGFt induce an impaired EGFR phosphorylation. It has recently been postulated that EGF family members that bind the same receptor are able to stimulate different biological responses both in cell culture and *in vivo*, due to distinctions in the conformation of the ligand-bound receptor and subsequent differences in the sites of receptor tyrosine phosphorylation (Wilson et al., 2009; Foley et al., 2010). Moreover, it has been demonstrated that the structure of the EGFR extracellular domain dimer is distinct when bound to EGF or TGF-α. Thus, ligand-specific differences in the interaction with the receptor may lead to differences in the receptor tyrosine residue availability for the receptor kinase domain (Foley et al., 2010). EGFt may induce a distinct EGFR ectodomain

conformation than hEGF and, as a consequence, EGFt could be stimulating different downstream responses. We analysed different tyrosine and serine residues to address the phosphorylation activation status of two main cellular responses: proliferation and down-regulation of EGFR by internalization of the receptor. Receptor down-regulation is the most prominent regulatory system for EGFR signaling attenuation and involves the internalization and subsequent degradation of the activated receptor in lysosomes. This molecular event mainly involves phosphorylation of Tyr-1045 and Ser-1046/7 of EGFR (Leykowitz et al., 1999; Countaway et al., 1992; Theroux et al., 1992). As expected, hEGF strongly induced the phosphorylation of both residues while EGFt did it moderately, indicating that EGFt could be inducing some EGFR internalization thus promoting some EGFR pathway down- regulation. Regarding cell proliferation, signaling by EGFR involves activation of the downstream MAPK / ERK signaling pathway, which is triggered by the phosphorylation of Tyr-1068 and Tyr-1173 (Jorissen et al., 2003). The analysis of the Tyr-1068 and Tyr-1173 phosphorylated residues after activation with either hEGF or EGFt revealed that while hEGF strongly stimulated their phosphorylation, EGFt hardly stimulated them compared to untreated cells. This result indicated that EGFt might not be activating cell growth, a similar result that was observed using PCI (Blanco-Aparicio et al., 1998; Sitjà-Arnau et al., 2005).

We also explored the effect of EGFt on EGFR dimerization. As expected, EGFt failed to induce both EGFR homo- and heterodimers, while hEGF treatment led to EGFR dimerization. These differences between hEGF and EGFt might be related to the different ability of the peptides to stabilize the untethered configuration of the receptor. As previously mentioned, EGFt does not interact with all three interaction sites required to promote the dramatic domain rearrangement that will shift the EGFR ectodomain into an untethered configuration in which its dimerization arm is exposed. In agreement, some authors have previously proposed that a ligand that competes effectively with EGF for EGFR binding, but which fails to promote the domain

rearrangement, would be a potent antagonist, and also predicted that a monovalent ligand that binds with very high affinity to only domain I or domain III (but not both) would fulfil these criteria (Ferguson et al., 2003). Moreover, recent understanding of the mechanism of action of suramin as a growth factor blocker with anti-cancer activity supports this idea. Suramin binds to EGFR by its C-terminal domain, and the authors suggested that suramin prevents hEGF from interacting with EGFR at site 3 and, as a consequence, EGFR cannot undergo the proper conformational change to dimerize and initiate signal transduction (Huang et al., 2010).

All together these results indicate that even though it is not possible to detect EGFR dimerization, EGFt is still causing EGFR trans-phosphorylation. Thus, EGFt is likely inducing a small EGFR conformational re-arrangement that could expose the dimerization arm in part, but probably not sufficient to stabilize the dimer. Consequently, the kinase domain is not fully activated to proper trans-phosphorylate all tyrosine residues. When investigating the effects of EGFt at the cellular level, we found that it was able to induce EGFR internalization, although in a much lesser extent than hEGF, what is in agreement with the reduced phosphorylation of residues involved in down regulation of EGFR. It is known that activated EGFR traffics from the plasma membrane to the cytoplasm through endocytic vesicles. Then, internalized EGFR can be eventually degraded in lysosomes, or recycled to the plasma membrane. Moreover, several reports have identified additional intracellular destinations for the internalized receptor, including the nucleus (Brand et al., 2011; Lin et al., 2001; Han et al., 2012). Our confocal microscopy analysis revealed that the localization of the receptor after its activation with either hEGF or EGFt was similar in both cases. Interestingly, after 3 hours of induction, a small amount of EGFR staining was observed into the cell nucleus. Moreover, the ligands localization assay showed a similar distribution of fluorescently labelled EGFt and hEGF within MDA-MB-468 human breast cancer cells overexpressing EGFR after a 3 h incubation period at 37ºC, and confirmed that EGFt reaches the cell nucleus. Different studies have postulated

that intranuclear EGFR may act as a transcriptional co-activator for various oncogenic genes (Brand et al., 2011; Lin et al., 2001).

The study of EGFR degradation revealed that while hEGF stimulated EGFR degradation, EGFt did not. These results suggested that after EGFt binding, the receptor was not extensively routed to lysosomes. We hypothesize that these differences in ligand-receptor processing between hEGF and EGFt could be similar to what some authors have observed before with TGF-α. The EGF binding to EGFR is relatively more stable at the pH of endosomes, so upon EGF binding to EGFR it can be transported to lysosomes. In contrast, TGF-α rapidly dissociates from the receptor when exposed to the low pH of endosomes, and the receptor and ligand dissociate and are recycled back to the plasma membrane (Ebner et al., 1991; Reddy et al., 1998). If EGFt behaves as TGF-α with respect to internalization, it means that EGFt may be recycled back to the cell surface, where it can exert its blocking activity on the EGFR again. A similar result was observed with PCI (Blanco-Aparicio et al., 1998; Sitjà-Arnau et al., 2005).

Regarding the effect of EGFt on cell proliferation, we observed that EGFt did not stimulate the proliferation of either MCF-7 or Caco-2 cells. On the contrary, EGFt treatment led to an inhibition of about 20% of Caco-2 cells growth compared to untreated control cells. Caco-2 cells have a powerful autocrine loop of TGF-α, and are highly dependent on the autocrine production of TGF-α for their growth (Bishop et al., 1995; Beaulieu et al., 1991; Anzano et al., 1989). Thus, these results suggest that EGFt may inhibit the autocrine mitogenic activity by competing with TGF-α for EGFR binding. So, EGFt would be able to inhibit the *in vitro* growth of those cancer cell lines that depend on an autocrine induction of cell proliferation by secretion of EGFR ligands.

In conclusion, we have demonstrated that EGFt binds to EGFR but does not stabilize the dimer formation, leading to an impaired EGFR trans-phosphorylation on tyrosine residues involved in proliferation signaling. Interestingly, EGFt induces the internalization of the receptor and presumably promotes the translocation of the receptor to the cell nucleus. Furthermore, EGFt competes with EGFR native ligands, inhibiting the proliferation of cells with an autocrine growth control via EGFR, acting as an inverse agonist or EGFR blocker. These findings indicate the importance of the hydrophobic interaction of EGF with EGFR on site 3 interface to activate the mitogenic EGFR signaling, and open up the possibility to insert new amino acid changes that could increase EGFt affinity for EGFR and its blocking activity.

The results obtained in this first part of the work encouraged us to explore the use of EGFt as a targeted toxin delivery agent in cancer cell lines overexpressing EGFt.

2. Evaluation of truncated human epidermal growth factor (EGFt) as a vehicle for the delivery of Auger electron-emitting ^{111}In into the nucleus of EGFR-positive breast cancer cells

To enable continued proliferation many tumors overexpress peptide growth factor receptors, also present at low density in normal tissues. These proteins can be targeted by radiopharmaceuticals consisting of radiolabeled forms of endogenous peptides or monoclonal antibodies that recognize these overexpressed receptors, for either tumor imaging or targeted radiotherapy (Reilly et al., 2010; Jackson et al., 2013). Recently, there has been a growing interest in radiolabeled peptides for imaging and therapy in oncology, because of target specificity, shorter circulation half-life (compared to radiolabeled antibodies) and better tumor penetrating characteristics of these agents (Reilly et al., 2010; Jackson et al., 2013). In the present

work we have used indium-111, an Auger electron emitter (Cai et al., 2008), complexed through the metal chelator DTPA to hEGF, or to the novel truncated form (EGFt) as targeted radiopharmaceutical. Auger electrons are very low energy electrons, which are emitted by radionuclides that decay by electron capture. The ultra-short (nanometer-micrometer), subcellular range of Auger electron-emitting radiopharmaceuticals restricts their radiotoxicity only towards cancer cells that specifically internalize and translocate these agents to the cell nucleus. In this respect it is important to note that EGF and other EGFR ligands reach the cell nucleus, possibly due to a putative nuclear localization sequence in the EGFR (Han et al., 2012). It has been reported that hEGF is a specific targeting vehicle to insert ^{111}In into the cytoplasm and nucleus of human breast cancer cells overexpressing EGFR. The radiopharmaceutical was highly and selectively radiotoxic to breast cancer cells that display a high EGFR density (Reilly et al., 2000).

^{111}In-labeled hEGF is an Auger electron-emitting radiopharmaceutical which may be a promising treatment for hormone-resistant, poor prognosis breast cancers in which EGFR are often overexpressed (Reilly et al., 2000; Chen et al., 2002; Chen et al., 2003; Hu et al., 2005; Bailey et al., 2007; Reilly et al., 2006; Vallis et al., 2014; Brouckaert et al., 2012). ^{111}In-DTPA-hEGF may also have application for imaging EGFR-positive breast cancer (Reilly et al., 2000; Vallis et al., 2014). However, since the EGFR is activated following ligand binding leading to a downstream signaling cascade, it is important that these radiolabeled peptides used for therapy or imaging do not self-activate the receptor. In this sense, a phase I trial to evaluate ^{111}In-DTPA-hEGF in patients with metastatic EGFR-positive breast cancer revealed some common adverse events in the patients that include flushing, chills, nausea, and vomiting as well as transient hypotension in some patients which are believed attributable to the EGF peptide (Vallis et al., 2014).

To avoid the possibility of receptor self-activation, in this work we produced a human EGF derivative, EGFt, which lacks the eight C-terminal amino acids of EGF and does not activate the EGFR. In this part of the study we have developed a radiolabeled derivative of EGFt (^{111}In-DTPA-EGFt) as an Auger electron emitting radiotherapeutic for EGFR-positive cancers and investigated its in vitro and in vivo characteristics. First of all ^{111}In-DTPA-EGFt was used to asses the affinity of EGFt for EGFR. This approach has the limitation of the low conjugation efficiency of DTPA with hEGF or EGFt (conjugation ratio of 0.58 and 0.36 peptide/DTPA, respectively), and thus not all EGF or EGFt molecules were conjugated with DTPA, which may underestimate the Kd of the ligands. However, the objective of the affinity data is to have a rough idea of the order of magnitude of the Kd value and to compare the affinities of hEGF and EGFt for the EGFR. ^{111}In-DTPA-EGFt showed a dissociation constant of 60.1 nM which was lower but in the same order of magnitude as ^{111}In-DTPA-hEGF (Kd: 1.3 nM) (Reilly et al., 2000). Moreover, the receptor-binding assay determined that the binding of ^{111}In-DTPA-EGFt with EGFR was specific. Interestingly, the effective concentration of PCI was one order of magnitude higher (μM) (Blanco-Aparicio, et al., 1998; Sitja-Arnau et al., 2005). Thus, the adopted approach significantly increased the affinity of the peptide for the EGFR compared to PCI and maintaining the specific binding for EGFR. Probably, EGFt has a lower affinity for EGFR compared to wild type hEGF because the binding of EGF to its receptor relies mainly on three contact sites and EGFt lacks the Leu47 residue which is of great importance for one of the interactions in site 3 of the EGF-EGFR binding interfaces.

In this part of the study we also determined the cellular uptake of ^{111}In-DTPA-EGFt and its intracellular distribution. The difference in binding affinity for EGFR resulted in a decreased proportion of ^{111}In bound to cells after incubation with ^{111}In-DTPA-EGFt compared to ^{111}In-DTPA-EGF. Interestingly, the results of this assay revealed an increased efficiency of ^{111}In-DTPA-EGFt for translocating ^{111}In to the cell nucleus following cell binding and internalization compared to ^{111}In-DTPA-hEGF. As a

consequence, the overall accumulation of ^{111}In-DTPA-EGFt in the cell nucleus was only about two times lower than that of ^{111}In-DTPA-hEGF, despite 8-fold lower cell binding and internalization. Nonetheless, overall EGFt was less efficient than hEGF to deliver ^{111}In to the cell nucleus since less radioconjugate was bound and internalized by the cells. However, EGFt was still able to deliver a cytotoxic concentration of ^{111}In into the nucleus of EGFR overexpressing breast cancer cells as demonstrated by decreased clonogenic survival.

The greater efficiency of nuclear accumulation of ^{111}In-DTPA-EGFt may be due to the lower EGFt receptor affinity which causes the ligand to be released more readily than EGF from the receptor in endosomes avoiding lysosomal degradation, resulting in a higher EGFt availability to be translocated the nucleus; or as EGFt does not promote receptor dimerization, the nuclear translocation of receptor monomers, which are smaller, could be more efficient, and may not saturate the nuclear transport machinery (Li et al., 2009; Wang et al., 2012). In addition, as we previously discussed, the impaired phosphorylation at Tyr-1045 of the EGFR after EGFt binding to the receptor may also contribute to the increased nuclear uptake of ^{111}In-DTPA-EGFt. Phosphorylated-Tyr-1045 is necessary to recruit c-Cbl, which ubiquitinates EGFR, directing it to the lysosome for degradation (Hu et al., 2007). Thus, the impaired phosphorylation of EGFR by EGFt may enable the ligand-receptor complex to escape from lysosome-mediated degradation, increasing the amount available to accumulate in the cell nucleus.

^{111}In-DTPA-EGFt and ^{111}In-DTPA-hEGF both demonstrated EGFR-mediated cell killing, as evidenced by the relative reduction in clonogenic survival of MDA-MB-468 and MCF-7 breast cancer cells exposed to these radiolabeled peptides. ^{111}In-DTPA-hEGF induced a greater reduction in the clonogenic survival of MDA-MB-468 cells that overexpress EGFR (1×10^6 EGFR/cell) compared to ^{111}In-DTPA-EGFt. This greater potency was not as evident in MCF-7 cells with lower receptor density (1×10^4

EGFR/cell). These results were consistent with earlier reports, which showed that ^{111}In-DTPA-hEGF selectively inhibited the growth of MDA-MB-468 cells compared to cells with lower EGFR density (Reilly et al., 2000). The effect of the unconjugated peptides was also assessed in both cell lines, in order to determine whether they contribute to the cell killing activity of the corresponding radioconjugates. We found that only the proliferation of the EGFR overexpressing MDA-MB-468 cells was significantly inhibited by both hEGF and EGFt. These results are consistent with previous reports that human cancer cells with very high EGFR expression are growth inhibited by EGF due to its effect in promoting cell cycle arrest and apoptosis (Filmus et al., 1985; Rae et al., 2004; Kamer et al., 2004; Armstrong et al., 1994).

The pharmacokinetic parameters calculated (AUC, CL, half-lives of the distribution (t1/2α) and elimination phases (t1/2β), and V1)) revealed a significant difference ($P<0.05$) between ^{111}In-DTPA-hEGF and ^{111}In-DTPA-EGFt. Particularly, ^{111}In-DTPA-EGFt remained longer in the circulation possibly due to a lower affinity for EGFR on normal tissues, especially the liver that decreased sequestration by these organs.

The biodistribution of ^{111}In-DTPA-EGFt in athymic mice bearing tumor xenografts confirmed its lower affinity for EGFR in vivo. Tissues such as skin, liver and the MDA-MB-468 tumor xenografts, that express high levels of EGFR, showed significantly lower uptake of ^{111}In-DTPA-EGFt compared to ^{111}In-DTPA-hEGF. The uptake of ^{111}In-DTPA-EGFt in MDA-MB-468 tumors and some normal tissues was blocked by pre-injecting mice with an excess of anti-EGFR monoclonal antibody nimotuzumab showing a specific target delivery of the radioisotope through EGFR. Nimotuzumab blocks the active binding sites of EGFR (Talavera et al., 2009). ^{111}In-DTPA-hEGt was mainly retained by the kidneys, a different biodistribution than ^{111}In-DTPA-hEGF, which was sequestered mainly by the liver, spleen and kidneys. The truncation of the 8 C-terminal amino acids does not change the pI of EGFt, but would decrease its hydrophobicity.

This effect and a longer blood residence time could explain the higher kidney retention (Kunstler et al., 2010; Schottelius et al., 2002; Hackel et al., 2012).

The tumor uptake of ^{111}In-DTPA-hEGF was higher than ^{111}In-DTPA-EGFt, but ex vivo fractionation of the tumors revealed that ^{111}In-DTPA-EGFt translocated to the cell nucleus 2-fold more efficiently than ^{111}In-DTPA-hEGF. Increased nuclear uptake is an advantage for Auger electron radiotherapy of tumors due to the nanometer-micrometer range of these electrons, but would also be valuable for delivery of other cytotoxic agents that act in the cell nucleus (e.g. DNA intercalating agents). However, the lower tumor uptake of ^{111}In-DTPA-EGFt compared to ^{111}In-DTPA-hEGF may practically limit this advantage.

In conclusion, EGFt is an interesting competitive EGFR blocking agent that does not activate the EGFR but provides an effective vehicle for the delivery of cytotoxic agents to EGFR-positive tumor cells. In particular, ^{111}In-DTPA-EGFt effectively delivered ^{111}In to the nucleus of EGFR-positive breast cancer cells where the emitted Auger electrons decreased their clonogenic survival. ^{111}In-DTPA-EGFt also specifically localized in EGFR-positive breast cancer xenografts in athymic mice, although its uptake was lower than non-truncated ^{111}In-DTPA-hEGF. ^{111}In-DTPA-EGFt could be associated with lower EGFR-mediated side effects due to its lower binding affinity and absence of EGFR-activating properties. In humans, ^{111}In-DTPA-hEGF caused a range of side-effects (flushing, chills nausea and vomiting) that are believed to be due to binding of the radiolabeled peptide to EGFR on normal tissues including the vasculature (Vallis et al., 2014). These side effects may limit dose-escalation to achieve a therapeutic effect.

3. Potential future directions

Based on the results obtained in this work, it would be very interesting to develop new hEGF derivatives with higher EGFR affinity. Although the design of EGFt has improved

the affinity of PCI for EGFR, some of the experiments presented by this thesis showed that it is still not strong enough to compete with hEGF for EGFR binding, which, for example, could represent a limitation in targeting radiotherapy,. In addition, it has been probed that EGFt is a good vehicle to target toxins into the cell nucleus. For this reason it would be very interesting to exploit this strategy to deliver other types of toxins into cancer cells. One approach could be to conjugate EGFt to chemotherapeutic agents like platinum derivatives and other nonplatinum metal complexes such as ruthenium, which interact with DNA and induce the cell death, in order to target them to cancer cells overexpressing EGFR. The cytotoxic activity of these compounds has been previously validated in other studies by our group (Barragán et al., 2012).

On the other hand, after the promising results of EGFt as an EGFR blocker it would be very interesting to explore this strategy with different ligands of the HER family in order to block other ErbB receptors. In particular HER3, as a publication by our group revealed that the simultaneous blocking of EGFR and HER3 by monoclonal antibodies inhibits the ErbB pathway in a more efficient way (Carrión-Salip, et al. 2012).

CONCLUSIONS

1. Based on the superimposition of PCI and hEGF a truncated form of hEGF (EGFt) has been designed and cloned into an extracellular expression vector. Both EGFt and hEGF were expressed in E.coli and purified from the supernatant by a two-step chromatography protocol that provided pure EGFt and hEGF with their correct folding and a good recovery.

2. Scaling-up the production of the recombinant peptides from flasks to 10 L fermenter increased the production yield of the peptides by 25-fold.

3. Both recombinant proteins were able to activate the tyrosin kinase activity of EGFR. However, the phosphorylation induced by EGFt was notably impaired.

4. EGFt did not induce EGFR homodimerization or EGFR-HER2 heterodimerization even when using an excess of EGFt. In addition, EGFt co-treatment decreased hEGF-induced EGFR dimerization, indicating a competition between both peptides for receptor stimulation.

5. EGFt treatment led to a different EGFR phosphorylation pattern than hEGF. Interestingly, EGFt minimally activated phosphorylation of the tyrosines involved in proliferative signaling but it induced the phosphorylation of the residues involved in the receptor internalization.

6. EGFt stimulation induced lower EGFR internalization than hEGF, however the localization of EGFR once within the cell was equivalent for both treatments. Both EGFt and hEGF were detected within the cell nucleus. In contrast to hEGF, EGFt did not directed EGFR to lysosomes for degradation,

7. EGFt did not stimulate the proliferation of MCF-7 or Caco-2. In addition, EGFt inhibited the proliferation of Caco-2 cells probably because Caco-2 cells have a potent stimulatory autocrine loop of TGF-α and EGFt blocked TGF-α binding to EGFR.

8. The binding assay with the radiocompound ^{111}In-DTPA-EGFt indicated that EGFt has high affinity and specificity for EGFR, although the affinity was lower than that of hEGF. As a consequence, ^{111}In-DTPA-EGFt binding and internalization into MDA-MB-468 breast cancer cells was lower compared to ^{111}In-DTPA-hEGF. However, internalized ^{111}In-DTPA-EGFt was more efficiently imported into the cell nucleus than ^{111}In-DTPA-hEGF.

9. ^{111}In-DTPA-EGFt was selectively and highly radiotoxic to MDA-MB-468 cells, leading to an 8% reduction of the surviving fraction to at the higher radiopeptide concentration tested in vitro. The cytotoxic effect in MCF-7 human breast cancer cells, with lower EGFR density, was more modest, leading to a reduction of only 43,1% using the same concentration of radioconjugate.

10. In vivo studies in mice revealed that ^{111}In-DTPA-EGFt remained longer in the circulation possibly due to a lower affinity for EGFR in tissues, as ^{111}In-DTPA-EGFt sequestration on normal tissues, especially the liver, spleen and pancreas was lower compared to 111In-DTPA-hEGF. ^{111}In-DTPA-EGFt was mainly retained by the kidneys probably cause by its higher hydrophobicity.

11. The uptake of ^{111}In-DTPA-hEGF by tumors was higher than ^{111}In-DTPA-EGFt. However, intratumor ^{111}In-DTPA-EGFt was accumulated in a greater proportion within the cell nucleus than ^{111}In-DTPA-hEGF, allowing the

delivery of a cytotoxic concentration of ^{111}In into the nucleus of EGFR overexpressing breast cancer cells, despite its lower tumor accumulation.

REFERENCES

Abrams PG, Fritzberg AR. Antibodies and Novel Constructs for Tumor Targeting. In: Radioimmunotherapy of Cancer. CRC Press; 2000, p.137-66.

Adelstein SJ. Merrill C. Sosman Lecture. The Auger process: a therapeutic promise? AJR Am J Roentgenol. 1993; 160(4):707-13.

Akhtar MJ, Ahamed M, Alhadlaq HA, Alrokayan SA, Kumar S. Targeted anticancer therapy: Overexpressed receptors and nanotechnology. Clin Chim Acta. 2014; 436:78-92.

Amit I, Yakir L, Katz M, Zwang Y, Marmor MD, Citri A, et al. Tal, a Tsg101-specific E3 ubiquitin ligase, regulates receptor endocytosis and retrovirus budding. Genes Dev. 2004; 18(14):1737-52.

Anzano MA, Rieman D, Prichett W, Bowen-Pope DF, Greig R. Growth factor production by human colon carcinoma cell lines. Cancer Res 1989; 49:2898-904.

Armstrong DK, Kaufmann SH, Ottaviano YL, Furuya Y, Buckley JA, Isaacs JT, et al. Epidermal Growth Factor-mediated Apoptosis of MDA-MB-468 Human Breast Cancer Cells. Cancer Res. 1994; 54:5280-3.

Bailey KE, Costantini DL, Cai Z, Scollard DA, Chen Z, Reilly RM, et al. Epidermal growth factor receptor inhibition modulates the nuclear localization and cytotoxicity of the Auger electron emitting radiopharmaceutical 111In-DTPA human epidermal growth factor. J Nucl Med. 2007; 48(9): 1562-70.

Barragán F, Carrión-Salip D, Gómez-Pinto I, González-Cantó A, Sadler PJ, de Llorens R, et al. Bioconjug Chem. 2012; 23(9):1838-55.

Baselga J. Why the Epidermal Growth Factor Receptor? The rationale for cancer therapy. The Oncologist. 2002; 2(4):2-8.

Beaulieu JF, Quaroni A. Clonal analysis of sucrase-isomaltase expression in the human colon adenocarcinoma Caco-2 cells. Biochem J. 1991; 280:599-608.

Benavente S, Huang S, Armstrong EA, Chi A, Hsu KT, Wheeler DL, et al. Establishment and characterization of a model of acquired resistance to epidermal growth factor receptor targeting agents in human cancer cells. Clin Cancer Res. 2009; 15:1585-92.

Biscardi JS, Maa M-C, Tice DA, Cox ME, Leu TH, Parsons SJ. c-Src-mediated phosphorylation of the epidermal growth factor receptor on Tyr845 and Tyr1101 is associated with modulation of receptor function. J Biol Chem. 1999; 274:8335–43.

Bishop WP, Lin J, Stein CA, Krieg AM. Interruption of a transforming growth factor alpha autocrine loop in Caco-2 cells by antisense oligodeoxynucleotides. Gastroenterology. 1995; 109:1882-9.

Blanco-Aparicio C, Molina MA, Fernández-Salas E, Frazier ML, Mas JM, Querol E, et al. Potato carboxypeptidase inhibitor, a T-knot protein, is an epidermal growth factor antagonist that inhibits tumor cell growth. J Biol Chem. 1998; 273(20):12370-7.

Brand TM, Iida M, Li C, Wheeler DL. The nuclear epidermal growth factor receptor signaling network and its role in cancer. Discov Med 2011; 12:419-32.

Brouckaert O, Wildiers H, Floris G, Neven P. Update on triple-negative breast cancer: prognosis and management strategies. Int J Womens Health. 2012; 4:511-20.

Brumlik MJ, Daniel BJ, Waehler R, Curiel DT, Giles FJ, Curiel TJ. Trends in immunoconjugate and ligand-receptor based targeting development for cancer therapy. Expert Opin Drug Deliv. 2008; 5(1):87-103.

Bublil EM, Yarden Y. The EGFR family: spearheading a merger of signaling and therapeutics. Curr Opin Cell Biol. 2007; 19:124-34.

Cai Z, Chattopadhyay N, Liu WJ, Chan C, Pignol JP, Reilly RM. Optimized digital counting colonies of clonogenic assays using ImageJ software and customized macros: comparison with manual counting. Int J Radiat Biol. 2011; 87(11):1135-46.

Cai Z, Chen Z, Bailey KE, Scollard DA, Reilly RM, Vallis KA. Relationship between induction of phosphorylated H2AX and survival in breast cancer cells exposed to 111In-DTPA-hEGF. J Nucl Med. 2008; 49(8):1353-61.

Cai Z, Zhang H, Liu J, Berezov A, Murali R, Wang Q, et al. Targeting erbB receptors. Semin Cell Dev Biol. 2010; 21(9):961-6.

Canals F. Signal transmission by epidermal growth factor receptor: coincidence of activation and dimerization. Biochemistry. 1992; 31: 4493–501.

Cao H, Lei ZM, Bian L, Rao CV. Functional nuclear epidermal growth factor receptors in human choriocarcinoma JEG-3 cells and normal human placenta. Endocrinology. 1995; 136(7):3163-72.

Carrión-Salip D, Panosa C, Menendez JA, Puig T, Oliveras G, Pandiella A, et al. Androgen-independent prostate cancer cells circumvent EGFR inhibition by overexpression of alternative HER receptors and ligands. Int J Oncol. 2012; 41(3):1128-38.

Chang JY, Lu BY, Li L. Conformational impurity of disulfide proteins: detection, quantification, and properties. Anal Biochem. 2005; 342:78-85.

Chang JY, Schindler P, Ramseier U, Lai PH. The disulfide folding pathway of human epidermal growth factor. J Biol Chem. 1995; 270:9207-16.

Chen P, Cameron R, Wang J, Vallis KA, Reilly RM. Antitumor effects and normal tissue toxicity of ^{111}In-labeled epidermal growth factor administered to athymic mice bearing

epidermal growth factor receptor-positive human breast cancer xenografts. J Nucl Med. 2003; 44:1469–78.

Chen P, Mrkobrada M, Vallis KA, Cameron R, Sandhu J, Hendler A, et al. Comparative antiproliferative effects of ^{111}In-DTPA-hEGF, chemotherapeutic agents and gamma-radiation on EGFR positive breast cancer cells. Nucl Med Biol. 2002; 29:693–9.

Cho HS, Leahy DJ. Structure of the extracellular region of HER3 reveals an interdomain tether. Science. 2002; 297(5585):1330-3.

Choi JH, Lee SY. Secretory and extracellular production of recombinant proteins using Escherichia coli. Appl Microbiol Biotechnol. 2004; 64:625-35.

Citri A, Yarden Y. EGF-ERBB signalling: towards the systems level. Nat Rev Mol Cell Biol. 2006; 7:505-16.

Cohen S. Isolation and biological effects of an epidermal growth-stimulating protein. Natl Cancer Inst Monogr. 1964; 13:13-37.

Cohen S. Isolation of a mouse submaxillary gland protein accelerating incisor eruption and eyelid opening in the new-born animal. J Biol Chem. 1962; 237:1555-62.

Cohen S. Purification of a nerve-growth promoting protein from the mouse salivary gland and its neurocytotoxic antiserum. Proc Natl Acad Sci U S A. 1960; 46(3):302-11.

Cordero JB, Cozzolino M, Lu Y, Vidal M, Slatopolsky E, Stahl PD, et al. 1,25-Dihydroxyvitamin D down-regulates cell membrane growth- and nuclear growth-promoting signals by the epidermal growth factor receptor. J Biol Chem. 2002; 277(41):38965-71.

Countaway JL, Nairn AC, Davis RJ. Mechanism of desensitization of the epidermal growth factor receptor protein-tyrosine kinase. J Biol Chem. 1992; 267:1129-40.

Dawson JP, Berger MB, Lin CC, Schlessinger J, Lemmon MA, Ferguson KM. Epidermal growth factor receptor dimerization and activation require ligand-induced conformational changes in the dimer interface. Mol Cell Biol. 2005; 25(17):7734-42.

De Larco JE, Reynolds R, Carlberg K, Engle C, Todaro GJ. Sarcoma growth factor from mouse sarcoma virus-transformed cells. Purification by binding and elution from epidermal growth factor receptor-rich cells. J Biol Chem. 1980; 255(8):3685-90.

Diaz-Miqueli A, Martinez GS. Nimotuzumab as a radiosensitizing agent in the treatment of high grade glioma: challenges and opportunities. Onco Targets Ther. 2013; 6: 931-42.

Dittmann K, Mayer C, Fehrenbacher B, Schaller M, Raju U, Milas L, et al. Radiation-induced epidermal growth factor receptor nuclear import is linked to activation of DNA-dependent protein kinase. J Biol Chem. 2005; 280(35): 31182-9.

Downward J, Yarden Y, Mayes E, Scrace G, Totty N, Stockwell P, et al. Close similarity of epidermal growth factor receptor and v-erb-B oncogene protein sequences. Nature. 1984; 9-15;307(5951):521-7.

Dunn WA, Hubbard AL. Receptor-mediated endocytosis of epidermal growth factor by hepatocytes in the perfused rat liver: ligand and receptor dynamics. J Cell Biol. 1984; 98(6):2148-59.

Ebner R, Derynck R. Epidermal growth factor and transforming growth factor-alpha: differential intracellular routing and processing of ligand-receptor complexes. Cell Regul. 1991; 2:599-612.

Ferguson KM, Berger MB, Mendrola JM, Cho HS, Leahy DJ, Lemmon MA. EGF activates its receptor by removing interactions that autoinhibit ectodomain dimerization. Mol Cell. 2003; 11(2):507-17.

Ferrer Soler L, Cedano J, Querol E, de Llorens R. Cloning, expression and purification of human epidermal growth factor using different expression systems. J Chromatogr B Analyt Technol Biomed Life Sci. 2003; 788:113-23.

Ferrer-Soler L, Vazquez-Martin A, Brunet J, Menendez JA, De Llorens R, Colomer R. An update of the mechanisms of resistance to EGFR-tyrosine kinase inhibitors in breast cancer: Gefitinib (Iressa) -induced changes in the expression and nucleo-cytoplasmic trafficking of HER-ligands (Review). Int J Mol Med. 2007; 20(1):3-10.

Ferrer-Soler L. Estudi de l'acció de diferents bloquejadors de la via ErbB en la teràpia antitumoral. PhD Thesis. Universitat de Girona, 2007.

Filmus J, Pollak MN, Cailleau R, Buick RN. MDA-468, a human breast cancer cell line with a high number of epidermal growth factor (EGF) receptors, has an amplified EGF receptor gene and is growth inhibited by EGF. Biochem Biophys Res Commun. 1985; 128(2):898-905.

Foley J, Nickerson NK, Nam S, Allen KT, Gilmore JL, Nephew KP, et al. EGFR signaling in breast cancer: bad to the bone. Semin Cell Dev Biol. 2010; 21:951-60.

Franken NA, Rodermond HM, Stap J, Haveman J, van Bree C. Clonogenic assay of cells in vitro. Nat Protoc. 2006; 1:2315–9.

Garrett TP, McKern NM, Lou M, Elleman TC, Adams TE, Lovrecz GO, et al. Crystal structure of a truncated epidermal growth factor receptor extracellular domain bound to transforming growth factor alpha. Cell. 2002; 110(6):763-73.

Ghrayeb J, Kimura H, Takahara M, Hsiung H, Masui Y, Inouye M. Secretion cloning vectors in Escherichia coli. EMBO J. 1984; 3:2437-42.

Gregory H. Isolation and structure of urogastrone and its relationship to epidermal growth factor. Nature. 1975; 257(5524):325-7.

Grøvdal LM, Stang E, Sorkin A, Madshus IH. Direct interaction of Cbl with pTyr 1045 of the EGF receptor (EGFR) is required to sort the EGFR to lysosomes for degradation. Exp Cell Res. 2004; 300(2):388-95.

Hackel BJ, Sathirachinda A, Gambhir SS. Designed hydrophilic and charge mutations of the fibronectin domain: towards tailored protein biodistribution. Protein Eng Des Sel. 2012; 25(10):639-47.

Han W, Lo HW. Landscape of EGFR signaling network in human cancers: biology and therapeutic response in relation to receptor subcellular locations. Cancer Lett. 2012; 318:124-34.

Hanada N, Lo HW, Day CP, Pan Y, Nakajima Y, Hung MC. Co-regulation of B-Myb expression by E2F1 and EGF receptor. Mol Carcinog. 2006; 45(1):10-7.

Hanahan D, Weinberg RA. Hallmarks of cancer: the next generation. Cell. 2011; 144(5):646-74.

Hass GM, Ryan CA. Carboxypeptidase inhibitor from potatoes. Methods Enzymol. 1981; 80:778-91.

Herbst RS, Kim ES, Harari PM. IMC-C225, an anti-epidermal growth factor receptor monoclonal antibody, for treatment of head and neck cancer. Expert Opin Biol Ther. 2001; 1(4):719-32.

Herbst RS, Shin DM. Monoclonal antibodies to target epidermal growth factor receptor-positive tumors: a new paradigm or cancer therapy. Cancer. 2002; 94(5):1593-611.

Hsu SC, Hung MC. Characterization of a novel tripartite nuclear localization sequence in the EGFR family. J Biol Chem. 2007; 282(14):10432-40.

Hu M, Scollard D, Chan C, Chen P, Vallis K, Reilly RM. Effect of the EGFR density of breast cancer cells on nuclear importation, in vitro cytotoxicity, and tumor and normal-tissue uptake of [111In]DTPA-hEGF. Nucl Med Biol. 2007; 34:887-96.

Huang HW, Mohan SK, Yu C. The NMR solution structure of human epidermal growth factor (hEGF) at physiological pH and its interactions with suramin. Biochem Biophys Res Commun. 2010; 402:705-10.

Huang M, Shen A, Ding J, Geng M. Molecularly targeted cancer therapy: some lessons from the past decade. Trends Pharmacol Sci. 2014; 35(1):41-50.

Hung LY, Tseng JT, Lee YC, Xia W, Wang YN, Wu ML, et al. Nuclear epidermal growth factor receptor (EGFR) interacts with signal transducer and activator of transcription 5 (STAT5) in activating Aurora-A gene expression. Nucleic Acids Res. 2008; 36(13):4337-51.

Hynes NE, Horsch K, Olayioye MA, Badache A. The ErbB receptor tyrosine family as signal integrators. Endocr Relat Cancer. 2001; 8(3):151-9.

Imai K, Takaoka A. Comparing antibody and small-molecule therapies for cancer. Nat Rev Cancer. 2006; 6(9):714-27.

Jackson MR, Falzone N, Vallis KA. Advances in anticancer radio-pharmaceuticals. Clin Oncol. 2013; 25:604-9.

Joo WD, Visintin I, Mor G. Targeted cancer therapy--are the days of systemic chemotherapy numbered? Maturitas. 2013; 76(4):308-14.

Jorissen RN, Walker F, Pouliot N, Garrett TP, Ward CW, Burgess AW. Epidermal growth factor receptor: mechanisms of activation and signalling. Exp Cell Res. 2003; 284(1):31-53.

Kamer AR, Sacks PG, Vladutiu A, Liebow C. EGF mediates multiple signals: Dependence on the conditions. Int J Mol Med. 2004; 13:143–47.

Kamio T, Shigematsu K, Sou H, Kawai K, Tsuchiyama H. Immunohistochemical expression of epidermal growth factor receptors in human adrenocortical carcinoma. Hum Pathol. 1990; 21(3):277-82.

Kassis AI. Cancer therapy with Auger electrons: are we almost there? J Nucl Med. 2003; 44(9):1479-81.

King RGB, Robins MW. Principles of cancer treatment. In: Cancer Biology. Prentice Hall; 2007, p.231-62.

Kunstler JU, Seidel G, Bergmann R, Gniazdowska E, Walther M, Schiler E, et al. Novel 99mTc '4 + 1' peptide conjugates: tuning the biodistribution by variation of coligands. Eur J Med Chem. 2010; 45(9):3645-55.

Lemmon MA. Ligand-induced ErbB receptor dimerization. Exp Cell Res. 2009; 315(4):638-48.

Levi-Montalcini R, Cohen S. Effects of the extract of the mouse submaxillary salivary glands on the sympathetic system of mammals. Ann N Y Acad Sci. 1960; 85:324-41.

Levkowitz G, Waterman H, Ettenberg SA, Katz M, Tsygankov AY, Alroy I, et al. Ubiquitin ligase activity and tyrosine phosphorylation underlie suppression of growth factor signaling by c-Cbl/Sli-1. Mol Cell. 1999; 4(6):1029-40.

Li C, Iida M, Dunn EF, Ghia AJ, Wheeler DL. Nuclear EGFR contributes to acquired resistance to cetuximab. Oncogene. 2009; 28: 3801-13.

Liao HJ, Carpenter G. Role of the Sec61 translocon in EGF receptor trafficking to the nucleus and gene expression. Mol Biol Cell. 2007; 18(3):1064-72.

Lin SY, Makino K, Xia W, Matin A, Wen Y, Kwong KY, et al. Nuclear localization of EGF receptor and its potential new role as a transcription factor. Nat Cell Biol. 2001; 3:802-808.

Lipponen P, Eskelinen M. Expression of epidermal growth factor receptor in bladder cancer as related to established prognostic factors, oncoprotein (c-erbB-2, p53) expression and long-term prognosis. Brit J Cancer. 1994; 69(6):1120-5.

Lo HW, Cao X, Zhu H, Ali-Osman F. COX-2 is a novel transcriptional target of the nuclear EGFR-STAT3 and EGFRvIII-STAT3 signaling axes. Mol Cancer Res. 2010; 8(2):232-45.

Lo HW, Xia W, Wei Y, Ali-Seyed M, Huang SF, Hung MC. Novel prognostic value of nuclear epidermal growth factor receptor in breast cancer. Cancer Res. 2005; 65(1):338-48.

Madshus IH, Stang E. Internalization and intracellular sorting of the EGF receptor: a model for understanding the mechanisms of receptor trafficking. J Cell Sci. 2009; 122(Pt 19):3433-9.

Malvezzi M, Bertuccio P, Rosso T, Rota M, Levi F, La Vecchia C, et al. European cancer mortality predictions for the year 2015: does lung cancer have the highest death rate in EU women? Ann Oncol. 2015; 26(4):779-86.

Marshall J. Clinical implications of the mechanism of epidermal growth factor receptor inhibitors. Cancer. 2006; 107:1207-18.

Marti U, Burwen SJ, Wells A, Barker ME, Huling S, Feren AM, et al. Localization of epidermal growth factor receptor in hepatocyte nuclei. Hepatology. 1991; 13(1):15-20.

Marti U, Ruchti C, Kampf J, Thomas GA, Williams ED, Peter HJ, et al. Nuclear localization of epidermal growth factor and epidermal growth factor receptors in human thyroid tissues. Thyroid. 2004; 11(2):137-45.

Martin RF, Bradley TR, Hodgson GS. Cytotoxicity of an 125I-labeled DNA-binding compound that induces double-stranded DNA breaks. Cancer Res. 1979; 39(8):3244-7.

Mas JM, Aloy P, Martí-Renom MA, Oliva B, Blanco-Aparicio C, Molina MA, et al. Protein similarities beyond disulphide bridge topology. J Mol Biol. 1998; 284(3):541-8.

Matsunami RK, Yette ML, Stevens A, Niyogi SK. Mutational analysis of leucine 47 in human epidermal growth factor. J Cell Biochem. 1991; 46:242-9.

McLean JR, Blakey DH, Douglas GR, Bayley J. The Auger electron dosimetry of indium-111 in mammalian cells in vitro. Radiat Res. 1989; 119(2):205-18.

Mills IG. Nuclear translocation and functions of growth factor receptors. Semin Cell Dev Biol. 2012; 23:165-71.

Mills IG. The interplay between clathrin-coated vesicles and cell signaling. Semin Cell Dev Biol. 2007; 18 (4):459-70.

Motulsky HJ, Stannard P, Neubig R. Prism; GraphPad Software Inc. 2.0; 1995.

Normanno N, De Luca A, Bianco C, Strizzi L, Mancino M, Maiello MR, et al. Epidermal growth factor receptor (EGFR) signaling in cancer. Gene. 2006; 366(1):2-16.

Ogiso H, Ishitani R, Nureki O, Fukai S, Yamanaka M, Kim JH, et al. Crystal structure of the complex of human epidermal growth factor and receptor extracellular domains. Cell. 2002; 110(6):775-87.

Olayioye MA, Neve RM, Lane HA, Hynes NE. The ErbB signaling network: receptor heterodimerization in development and cancer. EMBO J. 2000; 19(13):3159-67.

Psyrri A, Yu Z, Weinberger PM, Sasaki C, Haffty B, Camp R, et al. Quantitative determination of nuclear and cytoplasmic epidermal growth factor receptor expression in oropharyngeal squamous cell cancer by using automated quantitative analysis. Clin Cancer Res. 2005; 11(16):5856-62.

Rae JM, Lippman ME. Evaluation of novel epidermal growth factor receptor tyrosine kinase inhibitors. Breast Cancer Res Treat. 2004; 83:99-107.

Rakowicz-Szulczynska EM, Rodeck U, Herlyn M, Koprowski H. Chromatin binding of epidermal growth factor, nerve growth factor, and platelet-derived growth factor in cells bearing the appropriate surface receptors. Proc Natl Acad Sci. 1986; 83: 3728–32.

Ramakrishnan MS, Eswaraiah A, Crombet T, Piedra P, Saurez G, Iyer H, et al. Nimotuzumab, a promising therapeutic monoclonal for treatment of tumors of epithelial origin. MAbs. 2009; 1(1):41-8.

Ray P, Moy FJ, Montelione GT, Liu JF, Narang SA, Scheraga HA, et al. Structure-function studies of murine epidermal growth factor: expression and site-directed mutagenesis of epidermal growth factor gene. Biochemistry. 1988; 27:7289-95.

Reddy CC, Wells A, Lauffenburger DA. Comparative mitogenic potencies of EGF and TGF alpha and their dependence on receptor-limitation versus ligand-limitation. Med Biol Eng Comput. 1998; 36:499-507.

Reilly RM. Monoclonal Antibody and Peptide-Targeted Radiotherapy of Cancer, John Wiley & Sons, Inc. Hoboken, 2010.

Reilly RM, Chen P, Wang J, Scollard D, Cameron R, Vallis KA. Preclinical pharmacokinetic, biodistribution, toxicology, and dosimetry studies of 111In-DTPA-

human epidermal growth factor: an auger electron-emitting radio-therapeutic agent for epidermal growth factor receptor-positive breast cancer. J Nucl Med. 2006; 47:1023-31.

Reilly RM, Kassis AI. Targeted Auger electron radiotherapy of malignancies. In: Reilly RM, editor. Monoclonal antibody and peptide-targeted radiotherapy of cancer. NJ: John Wiley & Sons Inc.; 2010, p.289-348.

Reilly RM, Kiarash R, Cameron RG, Porlier N, Sandhu J, Hill RP, et al. ^{111}In-Labeled EGF is selectively radiotoxic to human breast cancer cells overexpressing EGFR. J Nucl Med. 2000; 41:429–38.

Reilly RM, Kiarash R, Sandhu J, Lee YW, Cameron RG, Hendler A, et al. A comparison of EGF and mAb 528 labeled with 111In for imaging human breast cancer. J Nucl Med. 2000; 41:903–11.

Reilly RM, Scollard DA, Wang J, Mondal H, Chen P, Henderson LA, et al. A kit formulated under good manufacturing practices for labeling human epidermal growth factor with 111In for radiotherapeutic applications. J Nucl Med. 2004;45(4):701-8.

Révillion F, Lhotellier V, Hornez L, Bonneterre J, Peyrat JP. ErbB/HER ligands in human breast cancer, and relationships with their receptors, the bio-pathological features and prognosis. Ann Oncol. 2008; 19(1):73-80.

Saleh TB. Radiopharmacy: Basics. In: Khalil MM, editors. Basic Sciences of Nuclear Medicine, Springer-Verlag, Berlin; 2011, p.25-39.

Sato JD, Kawamoto T, Le AD, Mendelsohn J, Polikoff J, Sato GH. Biological effects in vitro of monoclonal antibodies to human epidermal growth factor receptors. Mol Biol Med. 1983; 1(5):511-29.

Schottelius M, Wester HJ, Reubi JC, Senekowitsch-Schmidtke R, Schwaiger M. Improvement of pharmacokinetics of radioiodinated Tyr(3)-octreotide by conjugation with carbohydrates. Bioconjug Chem. 2002; 13(5):1021-30.

Sebastian S, Settleman J, Reshkin SJ, Azzariti A, Bellizzi A, Paradiso A. The complexity of targeting EGFR signalling in cancer: from expression to turnover. Biochim Biophys Acta. 2006; 1766(1):120-39.

Seshacharyulu P, Ponnusamy MP, Haridas D, Jain M, Ganti AK, Batra SK. Targeting the EGFR signaling pathway in cancer therapy. Expert Opin Ther Targets. 2012; 16(1):15-31.

Siegel RL, Miller KD, Jemal A. Cancer statistics, 2015. CA Cancer J Clin. 2015; 65(1):5-29

Sitjà-Arnau M, Molina MA, Blanco-Aparicio C, Ferrer-Soler L, Lorenzo J, Avilés FX, et al. Mechanism of action of potato carboxypeptidase inhibitor (PCI) as an EGF blocker. Cancer Lett. 2005; 226(2):169-84.

Sorensen HP, Mortensen KK. Advanced genetic strategies for recombinant protein expression in Escherichia coli. J Biotechnol. 2005; 115:113-28.

Sorkin A, Goh LK. Endocytosis and intracellular trafficking of ErbBs. Exp Cell Res. 2008; 314(17):3093-106.

Stoffel A. Targeted therapies for solid tumors: current status and future perspectives. BioDrugs. 2010; 24(5):303-16.

Talavera A, Friemann R, Gómez-Puerta S, Martinez-Fleites C, Garrido G, Rabasa A, et al. Nimotuzumab, an antitumor antibody that targets the epidermal growth factor receptor, blocks ligand binding while permitting the active receptor conformation. Cancer Res. 2009; 69(14):5851-9.

Theroux SJ, Latour DA, Stanley K, Raden DL, Davis RJ. Signal transduction by the epidermal growth factor receptor is attenuated by COOH_terminal domain serine phosphorylation site. J Biol Chem. 1992; 267(23):16620-6.

Vallis KA, Reilly RM, Scollard D, Merante P, Brade A, Velauthapillai S, et al. Phase I trial to evaluate the tumor and normal tissue uptake, radiation dosimetry and safety of (111)In-DTPA-human epidermal growth factor in patients with metastatic EGFR-positive breast cancer. Am J Nucl Med Mol Imaging. 2014; 4(2):181-92.

Wang SC, Nakajima Y, Yu YL, Xia W, Chen CT, Yang CC, et al. Tyrosine phosphorylation controls PCNA function through protein stability. Nat Cell Biol. 2006;8(12):1359-68.

Wang YN, Hung MC. Nuclear functions and subcellular trafficking mechanisms of the epidermal growth factor receptor family.Cell Biosci. 2012; 2: 1-13.

Wang YN, Wang H, Yamaguchi H, Lee HJ, Lee HH, Hung MC. COPI-mediated retrograde trafficking from the Golgi to the ER regulates EGFR nuclear transport. Biochem Biophys Res Commun. 2010; 399(4):498-504.

Weinberg RA. Cancer: a genetic disorder. In: Mendelsohn J, Howley P, Israel M, Gray J, Thompson C, editors. The molecular basis of cancer. Philadelphia: Saunders Elsevier; 2008, p.2-16.

Wheeler DL, Dunn EF, Harari PM. Understanding resistance to EGFR inhibitors-impact on future treatment strategies. Nat Rev Clin Oncol. 2010; 7(9):493-507.

Wilson KJ, Gilmore JL, Foley J, Lemmon MA, Riese DJ. Functional selectivity of EGF family peptide growth factors: implications for cancer. Pharmacol Ther. 2009; 122:1-8.

Yewale C, Baradia D, Vhora I, Patil S, Misra A. Epidermal growth factor receptor targeting in cancer: a review of trends and strategies. Biomaterials. 2013; 34(34):8690-707.

Yotsumoto F, Sanui A, Fukami T, Shirota K, Horiuchi S, Tsujioka H, et al. Efficacy of ligand-based targeting for the EGF system in cancer. Anticancer Res. 2009; 29(11):4879-85.

Zahnow CA. ErbB receptors and their ligands in the breast. Expert Rev Mol Med. 2006; 8(23):1-21.

Zahorowska B, Crowe PJ, Yang JL. Combined therapies for cancer: a review of EGFR-targeted monotherapy and combination treatment with other drugs. J Cancer Res Clin Oncol. 2009; 135(9):1137-48.